Patterning Strategies of Poly(ethylene glycol) Based Hydroxyapatite Composites for Biomedical Applications

Vorgelegt von

Dipl.-Ing. Axel Löbus

aus Leipzig

Von der Fakultät II - Mathematik und Naturwissenschaften

der Technischen Universität Berlin

zur Erlangung des akademischen Grades

Doktor der Ingenieurwissenschaften

Dr.-Ing.

Genehmigte Dissertation

Promotionsausschuss:

Vorsitzender: Prof. Dr.-Ing. Matthias Bickermann
Berichter/Gutachter: Prof. Dr. Ir. Marga C. Lensen
Berichter/Gutachter: Prof. Dr. rer. nat. Andreas Taubert

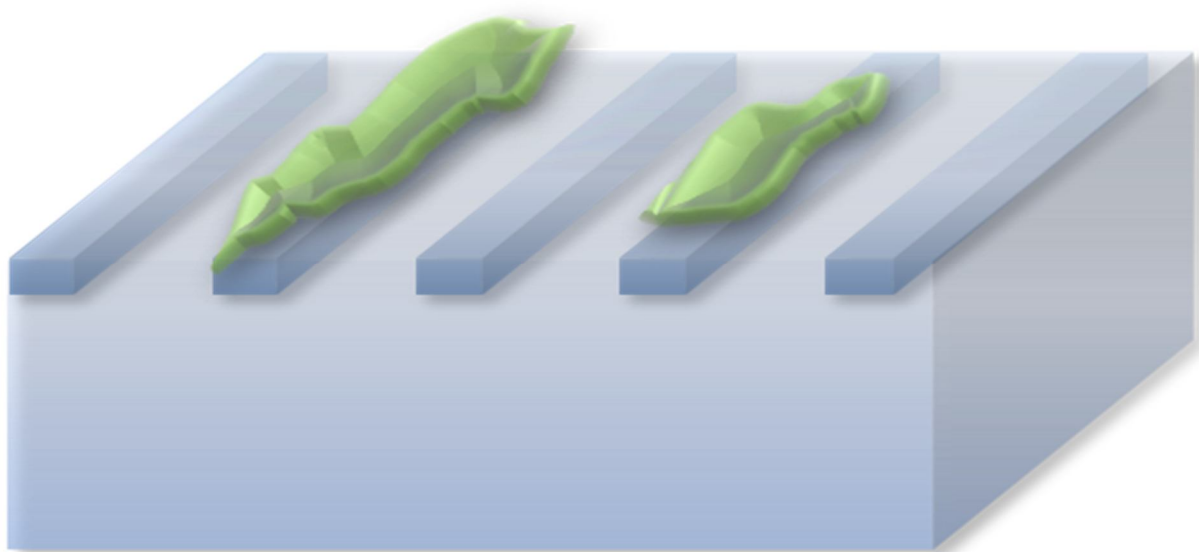Tag der wissenschaftlichen Aussprache: 6. September 2013

Berlin 2013

D 83

Table of Contents

List of Abbreviations

3BC - PEG-*b*-PPG-*b*-PEG

8PEG – 8arm star Poly(ethylene glycol)

ACP – Amorphous Calcium Phosphate

AFM - Atomic Force Microscopy

ATR FtIR – Attenuated Total Reflection Fourier Transformed Infrared Spectroscopy

BSA – Bovine Serum Albumin

CL - Crosslinker

CLSM - Confocal Laser Scanning Microscopy

E – Young's Modulus

EDX - Energy Dispersive X-Ray diffraction

F/d curve – Force-distance curve

FIMIC – Fillmolding In Capillaries

G'' – Storage Modulus

G' – Loss Modulus

HAp - hydroxyapatite

M_w – Molecular weight

NPs – nanoparticles

PDMS - Polydimethylsiloxane

PEG - Poly(ethylene glycol)

PETA - Pentaerythritol triacrylate

PI - Photoinitiator

PMMA - Poly(methyl methacrylate)

PPG – Poly(propylene glycol)

PS - Polystyrene

PUA - Poly(urethane acrylate)

R_a - Arithmetic Average (common measure for surface roughness)

RM - Replica Molding

RMS - Root Mean Square (common measure for surface roughness)

SBF – Simulated Body Fluid

SEM - Scanning Electron Microscopy

TEM - Transmission Electron Microscopy

T_g – Glass Transition Temperature

TGA - Thermogravimetric Analysis

UV – ultraviolet

XRD - X-ray diffraction

ε – Elongation at Break/ Compression Strain at Break

σ_{db} – Ultimate Compressive Strength

σ_{df} – Compressive Yield Point

σ_{max} – Ultimate tensile Strength

σ_y – Yield Strength

Chapter 1

Scope and Organization of the Thesis

The idea of substituting injured or malfunctioning parts of the human body in order to regain lost functionality is almost as old as mankind. Already in the ancient times, efforts were made to replace teeth or fix broken or injured bones and cartilages. Those devices were designed empirically by experience and fabricated from materials found in nature such as ivory or animal bone. Concerted construction and investigation of what is nowadays called biomaterials only started in the beginning of the 20th century. It was only then, when medicine emerged to the discipline as it is known today with the development of modern implants and diagnostics. As natural science evolved, it was discovered that the implants' biological performance is greatly affected not only by the type of material employed but also by its inherent surface characteristics. Considering the complexity of natural surfaces, which were aimed to mimic, it was revealed that each bears a specific design, intended to meet all the requirements of the concrete purpose. However, natural materials are hardly ever of morphologically simple or chemically pure nature, but are composites, which are structured from the macro level down to the nanometer scale. Most famously of those might be bone and nacre, which have been vastly examined in order to understand their outstanding properties and to give new insight of how to mimic biological materials[1]. Thus, it was revealed that an intriguing combination of different substances along with complex patterns of all relevant length scales result in the extraordinary performance of natural composites. That extends to surface properties, determining the interaction with the respective surrounding such as biological interfaces or ambient environment. The most famous example may be that of the lotus leaf, a self-cleaning super hydrophobic surface, which derives its intriguing properties solely from the micropatterned surface structure of its leaves. Having grasped the paramount importance of patterning in order to mimic natural composites such as bone in a successful manner, implant design was extensively investigated in terms of physical, mechanical and chemical structures, paying special attention to surface properties.

Surface modification and patterning is not restricted to tissue engineering, but is of essential interest for biomedical applications such as biosensors or diagnostic devices as well. The avoidance of nonspecific protein adsorption and consequent cell adhesion due to surface characteristics is of common interest, but poses several challenges. Among those is the respective determination of the isolated single influences of physical, mechanical and chemical features to interface interaction, which is still discussed in the scientific community. The discrimination and understanding of these effects towards protein adsorption and cell adhesion are centered in this thesis. The main goal was the fabrication of surface substrates, which allow attributing cellular response to designed surface properties. Thus, it was aimed to produce platforms, which exhibit the contrast of bioinert versus bioactive sites, displaying protein repellent and protein attracting behavior, respectively. Pursuing this objective, substrates were manufactured, which promote spatially controlled selective cell adhesion. Such platforms allow the attribution of single surface properties on cellular response, essential to profound understanding of biomaterials surface reaction and necessary for the design of novel devices, which prevent undesired interface interaction between substrate and biological environment.

This thesis is organized in four main chapters, which include "Introduction", "Materials and Methods", "Results and Discussion" and finally "Conclusion and Outlook" and are in the following briefly described. The chapter "Results and Discussion" is organized that each subchapter represents in large parts an own publication or manuscript in preparation.

Introduction: This chapter aims to explain the plausibility of this thesis including the major scientific principles and investigation techniques. Therefore, the importance of patterning in biomaterials surface engineering is outlined and soft lithographic techniques as major method are introduced. Furthermore, Fillmolding in Capillaries (FIMIC) is described in detail, as it is the dominant surface patterning method applied in this thesis. Atomic Force Microscopy (AFM) involving topographic imaging and Force spectroscopy are explained in a manner that aids the understanding of the respective figures in the "Result and Discussion" chapter.

Materials and Methods: This chapter states all employed chemical substances, preparation methods and characterization techniques relevant to this thesis in a comprehensive and detailed manner.

Results and Discussion: This chapter contains the major findings of this thesis organized in four subchapters. The first three subchapters (4.1-4.3) deal with different aspects of FIMIC sample preparation and characterization and are designed in a consecutive manner in order to build up a final result in chapter 4.3. The chapter 4.4 constitutes a subchapter of separate content, describing the 3D formation and characterization of hydrogel composite scaffolds.

Conclusion and Outlook: This chapter summarizes the main results of this thesis, comments on those and states potential challenges worth addressing in future research.

Note: The research project was part of a joint effort from three PhD students of the Lensen Lab; Christine Strehmel, Zhenfang Zhang and Axel Loebus, each possessing different scientific background. Consequently, due to the interdisciplinary nature of the here presented research, many of the attained results could only be achieved in close collaboration with Zhenfang Zhang and Christine Strehmel. Whenever the main intellectual contribution or experimental processing was conducted by (one of) those two colleagues, it will be clearly referred to their respective PhD theses[2,3]. In case any other person contributed significantly to the herein displayed results, it will be clearly indicated, e.g. in the "Materials and Methods" chapter.

Chapter 2

Introduction

First of all, three definitions are introduced, which find application throughout this thesis. However, the author is aware that diversions of these definitions exist.

A **Biomaterial** is nonviable material used in a medical device, intended to interact with biological systems[4].

Biocompatibility is the ability of a material to perform with an appropriate host response in a specific application[4].

Cytocompatibility can be tested by several standardized methods e.g. according to ISO10993, "CytoTox-OneTM Homogeneous Membrane Integrity Assay" and "Trypan Blue Life/Dead Staining", to name a few popular examples.

2.1 Surface Patterning of Materials for Potential Biomedical Application

Surface patterning has been of paramount importance within the biomaterial science community over the last decades[5,6]. In the course of exploring biomaterials and their design, characterizing surface properties has proven to be essential, since the initial interaction taking place at the interface implant - host may decisively impact the host's reaction towards the implant. Consequently, substantial effort has been invested and many systems have been scrutinized in order to reveal influential factors, allow classification and set standards for evaluation methods[7,8]. Hence, it was elaborated that (I) topography[5–7], (II) chemistry[8,9] and (III) elasticity[9] serve as determining factors in order to assess function and host response of biomaterials surface patterns. The need to ascertain these key influential factors experimentally in order to comprehend individual and combined impact was recently reviewed in a very

concise manner by Anseth and co-workers[10]. Surface patterning comprises physical, mechanical and chemical structuring from the macro- down to nano-scale. Physical patterns, which describe topographic features determine the surface's roughness and may be of regular or irregular nature. Mechanical patterns describe the characteristic of different adjacent surface elasticities on investigated substrates, while chemical patterns regard to distinct chemical surface cues leading to e.g. altering wettability or reactivity. They can be combined in almost any desired manner. The principles of surface patterning methods are depicted in Figure 1.

a) Physcial patterning (I lines, II dots)
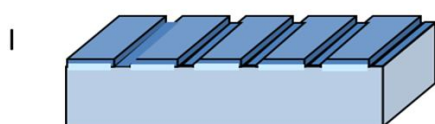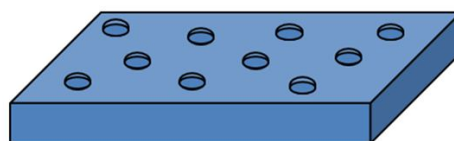
b) Mechanical patterning (I gradual change , II binary pattern)
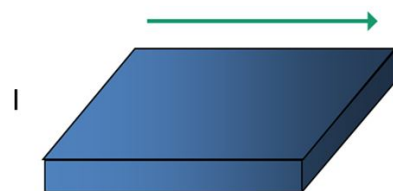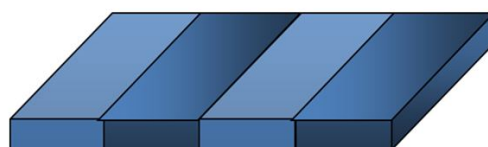
c) Chemical patterning e.g. Au nanodots
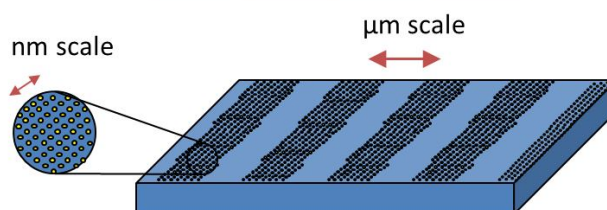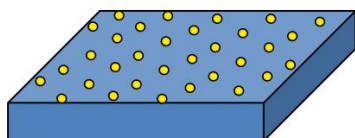
d) Combination of chemical nm-pattern with physical µm pattern
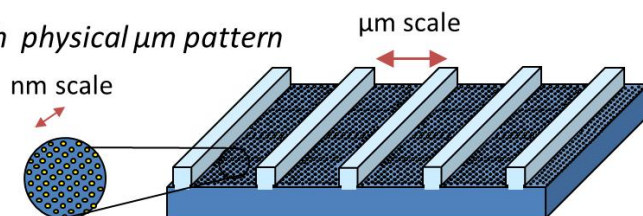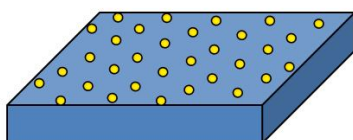
Figure 1: Schematic representation of the most common principles of soft lithographic surface patterning techniques: (a) physical patterns (topography e.g. lines, dots); (b) mechanical patterns (elasticity e.g. gradual change, alternating); (c) chemical patterns (biological or chemical cues e.g. Au nanodots, proteins); (d) example of a combination of patterns.

Physical patterning (topographic features) can be elegantly introduced via e.g. soft lithographic methods such as Molding or Imprinting, which were developed by Whitesides et al. in the 1990s[11]. Alves and co-workers reviewed that resulting micrometer-sized structures on polymer surfaces may promote selective cell adhesion or prevent cellular interaction as schematically depicted in Figure 2[7]. Thus, arrays may be designed, which spatially control protein adsorption and cell adhesion and may even allow discrimination between different kinds of cell types for example for application in diagnostics.
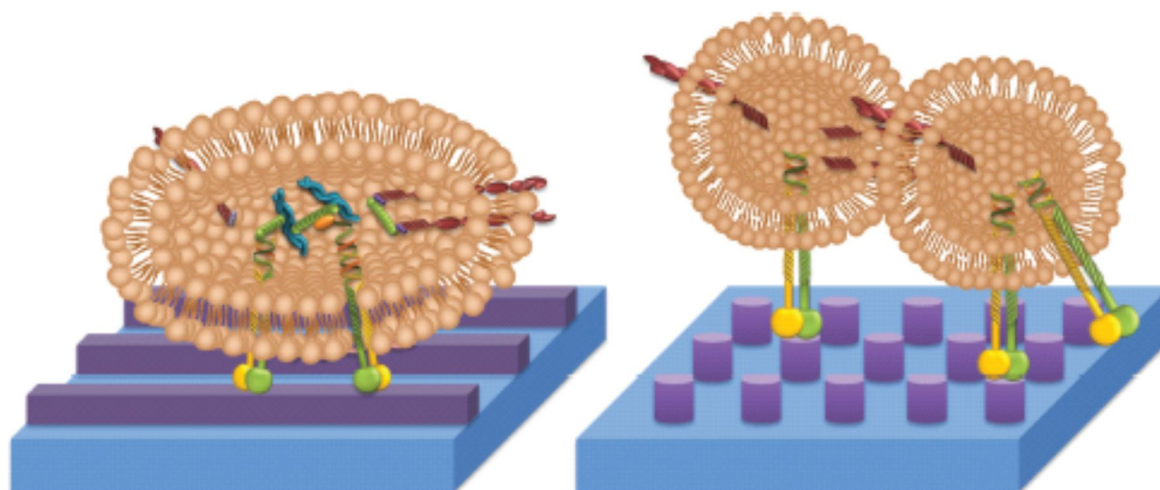
Figure 2: Schematic presentation of surface patterns employing different polymers, which promote or prevent cellular adhesion and spreading. Modified image reprinted from reference [7.]

The patterning techniques however are not limited to pure chemical substances, but may also include hybrid composite materials. One among many options is represented by mineralization of polymer hydrogels employed in soft lithography. Mineralization of patterned substrates by simple inorganic salts is conducted in various forms by nature[1] and has hence drawn great interest to this field of research elaborating profound comprehension regarding many aspects of this issue. Among that, the biomineralization by calcium carbonates[12] and calcium phosphates[13] seems best understood. Deposition of HAp by thermal spraying[14], sol-gel techniques[15], electrophoretic deposition[16,17] and deposition from Simulated Body Fluid (SBF)[18]

on metal, ceramic and polymer substrates, respectively, have elicited great interest, due to the ease and high control in processing and the resulting elevated degree of bioactivity. Among those techniques, deposition from SBF may be the most promising one in consequence of the biomimetic process and inherent mild reaction conditions, which allow serving as drug carrier[19] or the incorporation of e.g. osteoinductive biomolecules[20]. Although HAp nucleation and deposition may be spatially controlled by varying surfaces charges[21], sharp interfaces and precise morphology tunability in order to obtain multifunctional materials containing distinct bioaffinities, without subjecting to lavish and costly processing, remain a challenge[22–27].

Latest developments describe new ways of patterning or the combination of commonly utilized methods. Since it is impossible to summarize this vast research field in a few pages, the author restricts to three examples, which are either related directly to the main objectives of the thesis (Figure 3 and Figure 4), or present an intriguing, completely new approach for potential biomedical applications (Figure 5). Figure 3 displays an approach by Luz and coworkers[22] of targeted inorganic deposition in order to obtain surface patterns of regular inorganic-organic nature via imprinting of bioactive glass nanoparticles. It demonstrates that by controlled incorporation of chemical cues, cell adhesion may be guided and HAp nucleation from SBF may be spatially tuned.

Figure 3: Example of mineralization of in soft lithographic patterning: Imprinting of bioactive glass on chitosan substrates in order to gain sites of preferential cell adhesion. Image reprinted from reference [22].

Another example concerns the combination of physical micro- and nano-patterns by Farshchian et al.[28] as depicted in Figure 4. The feasibility of this approach is explained by the fact that natural materials generally possess physical patterns over various length scales, which exhibit distinct interaction characteristics to its environment. Incorporating different length scales has been a challenge addressed by many contributions in the research community.
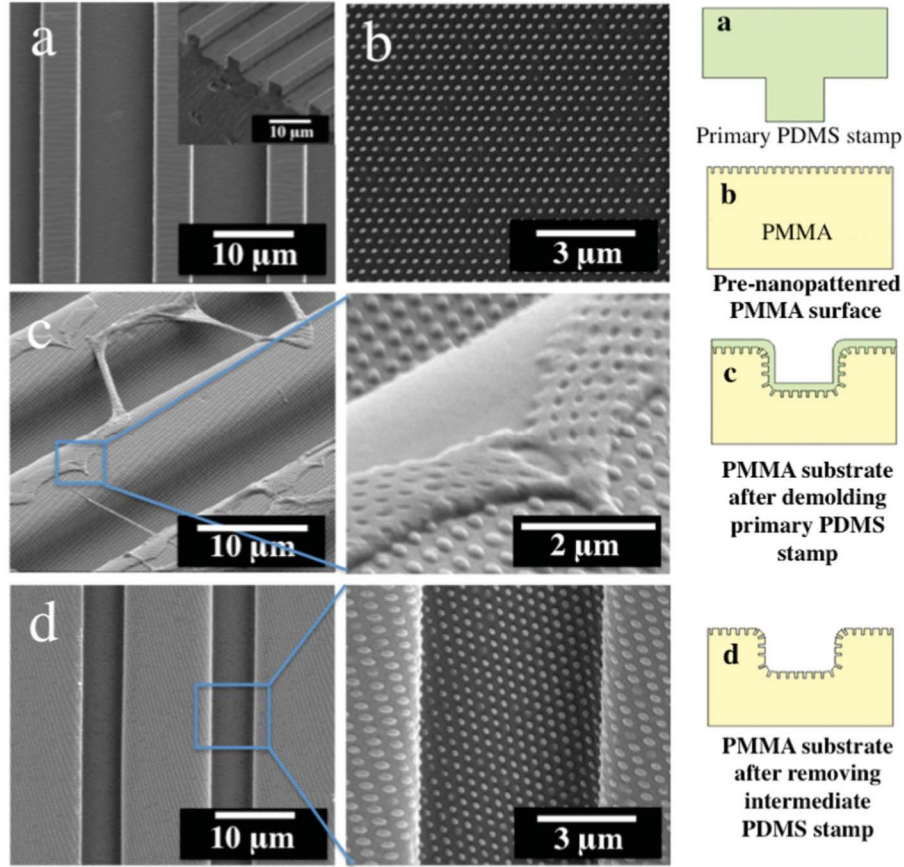
Figure 4: Scanning electron microscopy (SEM) micrographs of (a) primary PDMS stamp having microgratings; (b) pre-nanopatterned PMMA substrate imprinted using a PUA/PC composite stamp; (c) PMMA substrate imprinted using 3D nanomolding after demolding primary PDMS stamp; (d) 3D PMMA substrate after removing the ultra-thin PDMS stamp. Image reprinted from reference [25].

A completely new approach centers the goal of cellular patterning introduced by the research groups of Khademhosseini and Langer[29] (principle detailed in Figure 5). The general idea to this objective is to pattern different kinds of cell types in an adjacent manner in micrometer dimensions. Thereby, the volume change due to alteration of temperature of microwells is exploited.
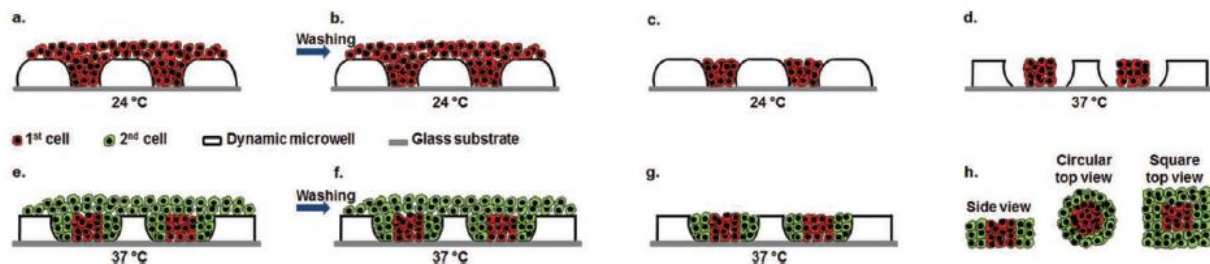
Figure 5: Schematic diagram of spatially controlled patterning of two different cell types with dynamic microwells. (a) Seeding the first cell type (red) at 24 °C when microwell structures were at swollen state. (b) Washing microwells to rinse off undocked cells on microwell surfaces. (c) Undocked cells were washed off the microwell surfaces. (d) Incubation at 37 °C to allow microwell structures to shrink, resulting in more free space for the second cell type. (e) Seeding the second cell type (green) within microwells. (f) Subsequently washing microwells to rinse off undocked cells on the surface. (g) Two cell types were spatially distributed within microwells and further incubated at 37 °C. (h) Side and top views of the resulting microtissues containing two spatially organized cell types. Image reprinted from reference [26].

2.2 Soft Lithography

Lithographic methods are often employed in order to achieve complex 2D or 3D patterns. This extremely versatile technique involves an ever growing number of different kinds of patterning approaches for almost any substrate imaginable covering all length scales from macro down to nano. All lithographic methods are employed in order to design surface characteristics of the goal-substrate in any desired way. Soft lithography is among the most successful techniques, due to its inherent versatility, ease of fabrication, accurate processing down to nanometer-scale and mass production availability. Invented by Whitesides and co-workers in the early 1990s, it has by now evolved into a great number of different methods among which Replica Molding (RM) may be the most famous one, since it represents the first preparation step of many other sophisticated techniques[11]. An incomplete overview of most relevant lithographic patterning techniques focusing on soft lithography is displayed in Figure 6. The methods finding extensive application in this thesis are highlighted.

Lithographic Patterning Techniques

Lithography

Photolithography
E-beam Lithography
Nano-Imprint Lithography
Dip-Pen Lithography
Soft lithography
…

Micro-Contact (De)Printing (µCP)
Replica Molding (RM)
Micro Transfer Molding (µTM)
Micromolding In Capillaries (MIMIC)
Solvent-Assisted Micromolding (SAMIM)
Fillmolding In Capillaries (FIMIC)
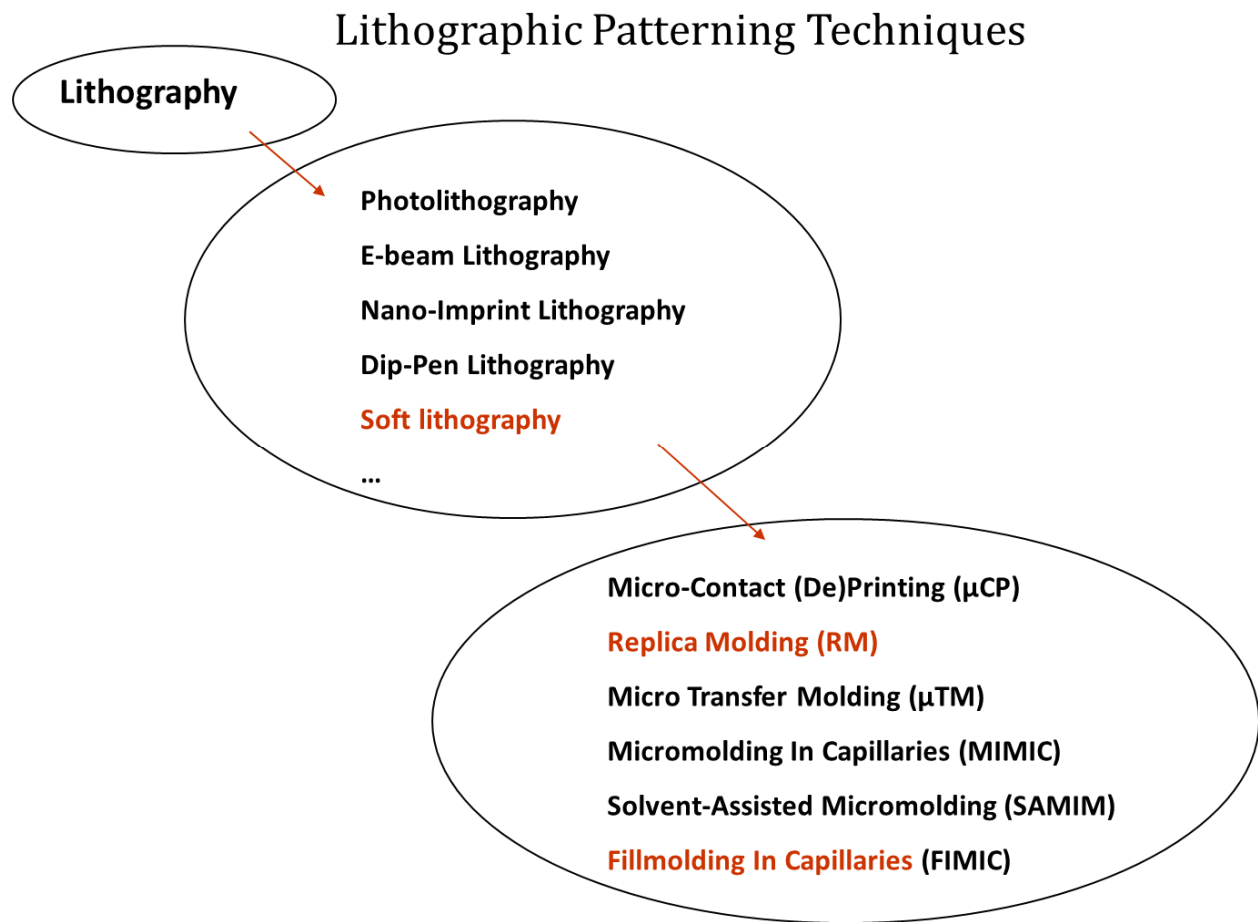
Figure 6: Lithographic patterning techniques, methods extensively applied during the course of this thesis are highlighted in red. Replica Molding (RM) and Fillmolding In Capillaries (FIMIC).

Replica Molding (RM) may be considered as one of the most important and widely applied soft lithographic techniques, since it is often an auxillary processing step to other techniques. RM application is basically restricted by a curable liquid precursor solution of sufficient viscosity allowing accurate penetration of the Silicon wafer pattern. In account to this fact, Figure 7 states details of the single processing steps. First, a Si wafer with the desired structural dimensions is selected (Figure 7a). Next, the desired liquid precursor solution is placed and cured via e.g. ultraviolett (UV) radiation as displayed in Figure 7b. As last step, the cured solution is peeled off the original Si wafer and represents a negative (replica) of the original master shown in Figure 7c, which is subsequently utilized as secondary mold for further

processing (replicating). RM denotes a process in which the negative (e.g. from PEG) from the first replication step is employed as secondary mold for a subsequent replication step; replication from a "soft mold".
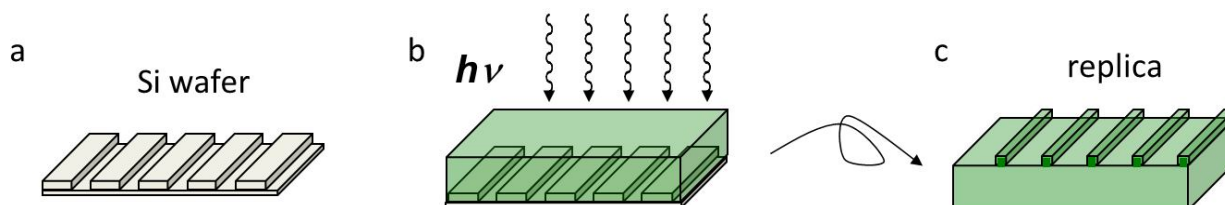
Figure 7: Processing steps of RM: (a) patterned Si wafer, serving as initial stamp; (b) polymer precursor covering Si wafer and subsequent ultraviolet radiation; (c) removing of cured patterned polymer negative (replica), which serves as secondary mold in a subsequent replication step.

With the help of RM, various kinds of surface patterns of differing magnitude such as dots, lines, squares or any given combination can be produced in great quantities (Figure 8) as reviewed in a concise manner by Roach and colleques[30]. Several polymeric formulations, such as PEG based hydrogels or Polydimethylsiloxane (PDMS) based organosilicon materials, have been vastly utilized.
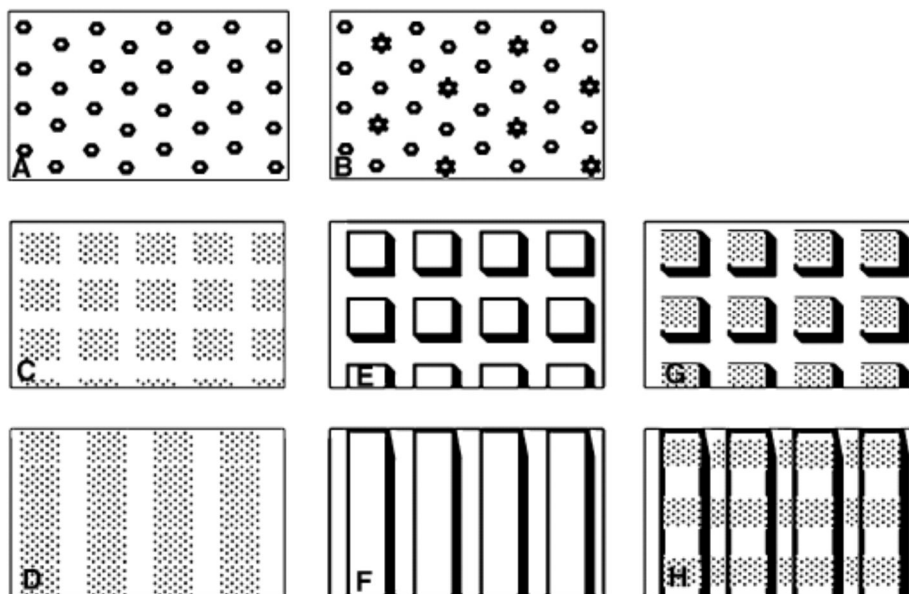
Figure 8: Surface chemical and topographic patterning examples. (a) isolated single molecule grafted pattern; (b) Isolated molecules grafted pattern; (c) island molecules pattern; (d) line molecules pattern; (e) pillar topographic pattern; (f) grooves topographic pattern; (g) and (h) mixed chemical and topographic patterns. Modified image reprinted from reference [30].

However, RM substrates may not be fabricated at any given aspect ratio. The limits of RM processing can be mainly summarized by three prevailing effects (Figure 9) as shown by Whitesides and coworkers[11]. A common problem is represented by *Pairing* (Figure 9a), that is when an aspect ratio of base and height of standout posts (lines may be just as affected) exists, which exceeds a specific material dependent value and the posts contact another. Patterns with relatively deep patterns and narrow distances between posts/lines are particlulary vulnerable to such defects. The second type of defect is called *Sagging* (Figure 9b), this is when due to the inherent weight of the applied polymer stamp mechanical integrity is lost and the stamps contacts the substrate in non-desired areas. Hence, the pattern gets lost. *Shrinking* (Figure 9c) is a very common phenomenon due to e.g. UV radiation. That is because secondary bondings such as Van der Waals bondings or hydrogen bonding are converted into covalent bonds, which

exhibit smaller binding distances and hence the bulk materials shrinks. For PEG based materials, commonly 10 vol% are stated[31].
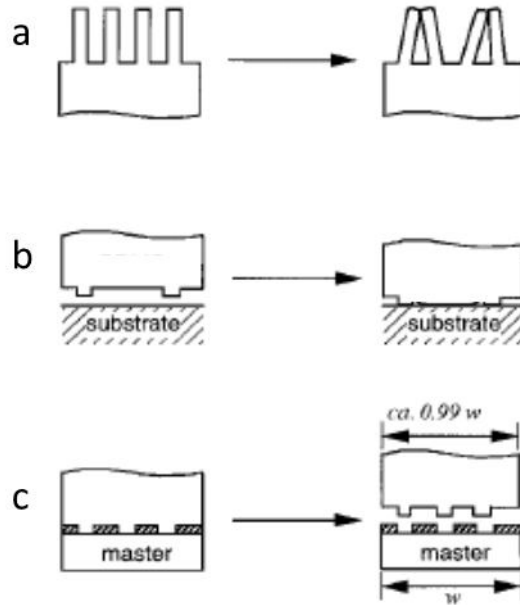
Figure 9: Schematic illustration of possible deformations and distortions of microstructures in the surfaces of polymers patterned via Replica Molding. a) Pairing; b) Sagging; c) Shrinking. Image reprinted from reference [11].

Micro-Contact Printing is considered as a very popular soft lithographic patterning method with a vast range of potential applications (Figure 10). The underlying principle of this easy and straight forward bench top method is the inking of a substrate with a stamp (e.g. PDMS stamp) during contact, a more elaborated version represents e.g. inking of liquid polymers or beads (Figure 10b) on the substrates, which may be already chemically functionalized. Patterns down to sub-micrometer dimensions have been realized as displayed by Zhou and coworkers[32].
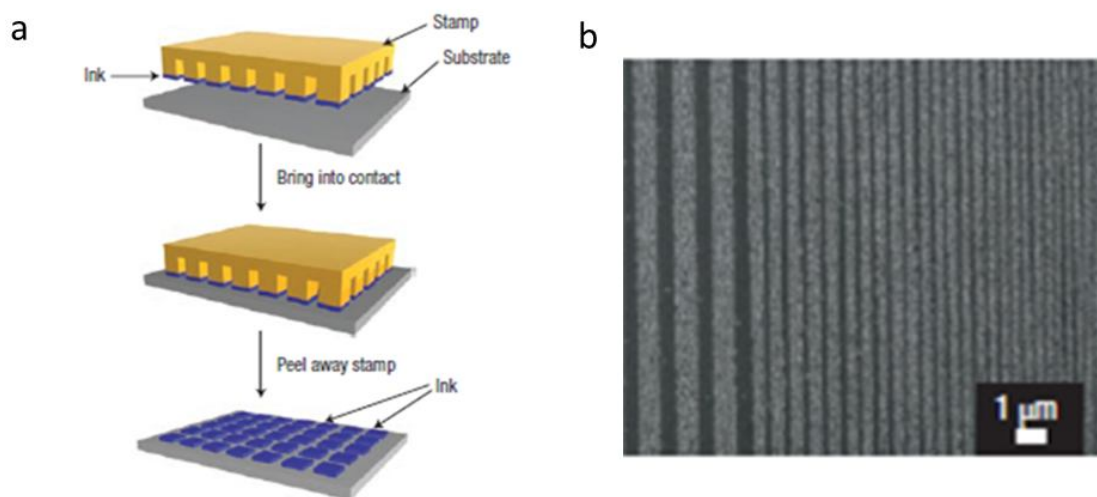
Figure 10: Micro-Contact Printing: (a) Schematic representation of polymer patterning; (b) Images of 96-nm polystyrene beads deposited on the lines of patterned polyelectrolyte complexes. Modified image reprinted from reference [32].

Another promising approach in this field is the recently developed Fillmolding In Capillaries (FIMIC) method[9] invented by the Lensen Lab, which enables the fabrication of sub micrometer-precise *Patterns of Elasticity*. Those are surface patterns, which ideally are horizontally perfectly plane in hydrated state and exhibit an alternating elasticity. In addition, the thus fabricated FIMIC platforms may incorporate chemical functionalities, which can be introduced in a spatially controlled manner. A more detailed description is found in the following chapter 2.3.

2.3 The Fillmolding In Capillaries (FIMIC) Method

Fillmolding In Capillaries was invented in the Lensen Lab and first reported by Diez et al.[9]. The main principle of this sophisticated, soft lithographic easy bench top method is to fill pre-prepared micropatterned hydrogel molds with a second elastomeric phase via capillary force. Figure 11 depicts the single steps along with the dimension-determining hydrogel mold produced via RM or simple replication from Si wafers. Figure 11a details the decisive characteristics of a hydrogel mold, in which d represents the pattern distance, w the pattern width and h the pattern height. Those dimensions may be in any given relation, but need to comply with the requirements stated in chapter 2.2 in order to refrain from defects. Figure 11b demonstrates schematically the FIMIC fabrication in 4 consecutive steps. (I) the hydrogel mold (e.g. fabricated via RM), (II) the hydrogel mold is turned upside down on a glass or Si wafer and a drop of the second liquid elastomeric phase is placed right in front of it. As a result of capillary action, the liquid precursor is driven into the channels and cured under the application of ultraviolet radiation (III). As final step, the as prepared FIMIC substrate can be released from the glass/silicon wafer and turned upside-down; in such a way that the topographically smooth, patterned surface faces upwards (IV). The resulting FIMIC is now ready for subsequent investigation/application.
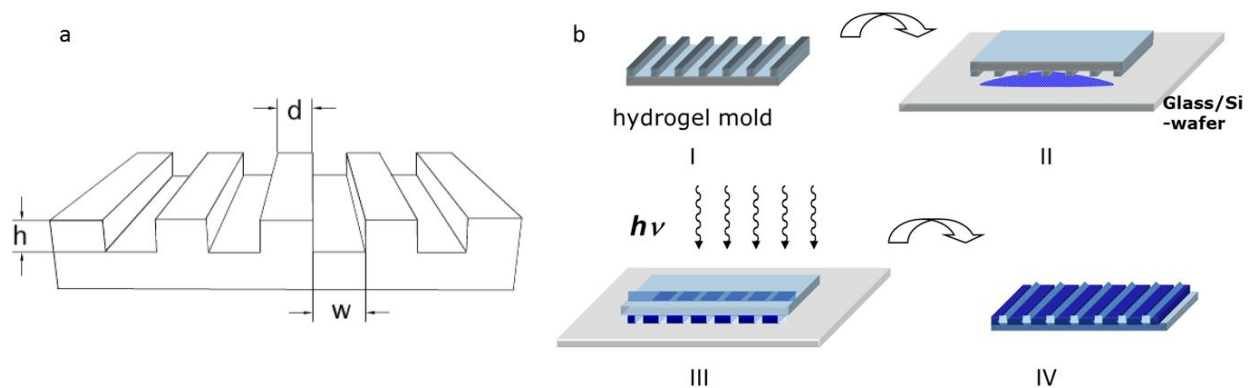
Figure 11: Processing Scheme of FIMIC substrates: (a) hydrogel mold with characteristic patterning dimensions (d- distance, w-width, h- height); (b) processing steps for FIMIC fabrication: (I) as-prepared hydrogel mold with defined distance, width and height characteristics, (II) placing of liquid polymer precursor in order to allow penetration of empty channels via capillary force, (III) ultraviolet radiation of filled lines, (IV) smooth final FIMIC substrate.

As important influential factors, surface tension at the liquid-vapor interface, capillary radius and the contact angle between substrate and liquid (measure for wetting behavior of the second phase on the hydrogel mold) were determined (Figure 12). Since all utilized hydrogel precursors showed sufficient wetting behavior, the capillary radius, and consequently the capillary force as driving force proved to be the most decisive factor for successful FIMIC substrate production. It showed that small radii yield in highly defective platforms, which result in enormous difficulties to fabricate FIMIC platforms with sub-micrometer dimensions. Hence, most platforms used throughout this thesis had dimensions of between 10 µm and 50 µm. Those are also the dimensions most relevant for cellular response investigations.

$$P_L = 2\mu \cdot \cos\theta / r$$

P_L **Laplace Pressure** (higher pressure
at the interface than in the center of a liquid drop)

μ **Surface Tension** liquid vapor interface

θ **Contact Angle** substrate-liquid

r **Capillary radius**

Figure12: Driving Force of Capillary Filling during FIMIC processing. Laplace Pressure with defining measures.

Figure 13 depicts optical and Scanning Electron Microscopy (SEM) images of successfully fabricated FIMIC platforms. The optical topview of a FIMIC platform at the end of filled channels is shown in Figure 13a, which demonstrates the ease in discriminating areas of filled grooves from unfilled ones. The cross-section recorded via SEM (Figure 13b) states the defined adjacent nature of the two applied phases and serves as an instrument to guarantee fabrication quality.
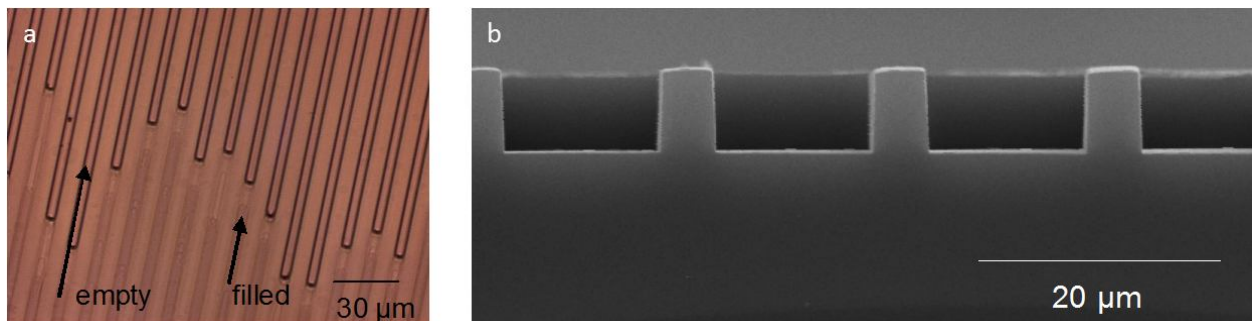
Figure 13: Depiction of FIMIC substrates: (a) optical microscopy image, topview; (b) Scanning electron microscopy image, cross-section.

Still, defects may occur, especially due to delamination in hydrated state as seen in Figure 14. The main cause for this phenomenon may be incomplete curing during UV-radiation or great differences in differential swelling behavior between the utilized hydrogel matrices. A weakness of the FIMIC concept is the missing control of chemical interaction between the hydrogel mold and the filled channels, which in particular in hydrated state becomes an issue. Then, the physical interaction (e.g. adhesive forces) between the involved phases is reduced and hydrated polymers may release from the hydrogel mold. This is less observed for materials exhibiting little swelling degree or in pattern combinations containing materials of similar hydration behavior.
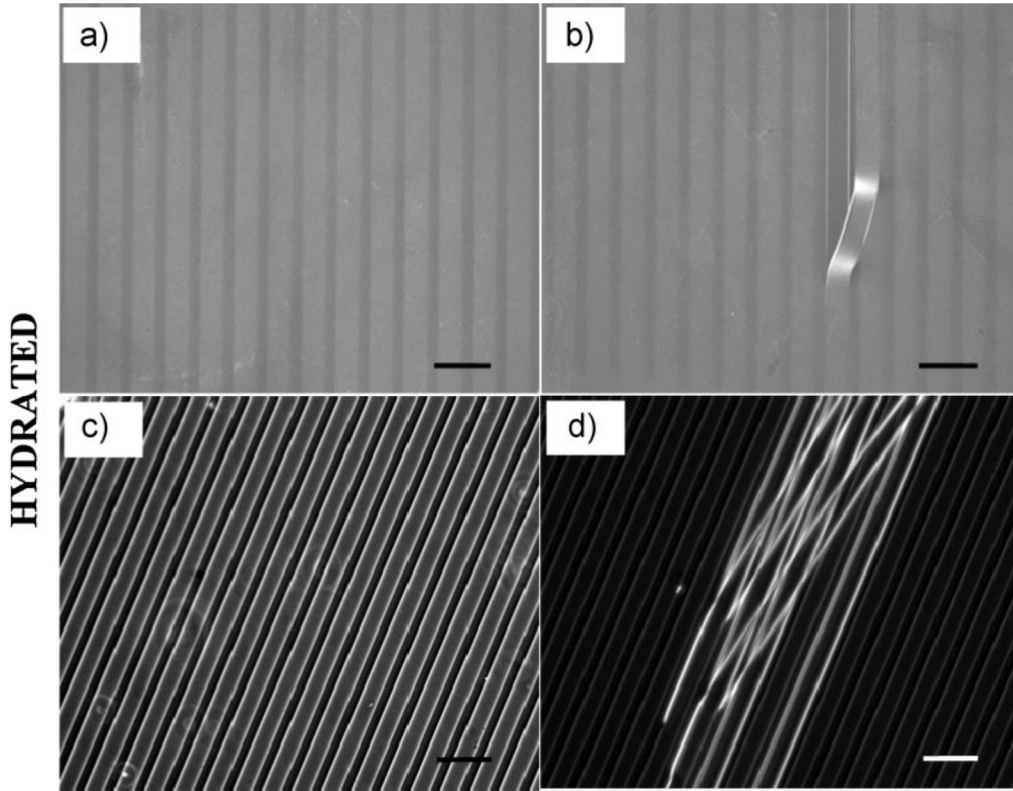
Figure 14: Hybrid hydrogel with pattern ''soft (20mm) in stiff (10mm)'' in hydrated state; (a) and (b) depict SEM images; showing one line coming loose in image (b). Light and dark gray are soft and stiff hydrogel, respectively. (c) and d) depict optical micrographs, revealing a defect area on the patterned surface in (d). Scale bars represent 50 µm. Image reprinted from reference [9].

2.4 Atomic Force Microscopy and Force Spectroscopy as Characterization Tool for Hydrogel Surface Patterns

Atomic Force Microscopy (AFM) may be readily applied for the physical and mechanical investigation of as prepared FIMIC platforms in dry or hydrated state. This versatile instrument allows for qualitative and quantitative characterization of relevant surface properties. Methods include physical measurement of topographic features as well as Force spectroscopy, which involves the determination of surface elasticities and the proof of present mechanical surface patterns, e.g. so called *Patterns of Elasticity* (Figure 15). There exist two fundamentally different techniques finding application in the investigation of the micropatterned hydrogel surfaces. First, the topographic imaging (Figure 15a), which allows physical surface characterization in dry and hydrated state. However, in particular measurements conducted in swollen state serve the purpose of the intended applications, since the main purpose of the fabricated platforms remains the investigation upon cellular response. The topographic imaging yields 2D topview image and cross-section at any given position. Thus, the real topography can be determined over an area up to 100 µm x 100 µm. Due to the size of cells of approximately 40 µm in maximum elongation, this is sufficient to scrutinize the areas, which single cells can sense. Second, Force spectroscopy records Force-distance-curves (F/d curve) (Figure 15b), which yield two main characteristics that are called adhesion and slope respectively. The information obtained includes the vertical position of the tip (thus indentation) and deflection (bending of the tip). Those two types of information are read out and converted via vertical displacement. In the next step, the two entities, slope and adhesion are derived. Adhesion represents the surface tip interaction via secondary interactions such as Van der Waals interaction, capillary action of water meniscuses, electrostatic interaction. Slope determines the resistance against elastic deformation, which represents the Young's Modulus at the investigated spot. Force spectroscopic methods are mainly applied to reveal regular mechanical patterns, which can be correlated to the respective topography (Figure 15b). Those measurements on the one hand may result in quantitative elastic analysis (F/d curve) of any chosen single surface spot, which represents the surface tip interaction at the very end of the AFM tip. On the other hand can

Force Mapping experiments be conducted for the areas of interest via gridwise visualization of recorded data points resulting in so-called *Force maps*. Precision is adjusted by the number of recorded single F/d curves regarding a specific investigation site.

Atomic Force Microscopy employed in FIMIC Characterization

a **Topographic - imaging**

Scheme of topographical imaging over FIMIC

Real topographic 2D image of a FIMIC

According real cross-section of the FIMIC

b **Force - spectroscopy**

Quantitative determination of surface elasticity

Real Force/Distance - Curve (F/d curve)

Force Mapping

Qualtitative comparison of surface elasticity (slope) and interaction tip-surface (adhesion)

Real Force-map of a FIMIC

Figure 15: Atomic Force Microscopy in FIMIC characterization: (a) topographical imaging, detailing scheme, 2D height imaging and according cross-section; (b) Force spectroscopy, detailing quantitative determination of elasticity and force mapping.

In order to better comprehend the potentials of AFM recording detailed interaction between AFM cantilever and investigated surface is depicted in Figure 16, as concisely displayed by

Shahin et al.[33]. During the recording process of one single F/d curve, the following steps of interaction are experienced by the cantilever and are exploited for the mechanical surface characterization: Point *A* defines the tip-surface interaction during the approach modus before any interaction takes place. The cantilever is not bent and no contact between tip and surface is yet observed. In point *B*, the tip jumps to the surface, due to secondary tip surface interaction. Now, the tip is in contact with the surface, but the cantilever is not yet bent, since no surface deformation has yet taken place. In state *C*, the AFM tip tries, resulting from applied pressure, to penetrate the sample surface. The samples shows resistance towards elastic deformation (Young's Modulus, defined as the slope of F/d curve during *C* or *D*), the cantilever is bent in a concave fashion. The tip deforms the substrate according to the adjusted pressure or distance and retracts as soon as the pre-set value is reached. During the retraction modus, the stress imposed on the sample is relieved and at point *D* the tip intends to separate from the sample surface. However, due to secondary interaction in state *E*, the tip is held at the surface and the cantilever bends in a convex fashion in order to retrieve the tip (adhesion force). Finally, the cantilever retracts further and can break away as adhesion forces are overcome.
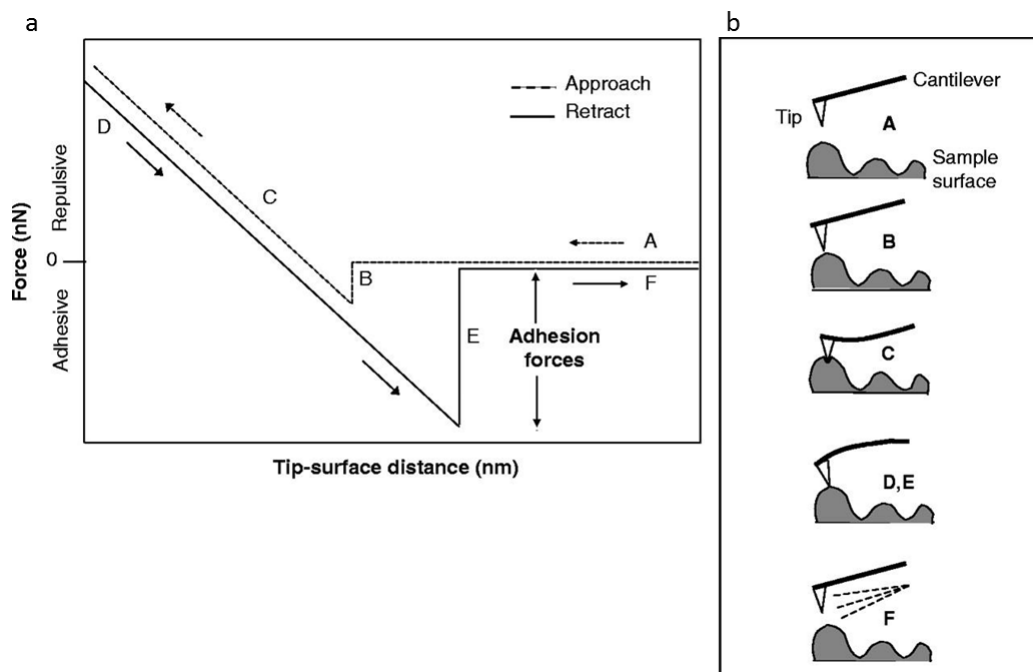
Figure 16: Details of Force Distance Curves (a) schematic approach and retract modus of an AFM tip on investigated surface; (b) according AFM cantilever bending due to experienced interaction with the surface during approach and retract modus. Image reprinted from reference [33].

Topographic imaging of hydrogel surfaces in hydrated state yield the challenge to determine the exact liquid-solid interface of sample and surrounding liquid due to the soft nature of the matter in hydrated state. This was further complicated, since regular surface patterns of low nanometer dimensions were to be revealed. Nevertheless, the feasibility of our approach to physically characterize patterned hydrogel surface in hydrated state was demonstrated by the detection of horizontal regular structures down to below 50 nm. Those measurements could be subsequently correlated with according *Force maps* from force spectroscopic investigations. Hence, topographic and mechanical AFM characterization of as prepared hydrogel surfaces proved to be vital and the instrument served as crucial investigation tool for the herein presented PhD project.

Chapter 3

Materials and Methods

3.1 Materials:

Any polymer utilized in this thesis was synthesized and processed by Zhenfang Zhang, a fellow PhD student of the Lensen Lab.

3.1.1 Poly(ethylene glycol) (PEG) diacrylate (DA):

PEG DA (Sigma Aldrich, M_w 575 Da) is mixed with various amounts of crosslinker (Pentaerythritol triacrylate, tech, Sigma Aldrich, M_w 298, 3 Da; 1 %, 5 % and 10 %) and one percent of photoinitiator (2-hydroxy-4'-(2hydroxy-ethoxy)-2 methyl-propiophenone, 98 %; Sigma Aldrich, M_w 224.26 Da) (PI) and subsequently UV cured under the exclusion of Oxygen.

3.1.2 PEG-based triblock copolymer of poly(propylene) glycol (PPG) and PEG,PEG-b-PPG-b-PEG (3BC):
See details in the PhD thesis of Zhenfang Zhang[2].

3.1.3 Polymer blends fabrication:
The gel networks were formed via ultraviolet (UV) radiation of an acrylated polymer in the presence of a photinitiator (PI) (Irgacure 2959) and pentaerythritol triacrylate (PETA) as a crosslinker (CL). In order to fabricate varying stiffness, pre-curing mixtures were prepared by mixing acrylate terminated **PEG** or **3BC** in a small amount of acetone with varying amounts of CL (0 - 10 wt%) and 1 % PI (with respect to the amount of polymer).

3.1.4 Hydroxyapatite nanoparticles (HAp NPs):

Hydroxyapatite nanoparticles (HAp NPs) were synthesized applying the precipitation method. Synthesis time and temperature, the two key factors, were adjusted to assure stable synthesis conditions and to control the properties of HAp. Calcium nitrate tetra hydrate ($Ca(NO_3)_2 \cdot 4H_2O$, Carl Roth GmbH & Co. KG) and diammonium hydrogen phosphate ((NH_4)HPO_4, Carl Roth GmbH & Co. KG) were used as starting materials. Ammonium hydroxide ((NH_4)OH) was used to adjust the desired pH value. 5.96 g of $Ca(NO_3)_2 \cdot 4H_2O$ were given into 200 mL distilled water and stirred thoroughly until all $Ca(NO_3)_2 \cdot 4H_2O$ was dissolved. A second solution was prepared by adding 1.92 g (NH_4)HPO_4 to 200 mL of distilled water. Both solutions were given simultaneously into a glass reaction vessel. Subsequent addition of 10 mL 33 % (NH_4)OH solution to adjust the pH of the resulting suspension to 10. The precipitation time was chosen to be 48 h, additionally 10 mL of 33 % (NH_4)OH solution were added after 24 h due to potential evaporation of Ammonium hydroxide. The precipitation reaction was performed at room temperature (22 °C). A constant temperature and magnetic stirring were maintained during the whole reaction time. During maturation the cover of the glass vessel was lifted several times to allow atmospheric exchange. After that, the suspension was quickly filtered and washed with sufficient distilled water until all (NH_4)OH was removed. The resulting cake was dried at 75 °C for at least 24 h and grinded to a homogeneous powder using a ball mill grinding jar.

3.1.5 PEG nHAp hydrogel composite synthesis:

PEG nHAp hydrogel composites made of PEG_{575} and HAp were fabricated as shown in Figure 1 in chapter 4.3.1. As prepared salt solutions of Calciumnitrate tetrahydrate ($Ca(NO_3)_2 \cdot 4H_2O$ analytical grade from Sigma Aldrich) and Diammonium hydrogen phosphate ((NH_4)$_2HPO_4$ analytical grade from Sigma Aldrich) were added to the precursor solution of PEG_{575} complemented with 1 % PI at room temperature under vigorous magnetic stirring. Maturation time was held constant at 24 h. Compositions were set in order to obtain 10 wt%, 20 wt% and 40 wt% PEG nHAp composites by weight (PEG 10nHAp, PEG 20nHAp and PEG 40nHAp

respectively). The resulting suspensions were thoroughly washed with distilled water and the resulting suspension was transferred to a glass flask for further processing.

The following synthesis steps were performed. Salt solutions containing $Ca(NO_3)_2 \cdot 4H_2O$ and $(NH_4)_2HPO_4$ respectively were added to acrylated PEG_{575} precursor in the reaction vessel. The resulting homogeneous suspension was kept at 22 °C under constant vigorous magnetic stirring for 24 h in order to allow for HAp nucleation. After a maturation-time of 24 h the suspension was filtered to remove all residual water and the viscous composite gel was transferred to a glass flask for further processing. Due to the incorporation of photo-initiator, UV curing was enabled and thus application in softlithography. In addition, the cured composite gels proved to be transparent and fluidic enough to be easily processed within the soft lithographic regime.

3.1.6 PEG HAp NPs hydrogel composite synthesis:

As prepared HAp NPs (synthesis see chapter 3.1.4) were given into the PEG_{575} precursor solution and homogenized to result in composite hydrogels containing 20 % NPs by weight (20 wt%). In order to achieve best distribution and least agglomeration behavior of the resulting PEG HAp NPs hydrogel composite, the composite precursor solutions were exposed extensively to vortexing and subsequent ultrasonic treatment prior to application.

3.1.7 8arm PEG:

8arm PEG-OH with a molecular weight of 15 KDa was purchased from Jenkem technology USA.

Acrylation-procedure:
For more details, see PhD thesis of Zhenfang Zhang[2].

The product we use is 8arm PEG-acrylate. After acrylation, the molecular weight is still around 15 KDa, because the acrylation group is quite small compared with 8arm PEG.

3.1.8 8arm PEG HAp Composite (8PEG HAp) Synthesis:

Composites made of 8arm PEG and HAp were fabricated as shown in Figure 2 in chapter 4.4.1. As prepared salt solutions of $Ca(NO_3)_2$ and $(NH_4)_2HPO_4$ were added to the precursor solution of 8arm PEG complemented with 1 % PI at room-temperature under vigorous magnetic stirring. Maturation-time was held constant at 24 h. Compositions were varied in order to receive 10 %, 20 %, and 40 % HAp – 8arm PEG composites by weight (8PEG 10HAp, 8PEG 20HAp and 8PEG 40HAp, respectively).

3.1.9 8arm PEG Composite Scaffold Synthesis:

The freeze drying process was conducted at 0.0019 mbar and -84 °C for 48 h (Alpha 2-4 L D plus, Christ). Samples were prepared as follows. First the salt solutions containing $Ca(NO_3)_2$ and $(NH_4)_2HPO_4$ were given simultaneously into a glass reaction vessel in the presence of the according amount of 8arm PEG. The precipitation reaction was performed over 24 h, after which a homogeneous gel was attained. The obtained gel was swollen different times (5, 15, 45 min) in deionized water and subsequently UV cured (wavelength of lamp 365 nm) in hydrated state over 15 min. Afterwards, the samples were frozen at -20 °C in a freezer.

3.1.10 Preparation of Simulated Body Fluid (SBF):

SBF solution was prepared as stated in detail by Müller and co-workers[34]. In summary, SBF solution with a HCO_3 content of 5 mmol/l was prepared by pipetting calculated amounts of concentrated solutions of KCl (59.64 g/l), NaCl(116.88 g/l), $NaHCO_3$ (45.37 g/l), $MgSO_4{\cdot}7H_2O$ (49.30 g/l), $CaCl_2$, TRIS(tris-hydroxymethyl aminomethane; 121.16 g/l), NaN_3(100 g/l) and KH_2PO_4 (27.22 g/l) into doubly distilled water. Concentrated salt solutions were added into a 1000 ml flask and filled up with double distilled H_2O. The 121.16 g of TRIS was dissolved in 650 ml double distilled H_2O. During stirring, the pH was adjusted to 7.6–7.7 at 25 °C, which is equal to a pH of 7.3–7.4 at 37 °C, by adding concentrated HCl. The clear solution of TRIS and HCl was quantitatively transfused into a 1000 ml flask and filled up with double distilled H_2O. All salt solutions were stored in polyethylene (PE) bottles in a refrigerator at a temperature of 4 °C. The

solutions were pipetted into 700 ml double distilled water in the sequence KCl, NaCl, NaHCO$_3$, MgSO$_4$·7H$_2$O, CaCl$_2$, (TRIS + HCl), NaN$_3$ and KH$_2$PO$_4$ to prevent precipitation. The pH of human blood plasma ranges from 7.3 to 7.4 at 37 °C. Since the pH of SBF depends on temperature the pH of SBF prepared at room temperature (21 °C) has to be adjusted between 7.75 and 7.85 in order to obtain 7.3 and 7.4 at 37 °C. The NaN$_3$ addition was conducted in order to inhibit the growth of bacteria.

3.2 Methods:

3.2.1 Soft lithographic methods:

3.2.1.1 Fabrication of micropatterned PEG$_{575}$ composite replicas:

Micro-patterned silicon wafers were rinsed with acetone, water and isopropanol and dried under a mild stream of nitrogen before use. Prior to the replication, the cleaned silicon masters were fluorinated with trichloro(1H,1H,2H,2H-perfluorooctyl)silane 97% (Sigma-Aldrich). The selected PEG$_{575}$ or PEG$_{575}$ composite pre-curing mixtures were dispensed on the silicon master, covered with a thin glass coverslip and exposed to UV light (340 nm) for 15 minutes. Following curing, the transparent polymeric film, with an inverse relief to that on the silicon master, was peeled off mechanically. The stand-alone film (250 – 300 μm in thickness) could be handled with tweezers.

3.2.1.2 Fabrication of Fillmolding In Capillaries (FIMIC) substrates:

More detailed description of the process is stated elsewhere[9], briefly: the PEG$_{575}$ replicas were placed upside down on a glass slide and a small amount of a second liquid prepolymer-composite (PEG nHAp or PEG HAp NPs) were carefully dispensed at the edge of the open channels. Si masters with e.g. 20 μm grooves, 10 μm wide ridges and 10 μm deep structures were applied for initial replica molding of elastomers. Subsequently, the viscous mixture was allowed to fill the capillaries for 1 minute, after which the assembly was exposed to UV radiation for 20 minutes. After exposure time was complete, the hybrid construct was easily mechanically detached from the glass substrate and turned upside down to proceed with surface characterization (AFM), protein adsorption experiments and cell culture. The resultant polymer/polymer-composite FIMIC platforms were robust, free standing and transparent.

3.2.2 Characterization

3.2.2.1 Mechanical Characterization:

Rheological Measurements:

Rheology measurements were conducted using a Gemini 200 HR (Malvern Instruments) by determining the appropriate frequency and vertical force on the sample (strain-controlled mode). An 8 mm plate was used and measurements were taken at room temperature. Samples were swollen min. 12 h prior to measurement. During the recording of data of swollen samples were kept in a solvent trap to avoid loss of water during the experimental run. First, the linear elastic range of the samples was determined with the help of the amplitude sweep. This is observed, when Storage Modulus (G′) (indicating the elastic property of the network) and the Loss Modulus (G″) (indicating viscous properties of the fluid) are yielding a constant plateau) run over a certain frequency range in a horizontal and parallel fashion to each other. The value was transferred to the frequency sweep, where the suitable values were ascertained within a range of 0.01 to 10 Hz. 1 Hz as applied frequency and 0.0001 – 0.01 as deformation value (γ) were chosen as appropriate parameters for all measured samples. The value of the observed plateau was recorded and the bulk elasticity was calculated by the following equation as described by Flory[35],

$$E = 3\,G'\hspace{4cm}(1)$$

where E is the Young's Modulus and G′ is the Storage Modulus. Each material composition was measured at least 3 times.

Tensile Test:

Tensile testing (Universal Testing Device, Zwick) was conducted in order to ascertain Young's Modulus (E), Yield Strength (σ_y), Ultimate Tensile Strength (σ_{max}), and Elongation at Break (ε) of the UV-cured composite hydrogels in hydrated state. Prior to measurements, dog-bone shaped samples were immersed in deionized water for at least 12 h at 23 °C. For each set of hydrogel

composites 5 samples were prepared. Measurements were carried out at 1 mm/min deformation velocity with a set-off of 2 N.

Compression Test:

Uniaxial Compression testing (Universal Testing Device, Zwick) was conducted in order to ascertain Young's Modulus (E), Compression Yield Point (σ_{df}), Ultimate Compressive Strength (σ_{db}) and Compression strain at Break (ε) of the UV-cured composite hydrogel scaffolds in hydrated state. Prior to measurements, cylindrical samples were immersed in deionized water for at least 12 h at 23 °C. For each set of composites 5 samples were prepared. Measurements were carried out at 1 mm/min deformation velocity with a set-off of 2 N.

3.2.2.2 Spectroscopic Methods:

RAMAN Spectroscopy:

Surface Resonance RAMAN Spectroscopy (LABRAM, HR Horiba Scientific) was conducted with an excitation wavelength of 514 nm. Spectra of the as prepared samples were recorded between 500 cm^{-1} and 1300 cm^{-1}.

ATR Fourier Transformed Infrared Spectroscopy (ATR FtIR):

ATR FtIR measurements were conducted (Bruker Optics GmbH Equinox 55 with ATR golden gate unit head) in order to qualitatively examine the presence of characteristic functional groups of HAp formation in the range of 450 cm^{-1} to 4000 cm^{-1} within the composite materials and pure HAp. The samples were vacuum-dried for 24 h prior to investigation.

3.2.2.3 X-ray diffraction (XRD):

XRD was conducted applying a powder-diffractometer (X'Pert Pro, PANalytical) in the range of 5 to 80 ° 2 theta. Samples were vacuum-dried at room temperature and grinded into powder prior to measurement. The X-ray generator was operated at a voltage of 40 kV and 40 mA producing Cu$K\alpha$ radiation with a wavelength λ of 0.154 nm. A scanning speed of 2300 s degree^{-1} was applied for measuring each sample.

3.2.2.4 Microscopy:

Atomic Force Microscopy (AFM):
An Atomic Force Microscope (JPK instruments, Nanowizard II) was used in order to measure the topography and surface elasticity of samples in dry and hydrated state.

Topographical Imaging:
Imaging was done in intermittent contact (hydrated samples) and contact mode (dry samples) using silicon nitride cantilevers (PNP TR, k ≈ 0.08 N/m, f_0 ≈ 17 kHz; Nanoworld Innovative technologies) with a chromium-gold coating. Images were edited with NanoWizard IP Version 3.3a (JPK instruments). Samples measured in hydrated state were immersed for at least 12 h in deionized water prior to measuring.

Force-Spectroscopy:
Force Mapping was conducted via qualitative comparing of surface elasticity using a set of Force-distance curves (F/d curves) on the same scanning probe microscope (JPK instruments, Nanowizard II). After every set of measurements, the cantilever was newly calibrated (by applying the thermal-noise-method) before starting with the next set of force-distance measurements. This value was then taken as surface elasticity. Silicon nitride cantilevers (PNP-TR) with a chromium-gold coating (k ≈ 0.08 N/m, f_0 ≈ 17 kHz; Nanoworld Innovative technologies) were used. Images were edited with NanoWizard IP Version 3.3a (JPK instruments). PNP TR tips (NanoWorld) exhibit a pyramidal tip-shape (face angle 35°), the tip-

geometry has been taken into account by applying the Bilodeau formula[36] in order to fit force distance curves. The fitting is implemented in the Nanowizard IP software and resulting values for the E-Modulus are accordingly obtained.

Optical microscopy:

Light microscopy images were taken with an inverted Axiovert 100A Imaging microscope (Carl Zeiss, Goettingen, Germany) using an AxioCam MRm digital camera and analyzed using the AxioVisionV4.8.1 software package (Carl Zeiss, Goettingen, Germany).

Electron microscopy:

Scanning electron microscopy (SEM) was performed to visualize resulting patterns as well as an in-situ electron _Energy dispersive x-ray spectroscopy (EDX)_ in order to identify elemental composition (in particular Ca/P ratios) and Elemental Mapping in defined areas of the respective each sample. Prior to image recording, samples were carbon-coated and an acceleration voltage of 8 keV was applied yielding EDX spectra at a penetration depth of approximately 2.0 µm.

Transmission electron microscopy (TEM)(TECNAI $G^2$20) was used to identify and quantify the crystalline character of the respective PEG based PEG-HAp composites. In order to analyze elemental constitution in-situ _EDX_ was utilized. Prior to measurements samples were frozen in LN2 and subsequently grinded with the help of a little ethanol. Following this, a copper net was introduced and shortly after removed. As final step, the suspension on the copper net was left to dry under ambient conditions. The instrument was operated at 200 keV acceleration voltages with a LaB6-cathode and 0.24 nm point-resolution. TEM measurements were conducted by Dipl. Ing. Sören Selve of the ZELMI, the Central Institution of Electron Microscopy of the Technical University of Berlin.

Confocal Laser Scanning Microscopy (CLSM):

Confocal Laser Scanning Microscopy was conducted with the help and under supervision of Gonzalo de Vicente Lucas, a fellow PhD student of the Lensen Lab.

Confocal and 3D images were recorded using a Leica TCS SP5 II Confocal Microscope (Leica, Wetzlar, Germany) with a 20x and a water immersion objective 63x. The excitation wavelength used was 496 nm and the detector was set in the range of 501 nm - 666 nm for BSA-FITC. The applied scan speed was 10 Hz for images and 100 Hz for 3D series. Images were analysed and processed utilizing the program Bioimage XD (Free software).

3.2.3 Cell Culture:

Cell culture experiments were conducted by Christine Strehmel, a fellow PhD student in the LensenLab.

Mouse connective tissue fibroblasts (L-929) were kindly provided by Dr. J. Lehmann (Fraunhofer Institute for Cell Therapy and Immunology IZI, Leipzig). L-929 cells were cultured in RPMI 1640 containing 10 % Fetal Bovine Serum (FBS) and 1 % Penicillin/ Streptomycin (PS; all PAA Laboratories GmbH) at 37 °C and 5 % CO_2 in a humidified incubator. The cells were grown in 75 cm^2 cell culture flasks (SPL Life Sciences Inc.) until confluence, washed with Dulbecco's Phosphate Buffered Saline solution (DPBS, PAA Laboratories GmbH) and treated with Trypsin-EDTA (PAA Laboratories GmbH).

MC3T3-E1 osteoblast like cells (further denoted as osteoblasts), originally derived from mouse calvaria, were kindly provided by Prof. Z. Su (Beijing University of Chemical Technology, China). MC3T3- cells were grown in 75 cm^2 cell culture flasks containing Minimum Essential Medium (Sigma- Aldrich) supplemented with 10 % FBS and 1 % PS at 37 °C and 5 % CO_2 in a humidified incubator. The cells were grown until confluence, washed with DPBS and treated with Trypsin-EDTA.

3.2.3.1 Cell viability:

Murine fibroblast viability on smooth PEG and PEG-HAp substrates was studied using a live-dead assay. For this purpose, PEG and PEG-HAp substrates (1 cm x 1 cm) were washed with ethanol (70 %), rinsed in DPBS and placed in a µ-slide (Ibidi GmbH). 300 µl of a cell suspension containing 50.000 L-929 cells were seeded onto each substrate and incubated at 37 °C, 5 % CO2 atmosphere and 100 % humidity. The viability of cells on the distinct substrates was estimated after a 24 h incubation period. Following incubation, cells were stained with 100 µl of a vitality staining solution containing fluorescein diacetate (stock solution 0.5 mg/ml in acetone, Sigma-Aldrich) and propidium iodide (stock solution 0.5 mg/ml in DPBS, Fluka). Viable and dead cells were detected by fluorescence microscopy.

3.2.3.2 Cell Morphology:

Samples were washed with ethanol (70 %), rinsed in DPBS and were placed in 24 well-plates (Becton Dickinson). 50.000 cells/ ml were seeded on top of the samples and incubated for 24 h at 37 °C, 5 % CO_2 and 100% humidity. After 24 h, the cells were washed with DPBS to remove unattached cells as well as remaining medium components and fixed for 30 min with 4 % formaldehyde, pH 7 (Carl Roth GmbH). Prior to the observation of the cells with a scanning electron microscope (SEM, Hitachi S-520), samples were dehydrated in a graded acetone series. Finally, the samples were dried with critical point drying (CPD 030, Baltec), sputtered with gold using a sputter coater (SCD 030, Balzers) and observed with a SEM using an acceleration voltage of 20 kV and a working distance of 10 mm.

Chapter 4

Results and Discussion

The main findings of the thesis are presented and discussed in this chapter. The four subchapters each address a distinct topic, but are not to be considered separately, since the consecutive order imparts better project-understanding. Thus, the reader may follow the main research objectives with greater ease, since the several chapters describe various applied patterning techniques with growing materials complexity and augmenting method sophistication. The reader should in particular note that the chapters 4.1, 4.2 and 4.3 all comprise the soft lithographic surface patterning technique Fillmolding In Capillaries (FIMIC). Therefore, the consecutive order of the chapters starts with the general introduction and characterization of the FIMIC method in chapter 4.1 and concludes with the illustrating the vast patterning potential, namely by incorporation of novel composite materials and subsequent cellular experiments in chapter 4.3. Additionally, this thesis does not restrict to a single patterning method, but involves surface patterning techniques (e.g. FIMIC) in chapters 4.1 – 4.3 as well as controlled formation of 3D structures for potential tissue engineering application in Chapter 4.4.

Each subchapter represents a different publication manuscript stated in the respective front page. To the chapters 4.1 and 4.2, the author contributed patterning processing as well as surface and bulk characterization of the relevant substrates. Materials formation and cell studies were conducted by colleagues of the Lensen Lab. To chapter 4.3 and chapter 4.4, the author contributed, as author, to all relevant data presented and discussed except cell studies, which were conducted in collaboration with Lensen Lab group members.

Chapter 4.1 addresses the fabrication of FIMIC platform with different kinds of Poly(ethylene glycol) (PEG) based hydrogels and scrutinizes the feasibility of physical and mechanical surface characterization via AFM topographic imaging and Force spectroscopy, respectively. This results in so called *Patterns of Elasticity*, hydrogel surfaces which exhibit alternating stiffness in the

micrometer range. In addition, FIMIC substrate investigation is not only restricted to dry state, but extends to hydrated state revealing the necessity of considering differential swelling of hydrogels into the FIMIC design.

Chapter 4.2 addresses the issue of differential swelling, employing several PEG based polymer blends with different hydration properties in order to equilibrate the physical surface characteristics of the FIMIC platforms in completely hydrated state.

Chapter 4.3 addresses the application of different kinds of PEG hydroxyapatite (HAp) hydrogel composites, namely PEG HAp NPs and PEG nHAp into the FIMIC processing. PEG HAp NPs consists of PEG and 20 wt% of physically incorporated HAp NPs. PEG nHAp in contrast features chemically synthesized PEG HAp hydrogel composite by in-situ nucleation of HAp in the PEG precursor matrix. These materials were processed in a spatially controlled manner into FIMIC substrates and the resulting chemically and mechanically micropatterned platforms were investigated and compared upon post fabrication functionality with HAp from Simulated Body Fluid (SBF), protein adsorption ability of the model protein Bovine Serum Albumin (BSA) and cellular adhesion behavior of fibroblasts (L-929) and osteoblast like cells (MC3T3-E1). This is the concluding chapter to the FIMIC processing with varying PEG based hydrogels.

Chapter 4.4 addresses the scaffold formation of 8armPEG HAp nanocomposite (8PEG HAp) via freeze-drying technique. The composite scaffolds are characterized regarding chemistry, morphology, mechanical performance, protein adsorption ability of the model protein Bovine Serum Albumin (BSA) and cellular response comparing adhesion behavior of fibroblasts (L-929) and osteoblast like cells (MC3T3-E1) on as-prepared scaffolds. The determination of morphological properties was conducted in cooperation with the group of Prof. Dr. Christian Rüssel from the Otto Schott Institute of the Friedrich-Schiller University of Jena, Germany. Additional cellular experiments were conducted in collaboration with the group Prof. Su of the Department of Materials and Engineering of the Beijing Chemistry and Technology University, Beijing, China.

Chapter 4.1

AFM Characterisation of Elastically Micropatterned Surfaces Fabricated by Fillmolding In Capillaries (FIMIC) and Investigation of the Topographic Influence on Cell Adhesion to the Patterns

Abstract

The recently developed soft lithographic method Fillmolding In Capillaries (FIMIC) was utilised in order to fabricate micropatterned substrates of Poly(ethylene glycol) (PEG) derived hydrogels with varying elasticities, so called *Patterns of Elasticity*. Surface characteristics were scrutinized via Atomic Force Microscopy regarding surface roughness and surface elasticity. Topographic imaging demonstrated generally smooth surfaces; however the physical profile is greatly impacted, when applying materials exhibiting different degrees of volume change during hydration. Thus, it is displayed how the topographic landscape of the hydrogels substrates is defined by the swelling behaviour of the constituents.

This chapter contains results from the following journal publication:

Results and Discussion

4.1.1 Materials Characterisation

As initial step, the non-cytotoxic characteristics of all polymer gels prepared from PEG and 3BC were verified utilizing a colony forming ability assay. As expected no cytotoxic effect was observed (for details, see thesis of Christine Strehmel[3]).

Subsequently, the physical and mechanical properties of the employed hydrogels were investigated. Fabricating FIMIC samples (details in chapter 2.3) with different surface and hydration properties requires the use of tailormade prepolymers. Physical properties of crosslinked Poly(ethylene glycol) (PEG) hydrogels may be tuned and adjusted by varying degrees of crosslinker (CL) and photoinitiator (PI) of the polymer precursor mixture. Throughout the processing, the amount of PI was kept constant at 1 wt%, while the notation of the specific hydrogel formulation states the amount of CL incorporated e.g. "PEG 5%" represents a mixture of PEG (Figure 1a) with 1 wt% PI and 5 wt% CL. Both, the elastic and the hydration properties of the applied hydrogels were ascertained, since these characteristics are of crucial relevance with respect to the eventual physical nature of the FIMIC platforms. That is, because *Patterns of Elasticity* (patterns with adjacent areas exhibiting different elasticities) are manufactured, of which hydration softens the mechanical properties of employed hydrogels. Figure 1 outlines and compares the aforementioned properties for the hydrogel networks. These measurements have been conducted in dry and hydrated state in order to scrutinize the hydrogels in as prepared state as well as in aqueous medium, since the latter would become essential during cell testing.

The ability of hydrogels to take up water is dependent on the network structure, the degree of crosslinking and the hydrophilicity. Since hydrogel compositions are prepared from neat liquid precursors, they are tightly chemically crosslinked and do not swell to the extent as if they had been cured in a hydrated state (not necessarily equilibrium state). Figure 1c shows the water uptake of the hydrogels after 24 h in deionised water. For hydrogels with higher amounts of CL, the degree of the crosslinking increases and consequently the network is more tightly linked. Therefore, the amount of water that the system can take up into the system decreases. On the

other hand, despite any lower crosslinking density, 3BC gels have a lower swelling ratio than PEG due to the variance in chemical structure. Hence, 3BC exhibits significantly less hydrophilic behaviour than pure PEG.

	PEG 0%	PEG 5%	PEG 10%	3BC 0%	3BC 5%	3BC 10%
Swelling degree (24 hr)	28.3±0.47	22.7±1.06	18.1±0.87	6.22±0.27	5.61±0.49	4.25 ± 0.23
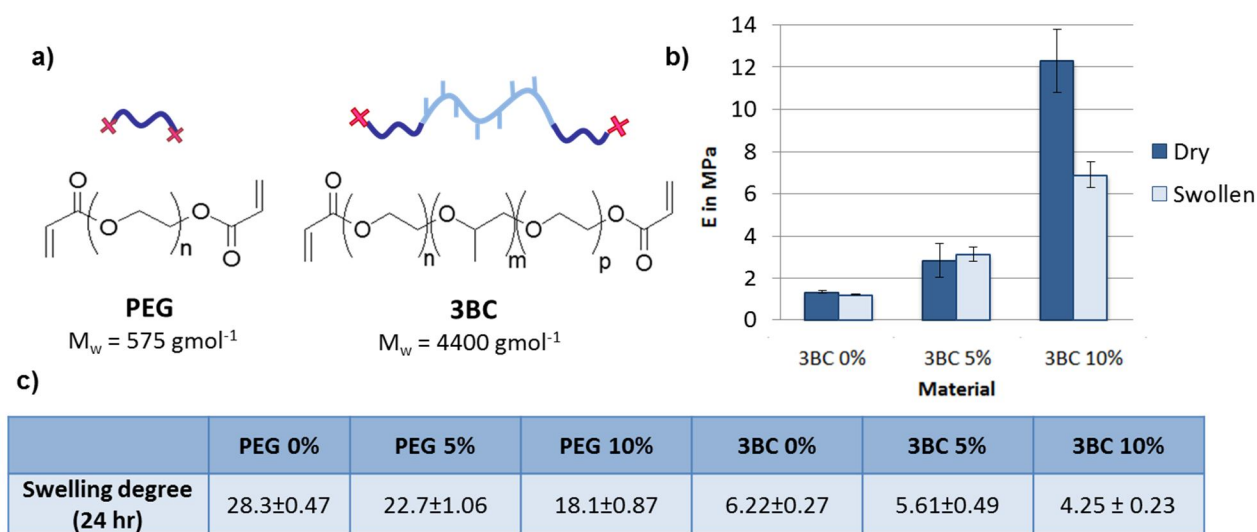
Figure 1: Chemical structures and some physical properties of the PEG-based gels: a) structure of the two pre-polymer diacrylates PEG and 3BC; b) bulk elasticity of the 3BC materials in dry and hydrated states; c) the swelling degree of the crosslinked hydrogels.

The degree of crosslinking also determines the elasticity of chemically crosslinked hydrogels in that less tightly bound hydrogels exhibit smaller Young's Moduli than those with a higher crosslinking density. Additionally, for linear polymer systems, the mechanical properties are impacted by the molecular weight (M_w) in the sense that the smaller M_w the higher the elasticity. Hence, it was expected that 3BC (higher M_w) displays lower elasticity than PEG (lower M_w). The values for the bulk elasticity of 3BC as calculated by rheological measurements are shown in Figure 1b. Unfortunately, the values for PEG could not be ascertained, as prepared PEG was too stiff for the experimental setup.

4.1.2 Microscopic Investigations of the FIMIC Platforms

The surface of the FIMIC substrates can be examined using optical microscopy in order to verify the successful processing or reveal potential defects. Sometimes, the formation of scum layers could be observed, which occurs when the pre-polymer does not only fill the designated FIMIC channels, but also covers residual areas of the replica, creating a layer of polymer across the replica.

Figure 2a depicts the top-view recorded via optical microscopy of a successfully fabricated FIMIC platform and Figure 2b shows a FIMIC substrate with a connected forward line of the meniscus indicating the presence of a scum layer. To gauge the thickness of any scum layer, real cross sections were recorded. Figure 2c shows a cross section of an as prepared FIMIC platform exhibiting a scum layer with approximately 1 µm in dimension. However, optical microscopy may not be the most suitable technique to quantify, due to limited accuracy reading the results and sample placing problems. For that reason, and to ensure that the liquid polymer had actually entirely filled into the corners of the channels, cross section images of FIMIC samples were recorded via Scanning Electron Microscopy (SEM). Figure 2d depicts an SEM image, which verifies that the channels have filled completely. FIMICs were made from a replica with [w-s-d] [50-10-10], whereas w represents groove width, s – spacing between grooves and d-depth (see chapter 2.3).
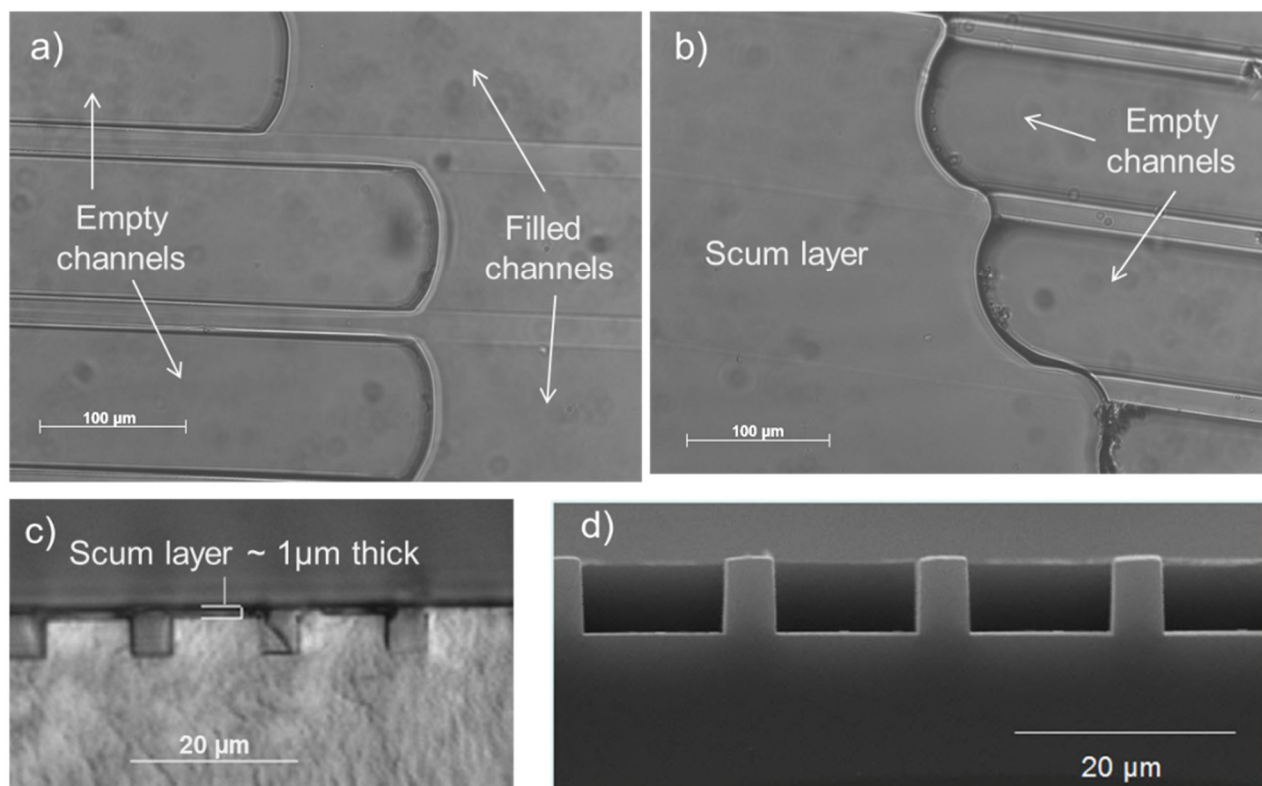
Figure 2: Scum layer on FIMIC samples: (a) and (b) Optical images of FIMICs made from replica where [w-s-d] is [50-10-10] showing a scum layer in (b); (c) and (d) respective optical and electron micrographs of real cross sections showing a scum layer in (c).

4.1.3 Atomic Force Microscopy and Force Spectroscopy Investigations

Atomic Force Microscopy (AFM) was employed in order to investigate the surface topography and the local mechanical differences of various FIMIC compositions; for that reason topographic imaging and *force mapping* were utilized respectively. Both, the microscopic and spectroscopic investigations were carried out under ambient conditions applying a liquid cell for measurements in aqueous conditions. Topographic imaging was conducted in intermittent contact mode, while Force spectroscopy was performed employing the same tip and recording

a set of Force-distance (F/d) curves on exactly the same area of the sample, where the microscopic investigation had been conducted beforehand. The set of spectroscopic measurements was subsequently employed to create so-called *Force-maps* (Figure 3), which are elaborated in the following paragraph.

The surface elasticity of materials can be calculated from the F/d-curves, which represent the elastic response of the material to indentation. Therefore, Figure 3a details the interaction-cycle between an AFM tip and the scrutinized substrate of a single force spectroscopic run. At large distances, there is no interaction between the tip and the substrate, and the force remains zero. However, upon approaching the surface, the tip starts to interact with the surface and attractive forces (such as capillary forces, Van der Waals interactions, hydrogen bonding and electrostatic interactions) make the tip snap into contact with the surface. This attraction can be recognised as the minimum in the F/d-curve, while the recorded F-values correlate with the strength of interaction. These attractive interactions are adhesive forces and can also be plotted as part of *Force-maps*.

The slope of the F/d-curve is a measure for the elastic response of the material upon indentation with the AFM tip, hence representing the elasticity (Young's Modulus)[36]. Stiffer materials are less easily deformed than softer ones and the slope will consequently be steeper, indicating that a larger force is needed to indent the surface. *Force-maps*, as depicted in Figure 3b and 3c, refer to qualitative mapping of surface elasticities (Figure 3b) and adhesive interactions (Figure 3c) and contain valuable information about the chemical homogeneity and elastic properties of the sample surface. Beyond that, they can reveal mechanical or chemical surface patterns of investigated substrates as extensively exploited in this thesis. The general colour code in *Force-maps* relates to; higher elastic values appear in a lighter colour and lower values in darker colour.
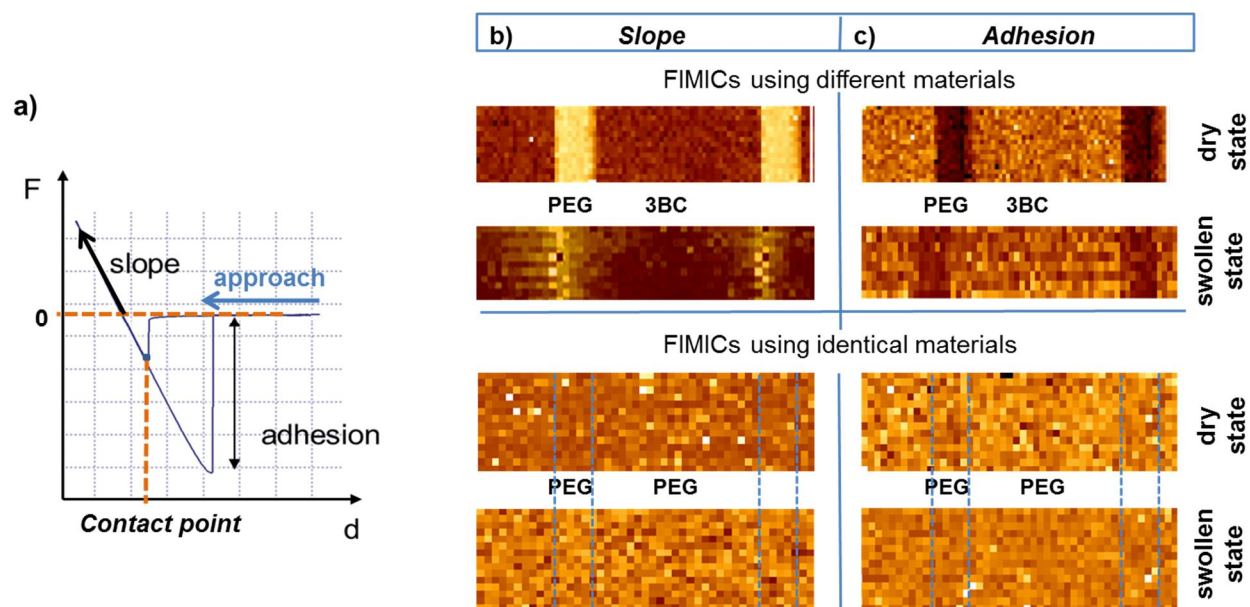
Figure 3: (a) Representative force-distance curve; (b) and (c) *Force-maps* created according to the slope of the F/d-curve; (b) adhesion forces between the tip and the substrate; (c) Distinction between different identical hydrogels materials applied.

The elasticity of the two different hydrogels, both in dry and in hydrated state, was quantitatively determined using Force spectroscopy as depicted in Figure 4. This method enables to determine the respective values of PEG based hydrogels, which was not possible by bulk rheological measurements. Nevertheless, the surface elasticity, as measured by AFM, cannot be directly compared to bulk values as measured by rheology, since the two methods are inherently different and assess different mechanical properties; AFM ascertains surface elasticity and rheology bulk elasticity. For cell culture studies, however, the surface elasticity in hydrated state is arguably the more important property, since cells sense the surface elasticity before any other mechanical property. In fact, there are different opinions existing, e.g. Buxboim et al. and Kuo et al. state as deep as the size of the magnitude of the cell itself[37,38], others limit it to a few micrometres (1 μm – 6 μm)[39–41]. A concise commentary of this controvert issue from Buxboim et al. summarizes the different standpoints[42].

It is obvious from Figure 4 that as prepared hydrogels from PEG possess much stiffer mechanical properties than those of 3BC, which can be expected on the basis of the relatively

low molecular weight of the precursor. Interestingly, the elasticity of PEG in hydrated state is drastically decreased in comparison to that in dry state (by 2 orders of magnitude) and due to this softening effect, the PEG 0% hydrogel becomes even softer than any of the 3BC hydrogels. The elasticity of 3BC also decreases by water uptake, but to a much smaller extent (only by a factor of about 2). This different behaviour can be explained by the differences in water uptake; PEG swells significantly more than 3BC.
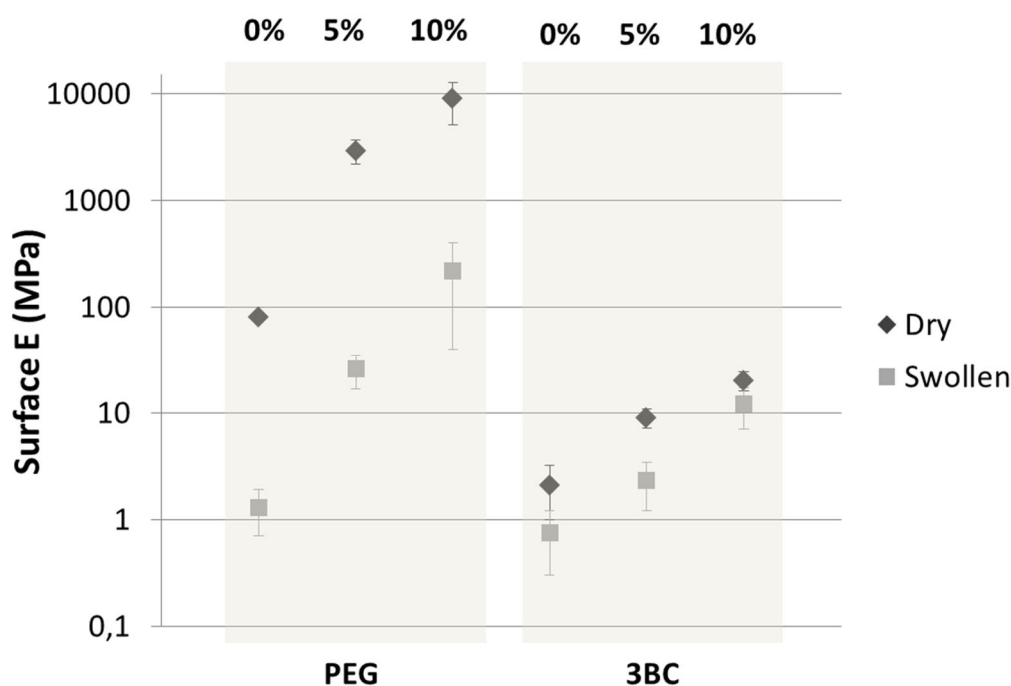
Figure 4: Surface elasticity of the hydrogels as measured by Force spectroscopy using the AFM.

Initially, replicas from PEG 5% and filled with 3BC 5% were created as surface pattern with sharp, clear boundaries and a distinct contrast in elasticity. The quality of the mechanical patterning of FIMIC platforms may be recognised from the *Force maps* (see Figure 3b and c), which display that PEG 5% possesses a higher Young's Modulus and a lower tip-surface interaction than 3BC 5%. In hydrated state, however the differences in adhesion forces are not as pronounced as in dry state, which can be attributed to the absence of a capillary water film between the tip and the substrate in immersed state.

The topography difference in the dry state verses hydrated state was examined using AFM topographic imaging combined with the analysis of according cross sections (Figure 5). In the dry state, the samples showed a topography difference of about 120 nm, which was shown to increase significantly to around 1.0 μm in the hydrated state. The increase in the height difference between dry and hydrated states leads to the conclusion that the topography change is related to the differential swelling properties of the two employed hydrogels resulting in the PEG replica protruding from the surface. Nevertheless, in order to exploit the differential swelling in an advantageous manner, it was attempted to level out this slight indentation by fabricating a FIMIC platform, in which the replica swells less than the filling material (Figure 5b) addressing to counteract the depression by allowing the filler to swell to the level of the replica. Since 3BC swells less than PEG, consequently, FIMIC substrates from a 3BC 5% replica and a PEG 5% filler were created. In this instance, AFM showed that the topography in the swollen state had indeed decreased (Figure 5d). Thus, it proved that this strategy seems successful to create patterned surfaces that display the least topographic difference in hydrated state, and hence in cell culture.
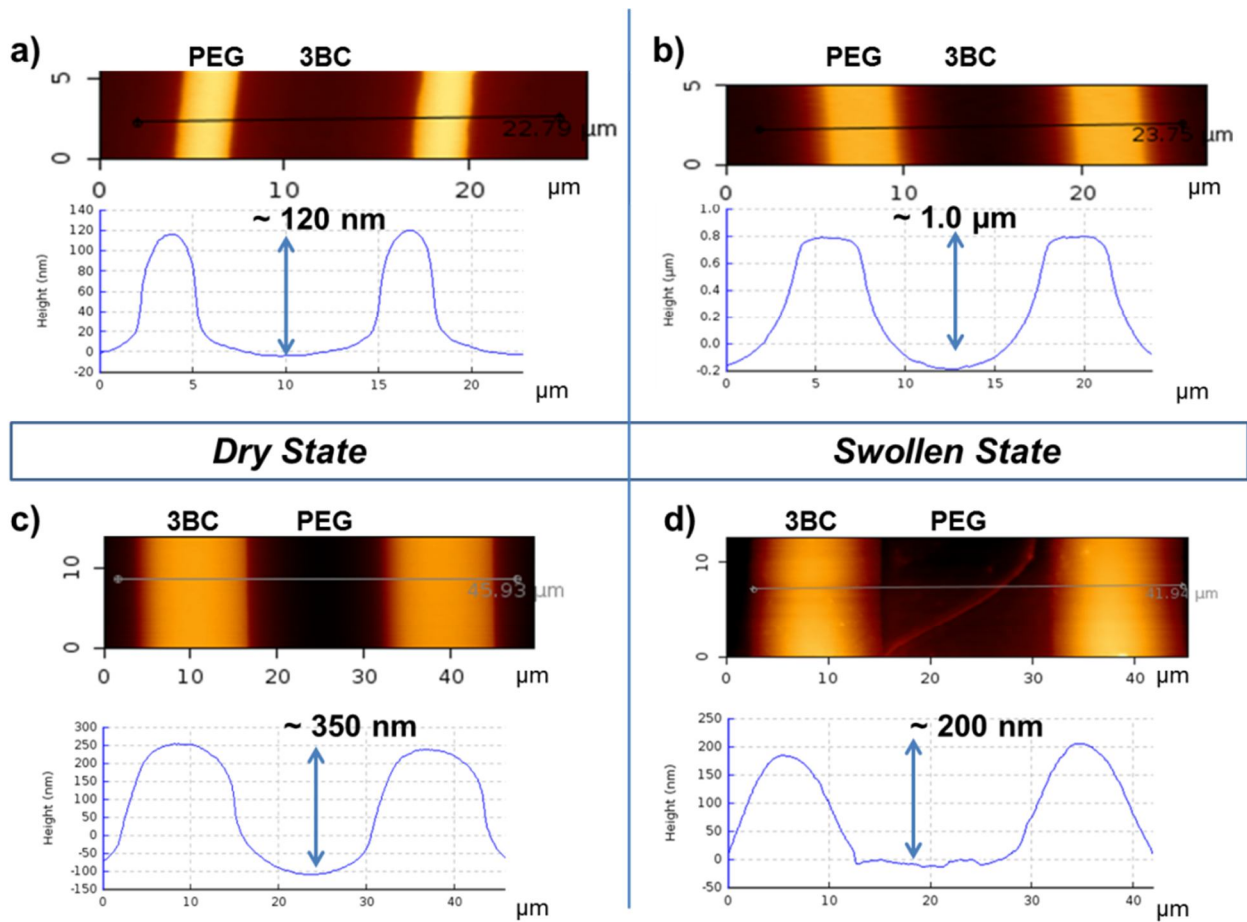
Figure 5: AFM topography images and corresponding cross sections of FIMICs consisting of (a) and (b) PEG 5% (Replica) and 3BC 5% (Filler); (c) and (d) 3BC 5% (Replica) and PEG 5% (Filler); left: dry state; right: swollen state.

To clarify the extent of the effect of differential swelling on the FIMIC topography, substrates with two components possessing identical swelling properties were examined. Utilizing PEG 5% as both the replica and as the filler material, it can be observed that there is little difference in topography between the dry and hydrated states, with a height difference of as little as 40 nm (see SI 1). This demonstrates that for identical hydrogel compositions with equal swelling properties, the change in topography between the replica and filled areas of the FIMIC surface is negligible. It should be noted that in dry state, the typical cross section profile always shows a small depression on the filler side, regardless of which material is employed as a mold and

which as the filler. This could be attributed to shrinking during UV-radiation. Table 1 summarizes the effects of differential swelling that either amplify or diminish topography.

Table 1. Exploiting differential swelling behaviour of 3BC and PEG to increase or decrease the topography in hydrated state.

FIMIC composition	Effect	Topography in dry state	Topography in hydrated state	Result
3BC in PEG	Mold swells more than filler	~120 nm	~ 1 µm	Increased topography
PEG in PEG	No differential swelling	~40 nm	~ 40 nm	No change
PEG in 3BC	Filler swells more than mold	~350 nm	~200 nm	Decreased topography
PEG 0% in PEG 10%	Filler swells more than mold	~400 nm	~125 nm	Decreased topography
3BC 0% in 3BC 10%	Filler swells more than mold	~ 250 nm	~ 100 nm	Decreased topography

In order to test the versatility of this approach and to arrive at very well controlled micro *Patterns of Elasticity* that are topographically smooth in cell culture, the fabrication of this type of FIMIC platform(replica that swells less, filling material that swells more) was repeated. Otherwise, contact guidance may be observed. That is, if significant topography remains, cellular response may be attributed to topography instead of chemistry or elasticity (for more detailed information see PhD thesis of Christine Strehmel[3]). Due to the selection of materials the chemistry of both constituents were kept the same. Replicas made of 3BC 10% and filled with 3BC 0%, where the two components exhibited slightly different swelling properties (a water uptake of 4 % versus 6 % respectively), were produced. Again, it was observed that there is a decrease in topography from approximately 250 nm to 100 nm (Table 1) and that the surface profile is levelling out due to the changes in degree of swelling. The same strategy was employed for PEG, whereas the effect of decreased topography by virtue of differential swelling (in this case comparing a water uptake of 18 % for PEG 10% with 28 % for PEG 0%, details see PhD thesis of Zhenfang Zhang[2]) was even larger, decreasing from approximately 400 nm in dry state to approximately 125 nm in hydrated state. It should be noted however, that the topographic differences not only vary between different samples, but also on the very same

sample. Variations can be observed between measurements on different areas of the same sample, which also can be attributed to the standard deviation in water-uptake, which hydrogels generally possess (more detailed information can be found in the PhD thesis of Zhenfang Zhang[2]).

4.1.4 Summary

The scope and limitation of the recently developed Fillmolding In Capillaries (FIMIC) method was investigated in order to fabricate elastically micropatterned substrates, so-called *Patterns of Elasticity*. The recent investigations employing Atomic Force Microscopy (AFM) however, have revealed that the surfaces of such FIMIC substrates are never completely smooth. A slight topographic landscape seems inherent to this particular fabrication method. The present results demonstrate that the topographic differences can even be enhanced, when the FIMIC platforms are immersed in water. This is due to differential swelling of the two PEG-based hydrogel materials.

Nevertheless, one can apply the differential swelling in a beneficiary nature to counteract volume shrinking of applied hydrogels observed during UV-radiation. The right choice of the two constituent hydrogel materials in FIMIC substrate production should be employed, namely by employing material that exhibit little tendency to water-uptake as the mold and a hydrogel that displays a higher degree of swelling as the filler. Thus, it was possible to successfully level out the topographic differences to some extent. Although no perfect levelling could be achieved, the presented results still prove the feasibility of this approach.

Chapter 4.2

Blending Poly(ethylene glycol) (PEG)-based Polymers in order to obtain a Library of New Biomaterials and their Application in Surface-Micro-Patterning by the Fillmolding In Capillaries (FIMIC) Method.

Abstract

A library of Poly(ethylene glycol) (PEG) based polymer blends with varying hydration properties were synthesized. They were fabricated in the absence of solvents, which makes them a suitable candidate for Fillmolding In Capillaries (FIMIC) processing. The main aim of this chapter is to include differential swelling properties of utilized hydrogels formulations in order to achieve FIMIC substrates without physical topography in hydrated state. This poses the challenge of levelling out the topography by adjusting shrinking properties during ultraviolet radiation with swelling differences of employed polymer blends. In consequence, genuine 2D *Patterns of Elasticity* of binary nature could be fabricated, which would allow studying cell migration phenomena in systematic detail.

Details in processing of pure polymers and blends can be found in the appendix of this thesis, since it was conducted by two colleagues of the Lensen Lab (Zhenfang Zhang and Dr. Susan Kelleher), and since my contribution to the blend fabrication was relatively limited. For a better understanding, here, only a short introduction to the hydrogels employed is given.

Results and Discussion

4.2.1 Materials Characterization

First, material notations with corresponding chemical properties finding application in this chapter are stated in Figure 1. One of the main reasons for applying Poly(ethylene glycol) (here denoted PEG1) (PEG, M_w 575 gmol^{-1}) and 3BC1, a tri-block copolymer (3BC) of PEG and Poly(propylene glycol) (PPG) (M_w 4400 kDa), in the fabrication of FIMIC platforms is the liquid nature of both hydrogels at room temperature (22 °C), which provides greater ease to FIMIC processing (for more processing details, see chapter2.3). The general idea of this project was to achieve successful levelling out of FIMICs. Therefore, employed hydrogels had to meet two principle characteristics: First processibility, since they are of non-linear nature e.g. multi-arm PEG poses the challenge of conversion from dry powder-like state into liquid state. Second cell repellence, since blends needed to contain more PEG than PPG in 3BC1 in order to ensure the perpetuation of cell-repellent behaviour. The polymers employed are presented in Figure 1. The table alongside shows the aggregation state of the polymer at room temperature with the according molecular weight and the calculated theoretical percentage of PEG in the polymer; pure PEG contains 100 % PEG and the block co-polymer contains either 30 % PEG in the case of 3BC1 or 80 % in the case of 3BC2. One should be aware that the PEG content in these blends is essential in order to understand the physicochemical properties of the herein presented hydrogels.

	Molecular weight	% PEG	State at r.t.
PEG1	575 gmol^{-1}	(100)	Liquid
PEG2	3400 Da	(100)	Solid
3BC1	4400 Da	30	Liquid
3BC2	8400 Da	80	Solid
8PEG	15,000 Da	(100)	Solid

Figure 1: The general structure of the three types of polymers used, i.e. PEG, 3BC and 8PEG and the properties of five selected examples that were investigated.

The addition of both pre-polymers with longer linear chains PEG2 (M_w 3400 Da), 3BC2 (M_w 8400 Da) and multiple arm 8PEG (M_w 15,000 Da), allows to fabricate polymer networks with very different characteristics than those utilized before, possessing more possible crosslinking points in the case of the multi-arm PEG or longer distances between either crosslinking points (higher M_w between crosslinks and corresponding larger mesh sizes). Thus, one can precisely tune the blends' elasticity and protein and cellular adhesiveness.

Important to remember is that one of the main requirements for the FIMIC patterning method is the need to apply liquid precursors, both to make replicas from silica masters via Replica Molding and subsequently to fill the grooves present on patterned hydrogel replica surfaces. The combination of specific chemistry and low molecular weight of these three new polymers (PEG2, 3BC2 and 8PEG) means that they are, in contrast to PEG1 and 3BC1, solid at room temperature and need to be processed into liquid state for blending and subsequent employment in FIMIC processing. This resulted in greater handling difficulty and poses therefore a substantial obstacle to the processing procedures. As a consequence of lavish trails, PEG2 was eliminated from further usage.

4.2.2 Application of Blends in the Fill Molding In Capillaries Method

In order to illustrate the challenge of addressing different hydration behaviours of employed hydrogel blends in FIMIC substrate fabrication. Figure 3 displays the three possible alternatives. Depicted are schematic cross sections as recorded from AFM topographic imaging. Figure 3a depicts the option 'Filler swells more', which refers to the former grooves standing out after hydration. Figure 3b refers to 'Filler swells less', which means that after complete hydration, the grooves still exhibit a depression. In rare cases (rather theoretically), that may also be the case, in which the swelling difference between the utilized hydrogel blends is lower than the volume shrinkage of the filler material during UV radiation. Figure 3c illustrates the ultimate, however very challenging objective of a completely levelled out FIMIC substrate in hydrated state.

Figure 3: Schematic illustration of hydrated FIMIC platforms employing hydrogel combinations with varying degrees of hydration. (a) Filler swells more; (b) Filler swells less; (c) perfectly levelled-out sample.

Hydrogel blends made of PEG1/3BC1 and of PEG1/8PEG were applied in order to produce FIMIC platforms. They were chosen, since they form the most promising combination of mechanical and protein and cell adhesion properties as well as to provide a necessary degree of processibility. To ensure that the polymers blends are in their liquid state for FIMIC processing, the PEG1/3BC1 blend is utilized as prepared and the PEG1/8PEG is melted and prepared using pre-heated glassware. Two different FIMIC-pattern-dimensions were finally selected, namely "20-10" and "10-50".

Blend 1: PEG1/3BC1

"20-10" FIMIC samples (filler occupies a groove of 10 μm in width) were produced, employing a blend ratio of PEG1:3BC1 (33:66). In the sample substrates, where the filler swells less than the mold, the filler contained 10 % CL and the mold contained 5 % CL. In an approach pursuing the opposite hydration behaviour, the filler contains 5 % CL and the mold contains 10 % CL. The topography of the substrate surfaces of these samples was measured by Atomic Force Microscopy (AFM) in the dry and the hydrated state.

The AFM results display that the strategy of levelling out the FIMIC substrates utilizing fillers with greater degree of water-uptake was generally working, but no complete levelling out of the investigated samples could be achieved (see SI 4). The contour of the FIMIC surfaces was still concave, with the filler appearing to be kind of retracted from the mold. Hence, it was concluded that the hydrogels made from PEG1/3BC1 blends do not take up sufficient amounts of water in order to level out the sample entirely and thus, the effort was focused on the set of blends fabricated from PEG1/8PEG, which exhibit greater swelling degrees. Therefore, they promise better chance to reduce the physical patterns of FIMIC substrates to a minimum.

Blend 2: PEG1/8PEG

The hydrogel blend PEG1/8PEG was selected, since firstly, these constituents are the easiest to handle and to process, and secondly they had a relatively high ability to take up water and beyond that, they consist of pure PEG-constituents. Consequently, the fabricated blends maintain the protein repellent nature of the pure substances. On PEG-surfaces, any aided protein adsorption and subsequent cell adhesion must be attributed to the designed elasticity pattern or to eventually remaining, undesired topographic effects. For these FIMIC substrates, regardless if mold or filler, blends were selected that contained the same ratio of the two components, PEG1 and 8PEG, but different amount of CL. A series of PEG1/8PEG FIMIC platforms were fabricated, applying a mold with "50-10" pattern dimensions. Hence, the master resulted in FIMIC substrates, where the filler spun 50 μm and the mold constituted of 10 μm lines. Seven different FIMIC samples using this blend were fabricated; for each sample, due

the maximum to water uptake ability, 0 % CL in the filler pre-polymer solution was chosen. The hydrogel molds contained a varied amount of CL ranging from 10 % down to 0 %. This series of substrates was produced in order to obtain FIMIC platforms perfectly levelled out. The samples were prepared and left to swell in deionised water for 12 h before the topography was measured via AFM. Upon measurement in the hydrated state, it was observed that in all samples, the filler in fact protruded from the mold. Thus, FIMIC substrates of previously unobserved convex patterning properties were formed (Figure 3). For the samples containing a high percentage of CL (e.g. 10 %), the filler protruded up to 1 µm from the mold. Consequently, as the CL percentage in the mold was reduced and the mold swelled more, the resulting FIMIC platform topography diminished.

Figure 4a plots the AFM topographic cross section of the filler protrusion of all investigated sample compositions with varying CL, showing that the decrease the in CL percentage of the mold leads to great reduction and eventual levelling out of topographic difference. Moreover, a schematic illustration is given for better understanding of the recorded FIMIC profiles. Figure 4b shows the height of the filler sticking out relative to the mold, which is plotted against the CL percentage of the mold. This work elegantly shows that one can use PEG based hydrogel blends to make FIMIC substrates that are either convex, concave or close to level. However, Figure 4b shows that although the series might incline a linear line with the crossing point to a height different of zero, a completely levelled out sample might never be achieved precisely. This is attributed to deviations in the FIMIC processing and standard deviations of water uptake behaviour of employed hydrogels. Hence, no FIMIC platform regardless of its composition can be absolutely identical to another (for more details, see PhD thesis of Zhenfang Zhang[2]). This applies especially, if hydrated hydrogels are investigated in a low nanometer-scale. However, considering a height difference of 100 nm over a distance of 50 µm, one can conclude that these samples are essentially smooth and effects on protein adsorption and cell adhesion due to physical patterns may be considered negligible. Any research known to the author deals with topographies far above the here present data[43–46]. A study conducted e.g. by Kunzler et al. demonstrates that osteoblasts prefer rougher areas of around R_a (arithmetic average) 5 µm, while fibroblasts tend to adhere more on smoother substrates with R_a 1 µm[45]. Cellular

responses on nano topographic substrates were e.g. carried out by Gelbinger et al., which pointed out that osteoclasts tend to interact more with surface roughnesses of R_a 500 nm, while surface roughnesses of around R_a 10 nm caused no profound interaction with osteoclasts[46]. Still, those are R_a values (RMS ~ 1.1 Ra) far beyond the here presented data. Apart from that, the author is convinced that not absolute roughness values determine the interaction cell-substrate but rather the curvature of the scrutinized substrate area. This means that the cell sense changes in physical substrate orientation rather than absolute topographic differences over a certain area. This means that the change in slope (referring to a surface area cross section) is considered to be the prevailing factor for cells in sensing topography.
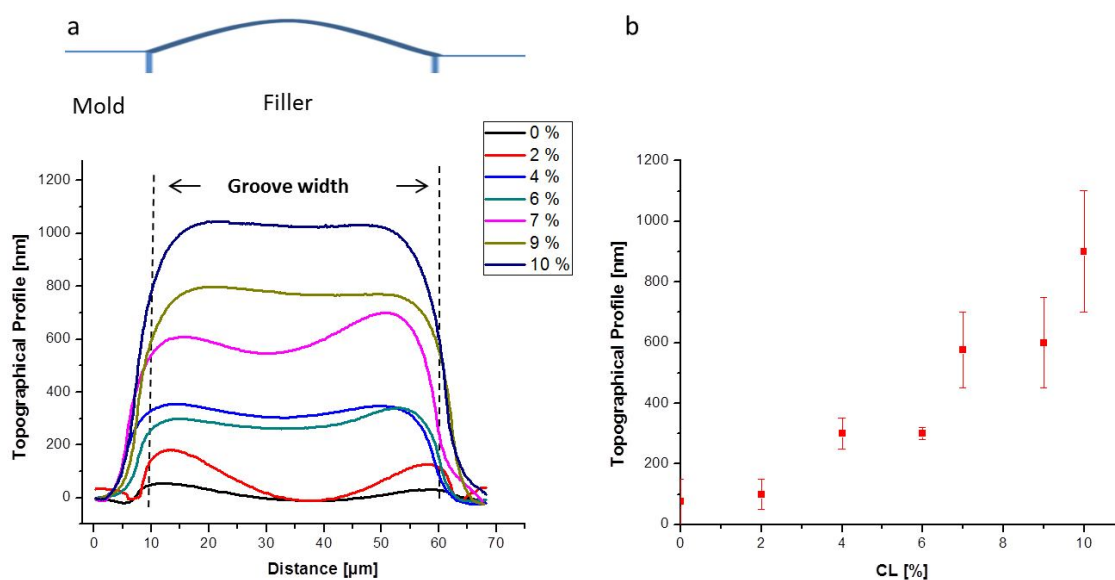
Figure 4: Graphs displaying the relationship between CL and topographic profile of the PEG1/8PEG blend: (a) representative topographic AFM profiles with varying CL in the filler with according schematic illustration; (b) topographic profile plotted over CL with according standard deviations.

4.2.3 Summary

First of all, the initial goal of levelling out FIMIC platforms with PEG based hydrogel blends, while maintaining protein repellent properties of PEG, could be achieved. That was attained by

employing a blend fabricated from PEG1 and 8PEG, which unite the FIMIC processibility requirements and water uptake ability in the desired manner. Hence, a model system with varying CL could be designed in order bring physical patterns of FIMIC substrates to a minimum, finding the matching combination regarding CL for both constituents; mold and filler. This demonstrated the feasibility of the FIMIC method aiming at true 2D *Patterns of Elasticity*, in which solely the hydrogels elasticity would determine the resulting cellular response to the substrate and no topographic overruling effect occurs. In addition, pursuing this method, one may even tune the elasticity according to the applied hydrogel systems in a manner that one could even control on the type of cells that adhere to the provided binary mechanical surface pattern.

Chapter 4.3

Soft Lithographic Surface Patterning of Physically and Chemically Mineralized Poly(ethylene glycol) Hydrogels for Selective Interface Interaction

Abstract

Understanding protein adsorption and cell adhesion behavior on engineered surfaces and interfaces is essential for the successful development of novel biomaterials. Therefore, the main influential factors, i.e. topography, chemistry and elasticity were examined, comparing (I) physically mixed Poly(ethylene glycol)-Hydroxyapatite (PEG HAp NPs) and (II) chemically synthesized Poly(ethyleneglycol)-Hydroxyapatite (PEG nHAp) based nanocomposite hydrogels. Both, the intrinsic protein repellent behavior of PEG-based hydrogels and the protein attractive properties of HAp-based ceramics were exploited in order to produce surface patterns of bioactive and bioinert properties. The recently developed soft lithographic method, Fillmolding In Capillaries (FIMIC), an easy bench top method with the employment of a new bioactive nanocomposite is paired in order to produce unique chemical and mechanical micro patterns. Aiming to focus on the impact of HAp to study preferred protein adsorption and cell adhesion, FIMIC patterns were tuned to exhibit virtually no topography in hydrated state (approximate height difference of 50 nm over 10 – 20 µm lateral dimensions). Materials characterization, investigating the chemical and morphological structure of PEG nHAp as a homogeneous nanocomposite hydrogel containing nanometer-sized domains of crystalline HAp were obtained via Electron microscopy, X-ray diffraction (XRD) and spectroscopic methods (FtIR, RAMAN). Physical surface properties of either FIMIC platforms in hydrated state were ascertained with Atomic Force Microscopy (AFM) and Energy-Dispersive X-ray spectroscopy (EDX) mapping, confirming the spatial control of physical, mechanical and chemical constitution, respectively. Still, only for chemically synthesized PEG nHAp hydrogel composites a pronounced level of differential protein adsorption and locally controlled homogeneous HAp deposition from

Simulated Body Fluid (SBF) possessing distinct interfaces could be observed. The FIMIC platforms that were processed with PEG nHAp, demonstrated a unique HAp deposition monolayer-pattern, which can be tuned over immersion-time in SBF and result in a micro-meter-sized pattern made of bioinert PEG and bioactive HAp globules. Ultimately, cell adhesion experiments were conducted, in which the cell adhesion behavior of fibroblasts and osteoblasts were scrutinized on PEG nHAp. These investigations revealed that calcium phosphate affine osteoblasts respond directly to the FIMIC platform and align along the incorporated HAp pattern, while in contrast, only a few fibroblasts adhere, not recognizing the surface pattern and distributing rather randomly. Beyond that, osteoblasts display a spread morphology indicating strong interaction with the FIMIC surface, while fibroblast exhibit a rather round morphology attributed to little surface-cell interaction.

Loebus A, Zhang Z, de Vicente Lucas G., Strehmel C, Arafeh M, Lensen MC, Soft lithographic Surface Patterning of Physically and Chemically Mineralized Poly(ethylene glycol) Hydrogels for Selective Interface Interaction; *to be submitted*

Incentives

Spatial control of cell-adhesion on biomaterials surface is of great interest in the understanding of cellular response in general. Consequently substantial effort has been invested and many systems have been investigated in order to reveal influential factors, allow classification and set standards for evaluation methods[7,8]. As main sources determining the final performance of biomaterials-surface-patterns topography[9,47,48], chemistry[49,50] and elasticity[51,52] could be elaborated.

Physical patterning (topographic features) can be elegantly induced via e.g. soft lithographic methods such as Molding or Imprinting, which were introduced by Whitesides et al. in the 1990s[11]. Another promising approach in this field is the recently developed Fillmolding In Capillaries (FIMIC) method [9], which enables the fabrication of sub micrometer *Patterns of Elasticity*; that are in hydrated state, horizontally perfectly plane surface patterns with alternating elasticity, which simultaneously allow chemical patterning in the lateral micrometer scale.

In this study, poly(ethylene glycol) (PEG)-based hydrogels and PEG nanocomposite materials containing hydroxyapatite (HAp) are utilized to fabricate patterned surfaces with defined areas of bioinert and bioactive properties, respectively. It is well known that PEG is widely recognized for its protein-repellent behavior, which have resulted in different applications such as contact lenses or protective coatings or drug-delivery vessels[18,53–55]. Moreover, PEG based hydrogels have been successfully applied as medium the illuminate cell-repellent surface behavior towards cell-adhesive cites[9,51]. In contrast, calcium phosphate based ceramics[12,13,56] e.g. Amorphous Calcium Phosphate (ACP), Tri Calcium Phosphate (TCP) or HAp often find application in biomaterials when increase in bioactivity or improved mechanical properties of polymer hydrogels are desired[54,57–60].

Results and Discussion

4.3.1 Materials Characterization

Polymeric composite materials may be fabricated by simple mixing of an inorganic material phase into a polymeric network. In this project, two fundamentally different approaches were pursued: First, the physical mixing of HAp nanoparticles (NPs) into a PEG matrix (denoted as PEG HAp NPs) and secondly, the chemical synthesis of a PEG HAp composite (denoted as PEG nHAp) via in-situ nucleation, in which the HAp domains nucleate and maturate within the PEG matrix. Details to synthesis of both formulations are given in chapters 3.1.5 and 3.1.6, respectively. The aim of the hydrogel composite synthesis via in-situ HAp nucleation was to avoid any influence from HAp aggregation and guarantee surface accessibility of introduced chemical functionalities in order to retain precise local control of post-gelation surface modification. Figure 1 depicts the materials synthesis and according materials notation as well as the lucency of the hydrogel composites and the suitability for FIMIC processing. Figure 1a displays the according details of the fabrication process for chemically synthesized PEG nHAp composite hydrogels. Step I depicts the Calcium- and Phosphate-salt solution addition to the photoinitiator (PI) containing PEG (M_w 575 g/mol) precursor. Step II displays the maturation stage of the hydrogel composite involving vigorous magnetic stirring, while filtering of the aqueous hydrogel composite was conducted in order to receive the final product as described in Step III. After step III, the composite precursor is processible for soft lithographic regime; subsequent ultraviolet (UV) radiation is applied when the liquid-to-solid conversion, e.g. for substrate fabrication, is desired. Three different types of chemically synthesized hydrogel composites (PEG nHAp) were fabricated. Hydrogel composite materials notations with according HAp content by weight, which find application in this chapter, are depicted in Figure 1b. One should note the absence of water in any of the stated materials compositions. Additionally, the table in Figure 1b displays the varying degrees of lucency of the respective hydrogels composites, an important aspect for the characterization of cell adherence patterns with optical microscopy. The ability to incorporate either hydrogel composite in FIMIC fabrication is also given, which relates to the viscosity of the hydrogel

composite pre-cursor. In case the viscosity is too high, capillary action cannot take place or grooves of the hydrogel molds are filled incompletely (for more details to FIMIC fabrication, see chapter 2.3).

composite hydrogel notation	HAp percentage by weight (wt%)	Lucency of hydrogel composites	Processibility in FIMIC design
PEG 10nHAp	10	transparent	+
PEG 20nHAp	20	transparent	+
PEG 40nHAp	40	opaque	-
PEG 20 HAp NPs	20	slightly opaque	+
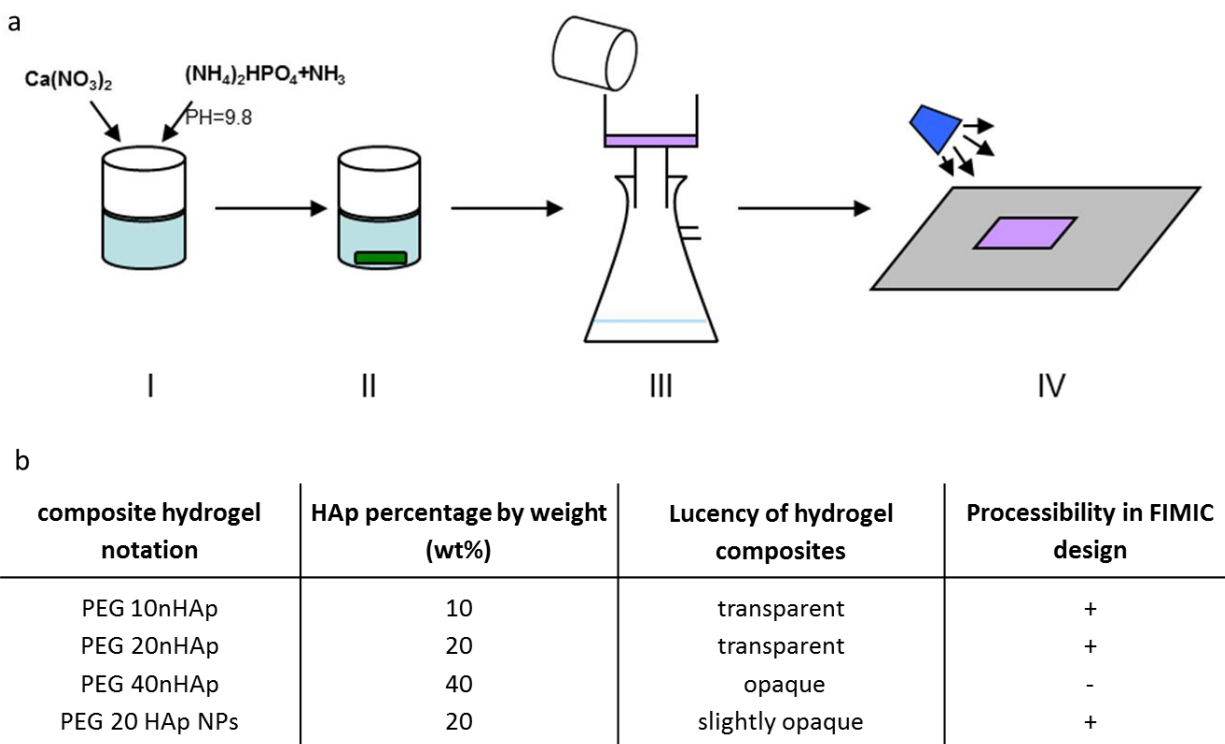
Figure 1: Materials: (a) synthesis process of PEG nHAp: adding of salt solutions (I), maturation (II), filtering (III) and UV curing (IV); (b) notation of applied hydrogel composites and according HAp percentage by weight, degree of lucency of the hydrogels and the processibility for FIMIC fabrication.

Materials characterization proving the chemical and morphological structure as a homogeneous nanocomposite hydrogel containing nanometer-sized domains of crystalline HAp were obtained via Electron microscopy, Elemental Mapping via EDX, X-ray diffraction (XRD) and spectrometrical methods (FtIR, RAMAN) (Figure 2). Since IR and RAMAN spectroscopy and X-ray diffraction are often used to qualitatively detect and discern calcium phosphate phases[56], the as prepared

samples were characterized with FtIR, RAMAN and XRD analysis in order to prove distinctive bands (FtIR), shifts (RAMAN) and reflections (XRD) for HAp formation.

FtIR measurements (Figure 2a) revealed distinctive bands at 560 cm^{-1} and 598 cm^{-1}, which can be attributed to the triply degenerated bending mode, v_4, of the O-P-O bond of the PO_4^{2-} group. Furthermore the weak peak at 474 cm^{-1} and the shoulder at 462 cm^{-1} indicate the doubly degenerated bending mode, v_2, which can be clearly discerned at least for PEG 40nHAp. All the other characteristic peaks e.g. 1032 cm^{-1}, 1046 cm^{-1} and 1087 cm^{-1} (triply degenerated asymmetric stretching mode vibration, v_3, of the P-O bond) for HAp formation are obscured by bands from the PEG_{575} polymer-matrix and therefore cannot be clearly identified. This shortcoming can be compensated by RAMAN spectroscopy.

The recorded RAMAN spectra (Figure 2b) exhibit an increasing peak at approximately 965 cm^{-1} (v_1PO_4) with augmenting HAp content, which derive from a totally symmetric non-degenerated stretching mode of the free tetrahedral phosphate ion. This is in agreement with literature, where this peak is widely recognized as identification site for HAp presence[56,61,62]. In addition, a broader peak at approximately 1050 cm^{-1} (v_3PO_4) was observed, which can be assigned to amorphous calcium phosphate-like mineral[62]. The decrease of the peak intensity ratio of 1050 cm^{-1} to 965 cm^{-1} with rising HAp content implies the transition from ACP to HAp. Furthermore, it is a widely accepted fact that ACP is a precursor for HAp formation[56,62]. The spectrum of HAp NPs is additionally given for comparison.

XRD measurements can be ideally used in order to verify phase purity[56]. In this case, it proved the presence of reflections typically assigned to HAp at 2theta-values of 26 ° and 32 ° (Figure 2c). The intensity of the signal increases with HAp content indicated by the black arrow. PEG 10nHAp is not depicted due to very small intensity of reflections in the according spectra. Furthermore, the spectra demonstrate that an increased incorporation of HAp also results in enhanced crystallinity of the HAp phase. In order to reliably quantify this aspect or even state about crystal sizes, Rietveld Refinement would be necessary[63], which was not conducted in the present study.

The morphology of as prepared PEG nHAp composite hydrogels was investigated via Transmission Electron Microscopy (TEM) in order to identify HAp formation and comment on HAp distribution within the PEG nHAp nanocomposites. As representative example of the three investigated compositions PEG 20nHAp is shown and analyzed. The TEM images (Figure 2d) reveal crystalline areas distributed throughout the composite sample, which implies a high level of uniformity down to the nanoscopic scale. This can be attributed to the in-situ nucleation of HAp, since thus, agglomeration as often observed for physically incorporated HAp NPs is prevented[64]. The in-situ X-Ray diffraction pattern (Figure 2e) demonstrates the crystalline character of the nucleated HAp-phase, where the recorded reflections were characterized and quantified starting from the most centered ring (largest crystallographic dimensions) to the outer ones. The diffraction data allowed identification of the present crystallographic net-planes with corresponding crystallographic net-plane distances and 2 theta angles. The obtained results are in very good agreement with the XRD spectrum, since the most characteristic reflections at 26 ° and 32 ° were amongst others detected and according net-plane distances calculated (see table Figure 2e). Moreover, it was found that the measured distances are in very good agreement with literature for crystalline HAp[56]. In-situ EDX analysis was applied in order to prove the presence of the elements Calcium (Figure 2g) and Phosphorous (Figure 2h). The traces of Silicon and Magnesium can be attributed to impurities during sample preparation, while grinding the particles. Copper can be explained by the usage of a copper TEM grid during sample preparation.

Number of Cycle counted from the center	2θ [°]	d [Å]	Miller Index of the Corresponding Reflection
1	25.9	3.44	(002)
2	29.14	3.08	(210)
3	31.86	2.9	(211)
4	32.2	2.79	(112)
5	34.22	2.66	(202)
6	39.86	2.29	(310)
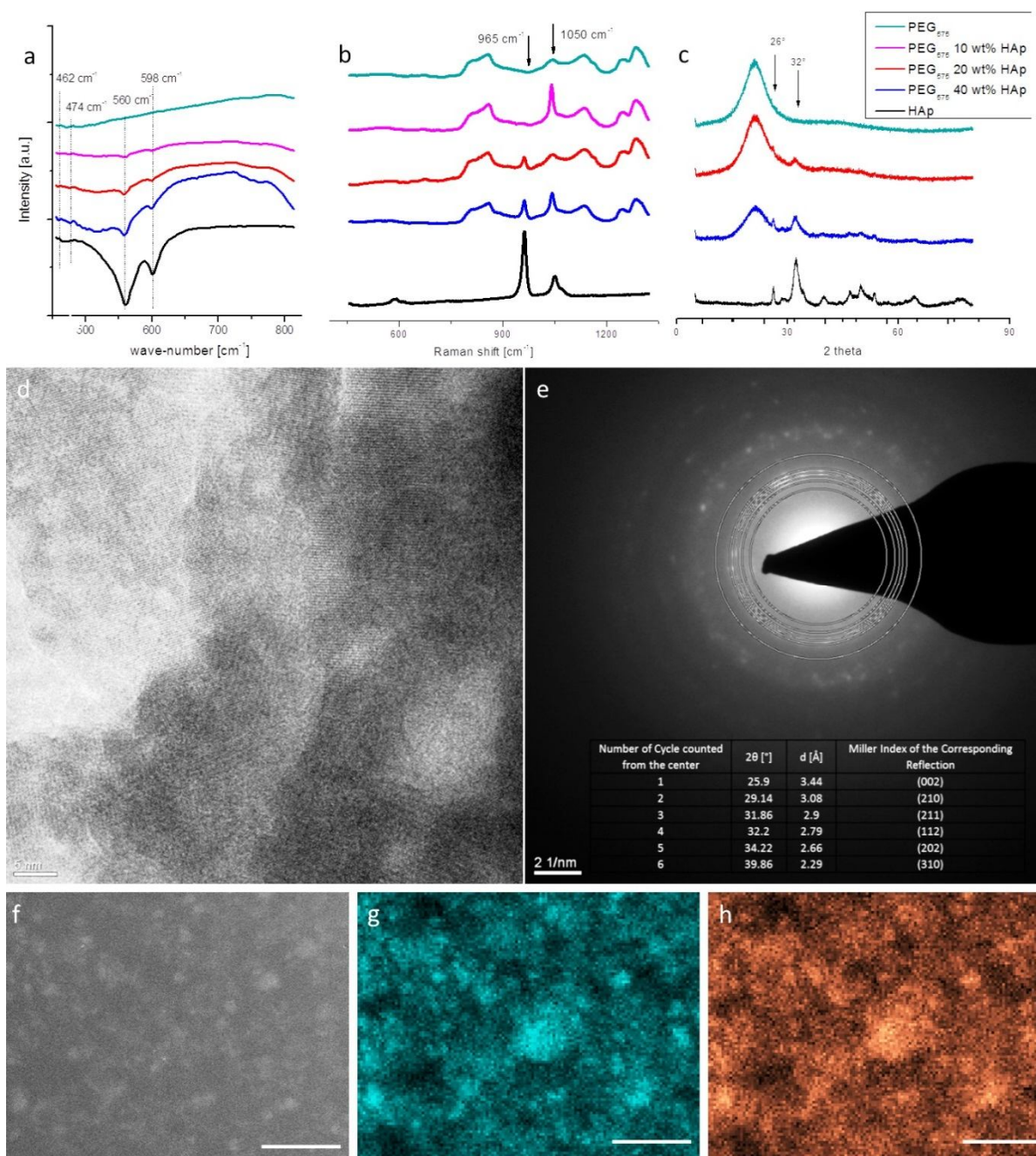
Figure 2: Chemical and morphological characterization of PEG nHAp. FtIR spectra (a) displaying distinctive bands at 560 cm^{-1} and 598 cm^{-1}, RAMAN absorption spectra; (b) with distinctive bands at ca. 965 cm^{-1} and approximately 1050 cm^{-1} and XRD analyses; (c) distinctive reflections of HAp of the different composite matrices at 26 ° and 32 °; (d) TEM micrograph with visible net-planes of the composite; (e) to the electron diffraction pattern (miller indices) with according diffraction angle net-plane distances; (f-h) elemental mapping of plane composite films with scale bar representing 20 µm (f) micrograph (g) Ca-map (h) P-map.

In addition, rheological measurements of the hydrogels in completely hydrated state were conducted in order to quantify the bulk mechanical properties of the hydrogel composite as detailed in Table 1. They revealed, that after ultraviolet (UV) radiation treatment the hydrogel composite are considerably softer than pure PEG (decrease almost 5-fold), which is tentatively attributed to the disturbance of chemical crosslinking in the presence of HAp nano-domains[65–68]. Remarkably though, it was observed that PEG 20nHAp exhibits the highest Young's Modulus (3.45 MPa) in comparison with PEG 10nHAp and PEG 40nHAp (2.38 MPa and 2.41 MPa respectively). For non-UV radiated hydrogel composites, it is presumed that the HAp domains increase the stiffness of the polymer-network[54,69–71]. In contrast, those crystallites may disturb chemical bond formation during UV-curing[72,73]. This effect is the more dominant the smaller the molecular weight of the polymer-matrix, since the crosslinking density increases with decreasing molecular weight. Thus, the introduction of HAp partially limits the hydrogel network formation and consequently the mechanical integrity, which strongly depends on the number of chemical crosslinks formed. Hence, in the case of PEG, one observes this effect at an elevated level leading to the here monitored result, in which small amounts of HAp interfere potentially very strongly in the curing process. However, results imply that HAp incorporation contributes only to a small degree to the strengthening of the composite hydrogel via physical interaction. The incorporation of greater amounts of HAp (as for PEG 40nHAp) nevertheless, either do not disturb significantly more the chemical bond-formation than little amounts of HAp during UV curing, or do not elicit stronger composite hydrogels due to limited secondary interaction processes between the organic and inorganic phase .

Table 1: Bulk elasticity obtained via rheology of the investigated PEG nHAp composite hydrogels with varying concentrations of HAp.

Bulk Elasticity [MPa] in hydrated state	
PEG$_{575}$	16.9 ±3.67
PEG 10nHAp	2.38 ± 0.43
PEG 20nHAp	3.45 ± 0.45
PEG 40nHAp	2.41 ± 0.36

The chemically synthesized composite hydrogels PEG 10nHAp and PEG 20nHAp were fluidic and transparent, while PEG 40nHAp had a considerably higher viscosity and appeared rather opaque, consequently PEG 20nHAp was chosen for further soft lithographic processing due to the highest amount of HAp incorporation and the processibility. The superb degree of patternability down to sub-micrometer range is demonstrated in Figure 3.
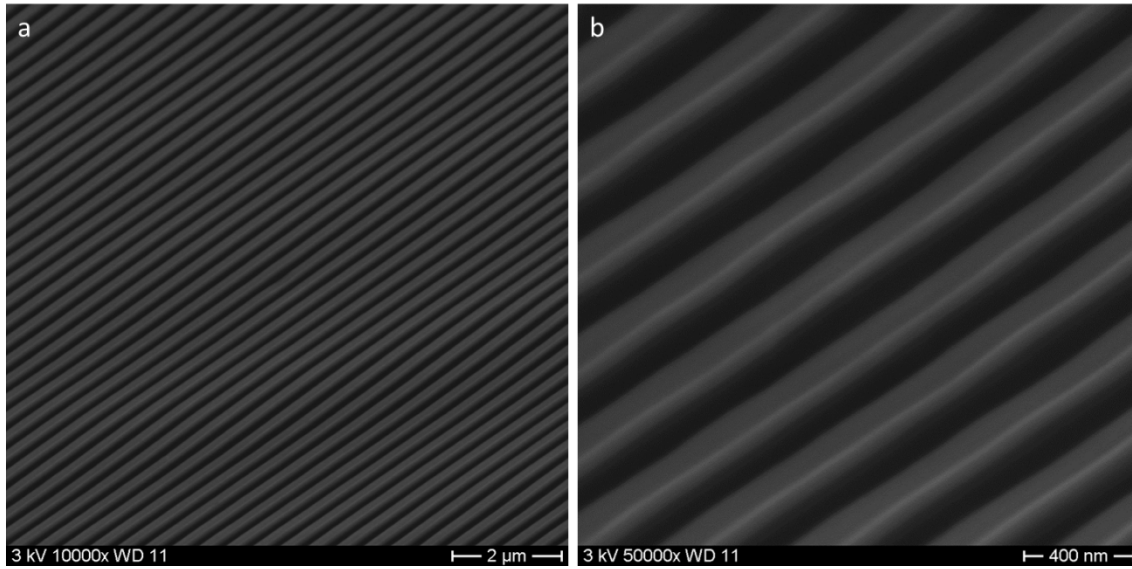

Figure 3: Line patterns in the sub-micrometer scale fabricated via Replica Molding applying PEG 20nHAp.

For comparison reason, a conventional, physically mixed hydrogel composite (PEG 20 HAp NPs) (HAp Ø 20 nm) was fabricated. Therefore, HAp NPs were successfully synthesized via the wet chemical route, which resulted in rod-like HAp NPs with a size of approximately 20 nm. Those were physically mixed into the PEG precursor solution with a weight percentage of 20 % with respect to the entire composite mass. In order to achieve best homogenicity of the resulting PEG HAp NPs hydrogel composite, extensive vortexing and subsequent ultrasonic treatment were applied. The final suspension was rather opaque exhibiting a low viscosity, which enabled easy application in soft lithographic regimes. Surface roughness in form of the Root-Mean-Square (RMS) measure was determined in hydrated state in order to verify that the unpatterned

plane RMS value would be in the range of the substrate used (glass or silicon wafer), hence guaranteeing processing quality. This is displayed in Figure 4, which demonstrates that although PEG 20nHAp exhibits expectedly a greater RMS value (approximately 2.0 nm) than that of pure PEG (approximately 0.6 nm), ascertained values are still in very low nanometer range and to the best of the author's knowledge not detectable by cells. At least any literature known to the author centers RMS far above the here stated values[43–46,74] (see chapter 4.2.2).
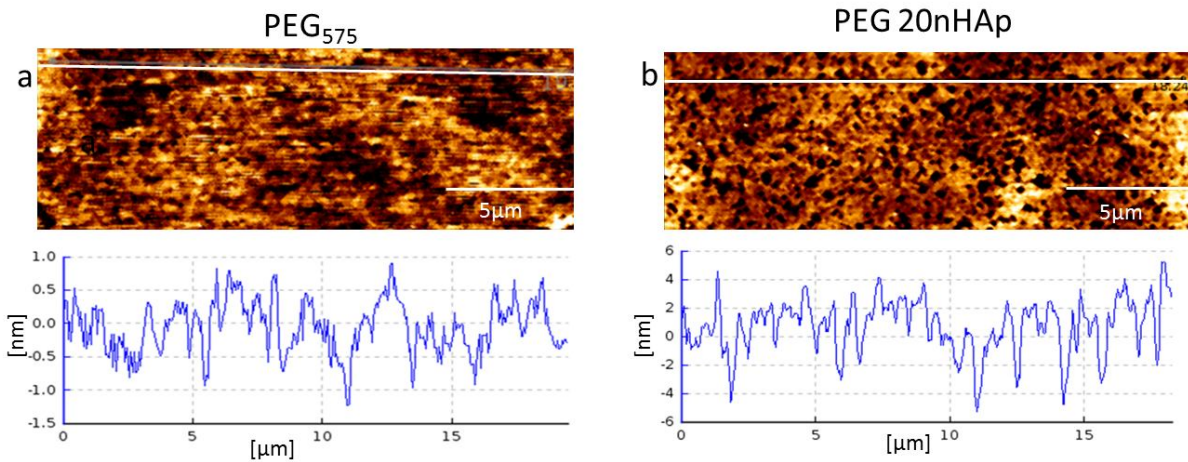
Figure 4: Surface Roughness in form of the Root-Mean-Square (RMS) value of (a) PEG$_{575}$ and (b) PEG 20nHAp in completely hydrated state.

4.3.2 Surface Patterning and Characterization

The general idea of the intended patterning process involving FIMIC production and selective HAp deposition from Simulated Body Fluid (SBF) is schematically depicted in Figure 5a. As shown two different FIMIC sample platforms are fabricated and compared. Those FIMIC platforms contain regions of pure PEG, which are in comparison stiff and bioinert as the

adjacent surface areas contain PEG HAp hydrogel composites and are rather soft and bioactive. As will be demonstrated, both physically mixed and chemically synthesized hydrogel composites (PEG HAp NPs and PEG nHAp respectively) were utilized in the FIMIC method in order to gain micropatterned surface structures, exhibiting defined areas with and without HAp presence. Subsequently, as fabricated FIMIC platforms were immersed into SBF up to 10 days in order to assess the locally controlled HAp deposition as final patterning step. Thus, it is intended to ascertain post-fabrication functionalization and to construct multiple-protein-affine substrates. Those are substrates, which exhibit different degrees of protein affinity on adjacent areas (may be in a regular pattern as for FIMIC platforms). Figure 5b depicts a schematic cross section of the fabricated FIMIC platforms which are chemically (introduction of HAp) and mechanically (different elasticity, see Table 1) patterned; either with PEG nHAp or with PEG HAp NPs. The hydrogel mold consists of pure PEG (only elements are Carbon, Hydrogen and Oxygen) and are cell anti adhesive, while the grooves contain Calcium and Phosphorus, are bioactive and are considerably softer than pure PEG in ultraviolet radiated state.
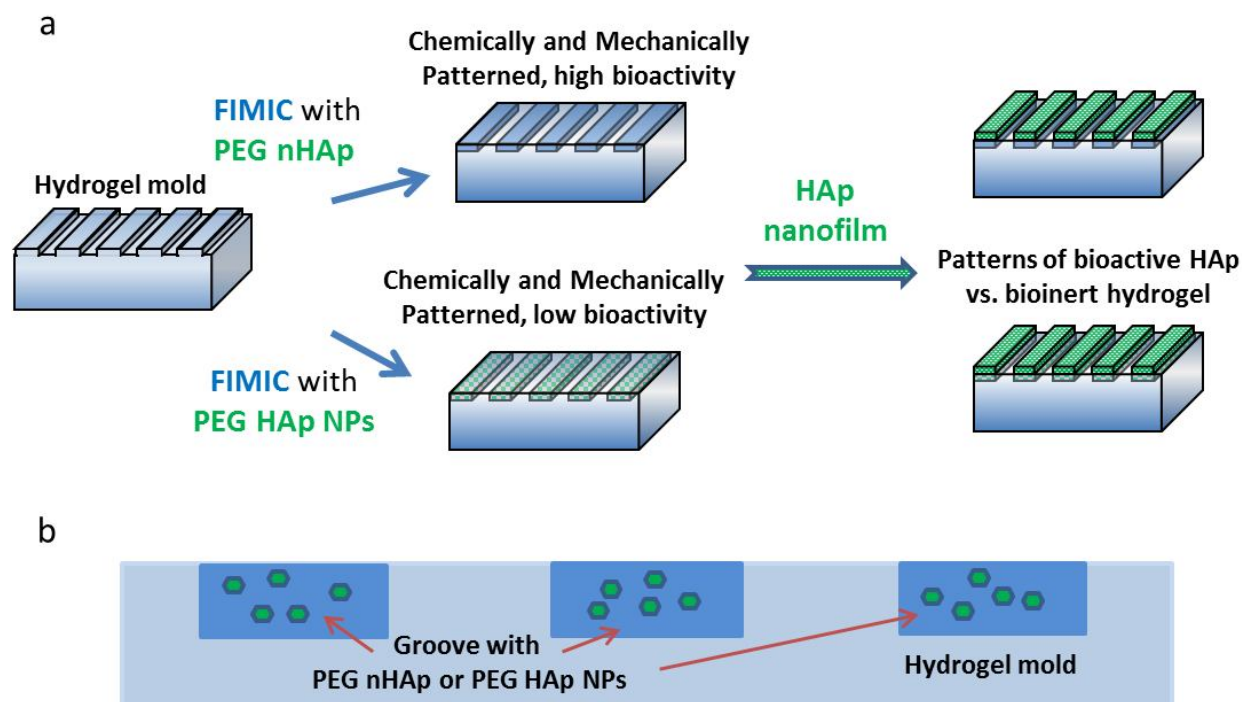
Figure 5: (a) Scheme of the intended patterning process involving FIMIC fabrication and HAp nucleation from SBF including PEG nHAp and PEG HAp NPs. (b) schematic depiction of FIMIC cross section.

FIMIC production (as shown in detail in chapter 2.3) is an easy bench-top method, which allows micrometer precise fabrication of hydrogel patterns suitable for the investigation of potential interface interactions. The application of this process with PEG HAp NPs proved to be straight forward; however the non-homogeneous nature of this class of physically interacting hydrogel composites demonstrated non-uniform HAp distribution as shown in Figure 6. Figure 6a displays two optical topviews of FIMIC substrates containing HAp NPs. The according PEG HAP NPs areas with according HAp NPs, visible as agglomerates, are indicated by the green arrows. Figure 6b depicts a SEM topview with indicated areas of EDX elemental analysis for Calcium (Ca) and Phosphorus (P) (areas 1 and 2). For area 1, both elements can be clearly detected, while in area 2 the absence of both is detected. Figure 6c shows a SEM cross section of Figure 6b investigating the volume distribution of HAp NPs within the PEG HAp NPs filled grooves via EDX analysis. For surface-near (area 3) and surface-far (area 4) areas, moreless equal amounts of

Calcium and Phosphorous can be measured implying a rather homogeneous distribution of HAp in the micro-scale.
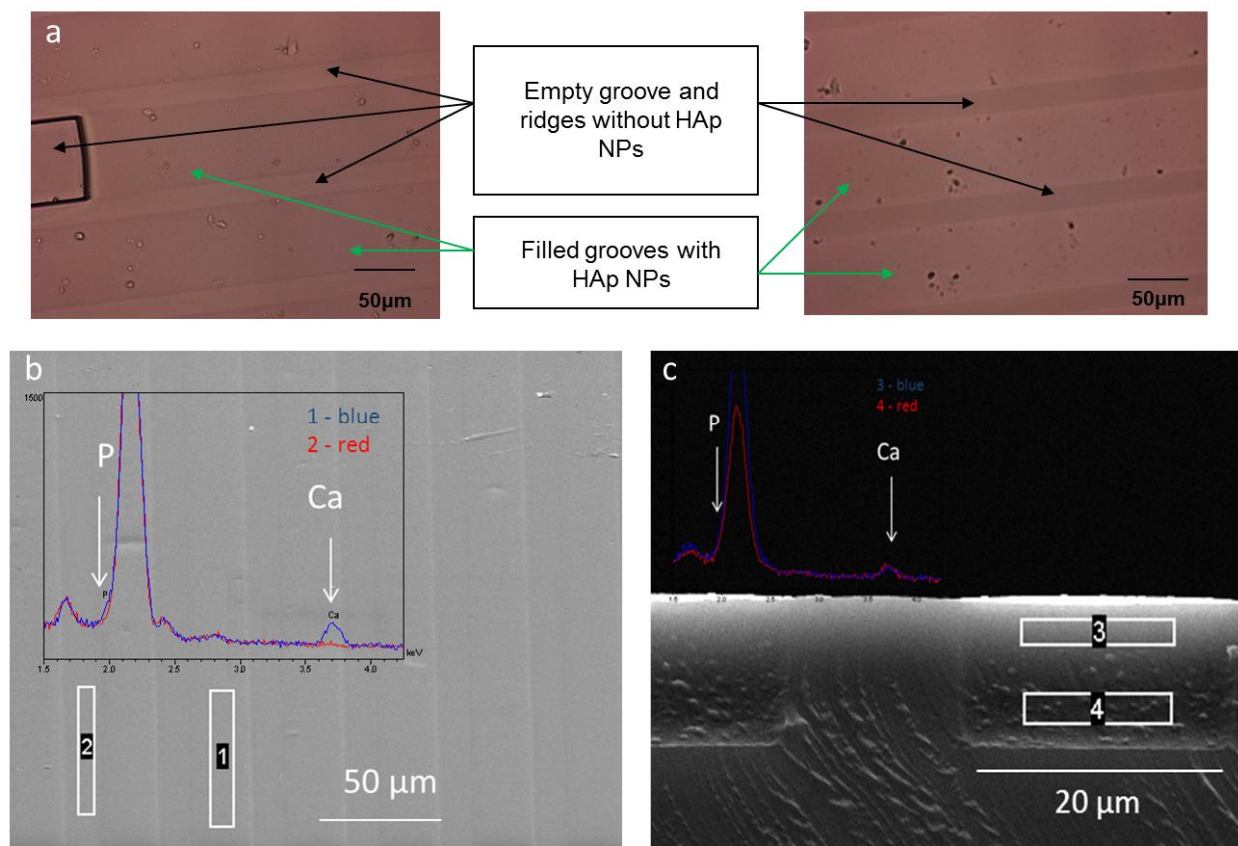
Figure 6: FIMICs containg PEG HAp NPs (a) optical image of FIMICs containing PEG HAp NPs with HAp agglomerates; (b) SEM image of FIMICs containing PEG HAp NPs with according EDX analysis from the top; (c) SEM image of cross-section of FIMICs containing PEG HAp NPs with according EDX analysis.

Even though the processed FIMIC platforms seem intact and well defined, still no final conclusion about successful HAp incorporation may be drawn. This is in particular the case when dealing with homogeneous HAp NPs distribution and surface accessibility in order to allow interface interaction. Some distributed HAp NPs agglomerates are detectable via optical microscopy, still precise control of amount and placing of HAp NPs is missing. In order to ascertain the difference of HAp incorporation of either hydrogel composite into the patterns,

SEM micrographs with according elemental mappings, namely of Calcium and Phosphorus were recorded (Figure 7). Distinction can be easily addressed, since elemental proof of Ca and P for PEG HAp NPs are restricted to the agglomerates or are of so little concentration that they fall below the threshold of detection (Figure 7a-c). On the contrary, homogeneous distribution covering the desired areas was achieved for PEG nHAp composites verifying the concept of homogeneously chemically functionalized 2D *Patterns of Elasticity* (Figure 7d-f). Thus it was possible to apply a novel hydrogel composite via soft lithographic processing regime, gaining spatial control of chemical patterns with micrometer precision.
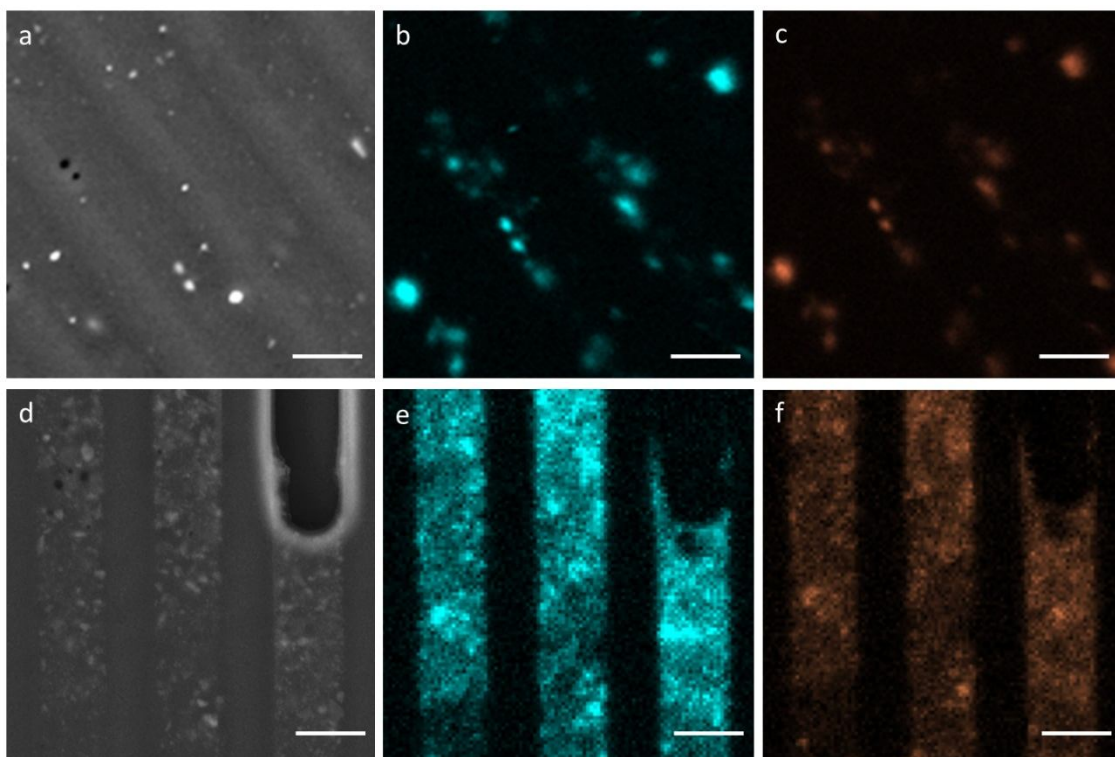
Figure 7: SEM micrographs and elemental mapping (Ca, P) of as prepared FIMIC platforms (PEG$_{575}$ PEG HAp NPs/PEG nHAp) containing physically mixed and chemically synthesized PEG-HAp composites. (a-c) physically mixed PEG HAp NPs composites (a) micrograph of FIMIC platform with PEG HAp NPs (b) Ca-map (c) P-map; (d-f) chemically synthesized PEG nHAp composites d) micrograph of FIMIC platform with PEG-nHAp composite; (e) Ca-map; (f) P-map; (scale bar 20 µm).

As concluding patterning step on FIMIC platforms, both sets of FIMIC substrates were incubated in SBF in order to achieve multiple-protein-affine surfaces and to assess the post-FIMIC fabrication patternability. Therefore, locally controlled, time-resolved HAp crystallite monolayer deposition with spatial micrometer precision was conducted to demonstrate the selective interface reactivity of the investigated FIMIC samples.

The general idea was to verify surface interaction potential, since HAp deposition from SBF requires nucleation sites (in general charged surface cues), not facilitated by the herein utilized PEG derived hydrogels[18,34,75]. Hence, any HAp deposition detectable can be attributed to chemical surface patterning with reactive ions from HAp domains. Therefore, pre-patterned FIMIC samples containing physically mixed PEG HAp NPs and chemically synthesized PEG nHAp hydrogel composites were immersed in SBF over a 2, 4, 6, 8 and 10 day period. Figure 8 displays the HAp crystallite deposition on PEG nHAp and PEG HAp NPs over several time spans. Figure 8a-e demonstrate the continuous homogeneous HAp deposition over time on PEG nHAp, in which Figure 8a depicts small isolated HAp nuclei after 4 days, Figure 8b the almost dense layer of single nuclei after 8 days and Figure 8c an uniform monolayer after 10 days. Figure 8d and Figure 8e confirm the density and monolayer morphology of the HAp nuclei, along with crystallite shape of the single HAp nuclei well known from literature[76–78]. Figure 8f displays the HAp deposition structure after 10 days on patterned substrates containing PEG-HAp NPs composite.

Precisely controlled spatial deposition of HAp nuclei from SBF over time on the as prepared FIMIC hydrogel patterns demonstrate the superior tailoring ability and versatility of the chemically synthesized hydrogel composite PEG nHAp over its physically mixed PEG HAp NPs counterpart. In contrast, even though HAp disposition to the designed areas could be observed, both, the non-uniformity of nucleated HAp crystallites together with the formation of large agglomerates verify the rather limited potential of PEG HAp NPs as platform for controlled interface interaction.

Consequently, this simple patterning method, combined with precise control of determining parameters yield common interest, since patterning via SBF deposition so far generally

generates perturbed interfaces[24], may only proceed after lavish processing[27] or result from transferred bioactive nanoparticles agglomerates[22].
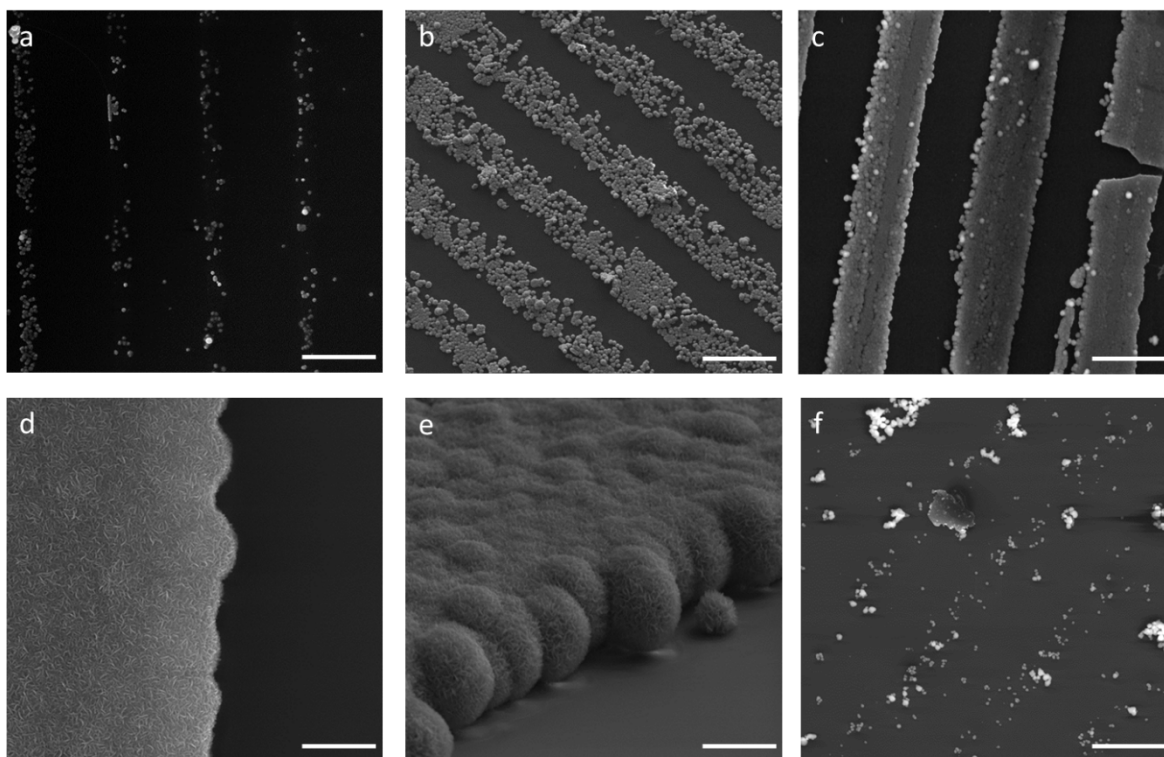
Figure 8: SEM micrographs of locally controlled time resolved HAp deposition from Simulated Body Fluid (SBF) on as prepared FIMIC platforms containing chemically synthesized hydrogel composites (PEG nHAp) and for comparison reason physically mixed hydrogel composites (PEG HAp NPs). (a-e) FIMICs containing PEG nHAp (a) HAp nuclei after 4 days of immersion in SBF; (b) HAp nuclei after 8 days of immersion in SBF; (c) HAp nuclei after 10 days of immersion in SBF; (d) HAp nuclei after 10 days of immersion in SBF - close up of interface; (e) HAp nuclei after 10 days of immersion-monolayer; (f)HAp nuclei and agglomerates on FIMIC containing PEG HAp NPs a after 10 days of immersion in SBF; (scale bar (a), (b), (c) and (f) 20 µm; scale bar (d) and (e) 2 µm).

4.3.3 Cell Adhesion of Fibroblasts and Osteoblasts on Fillmolding In Capillaries (FIMIC) Platforms Patterned with PEG nHAp

As preceding step to cellular response to biomaterials surfaces, proteins interact and may show more or less affinity towards the respective surface. In order to verify the anticipated differential protein adsorption pattern on either FIMIC platforms, the model protein Bovine Serum Albumin (BSA) was utilized to conduct protein adsorption measurements. It is well known from literature that BSA and calcium phosphates share electrostatic interaction between Ca^{2+} (HAp surface) and COO^- (protein surface), in particular when HAp exhibits amorphous characteristics [79,80] and may even impact the morphology of deposited HAp nuclei[77]. Hence, the experiment was designed to ascertain the accessibility of HAp domains to interface interaction, indispensable for successful chemical surface patterning.

As prepared FIMIC platforms with PEG HAp NPs and PEG nHAp were investigated and compared as shown in Figure 9. As expected, patterns exhibiting chemical composites PEG nHAp not only impart homogeneous BSA adsorption over the entire area functionalized with HAp, but possess in addition a precisely defined spatial interface of protein-repellent and protein-adhesive areas (Figure 9a-c). That makes the FIMIC platform a perfect tool for the investigation of selective protein adsorption experiments as well as for spatially controlled further functionalization with HAp affine chemical or biological cues.

Scrutinizing the adsorption pattern of proteins on composites containing PEG HAp NPs, a distinctively different image is gained. One can clearly see the HAp agglomerates as potential BSA adsorption sites (Figure 9d), however, no continuous HAp NPs incorporation can be determined as no homogeneous BSA adsorption pattern on the FIMIC substrate areas containing PEG HAp NPs can be detected (Figure 9e). This is in agreement with the findings depicted in Figure 7a-c, where Calcium and Phosphorus of PEG HAp NPs can only be detected locally as agglomerates; instead of a homogeneous distribution of HAp domains as for PEG nHAp (see Figure 7d-c). In some cases even, although the agglomerates are clearly visible in the optical image, no BSA adsorption can be noted, which can potentially be explained by a polymer

layer (cover) around the particles covering all potential sites of interaction. This can be seen in Figure 9f, in which the inset demonstrates the absence of any BSA adsorption in the investigated sample (inset of Figure 9f, image enlarged in appendix SI 1).

As consequence of the different BSA adsorption patterns for PEG nHAp and PEG HAp NPs, subsequent cell experiments with osteoblasts and fibroblasts were conducted on FIMIC platforms containing PEG 20nHAp. That formulation was selected due to the combination of highest degree in HAp incorporation yielding highest potential for cell adhesiveness and ease of pattern processibility.
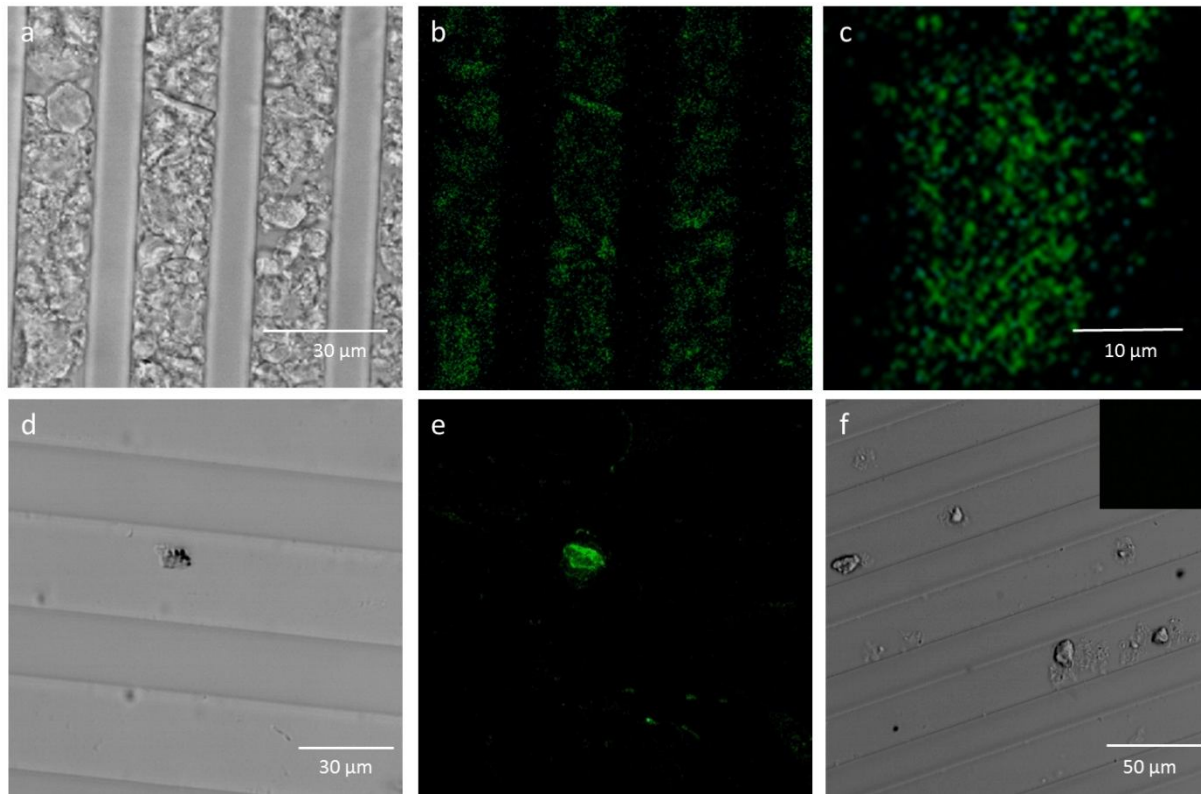
Figure 9: Confocal Laser Scanning Microscopy (CLSM) optical and fluorescent images of FIMIC platforms containing PEG NPs HAp and PEG nHAp hydrogel composites depicting selective adsorption of Bovine Serum Albumin (BSA). (a-c) PEG nHAp (a) optical image; (b) fluorescent image; (c) fluorescent image close up; (d-f) PEG NPs HAp composites (d)optical image depicting one large HAp and several small HAp clusters; (e) according fluorescent image depicting non homogeneous BSA adsorption; (f) HAp agglomerates visible within PEG NPs HAp but no BSA adsorption detectable (black inset).

The physical and mechanical properties of biomaterials surfaces impose great influence on cellular behavior[44,49,81], especially since cells respond to substrates exhibiting submicrometer-topographical features[46] and micrometer-sized tuned elasticity[82−84]. Therefore, it is of crucial importance to control the topographic and mechanical properties and determine these in hydrated state. This is of particular interest if, as in our case for PEG based hydrogels, one wants to assess the effectiveness of elastic and chemical patterning, which may be overruled by physical patterning as demonstrated by Lensen et al.[48].

In order to ascertain the physical and mechanical surface characteristics of as prepared FIMIC platforms, AFM was employed, assessing the topographic and elastic properties in dry and hydrated state (Figure 10). Among the great challenges in order to apply this technique in surface pattering proved to be the equilibration of the swelling level (and hence the swelling degree of the several hydrogels applied) of the investigated FIMIC platforms. While physical patterning in dry state exhibited values up to 300 nm in topography (Figure 10a), this was reduced to approximately 50 nm for samples in hydrated state (Figure 10c); an observation which is of extraordinary interest, since cellular spreading (positioning) may be dominantly guided by physical patterning such contact guidance. However, if topographic cues are in the sub-micrometer range, cells react chiefly to chemical ones, as demonstrated by Britland and colleagues[85]. This means that if the topographic features are in the nanometer range, the cellular response and subsequent adhesion patterns are dominated by the surface chemistry. In addition, incorporating two different sets of hydrogel systems (in this case PEG and PEG nHAp) result in mechanical patterning as characterized by AFM-based surface force spectroscopic experiments (according *Force-maps* denote areas of soft areas to light colour and stiff areas to dark colour) as stated in Figure 10b/d. These thus produced 2D *Patterns of Elasticity* exhibit micrometer-sized spatially controlled elastic properties and can moreover impart chemical cues (e.g. HAp), combining mechanical and chemical patterning, while simultaneously reducing topography to a minimum. These properties make FIMIC platforms with incorporated PEG nHAp a superb tool for scrutinizing the effect of mechanical and chemical patterning on interface interactions in the absence of topography.
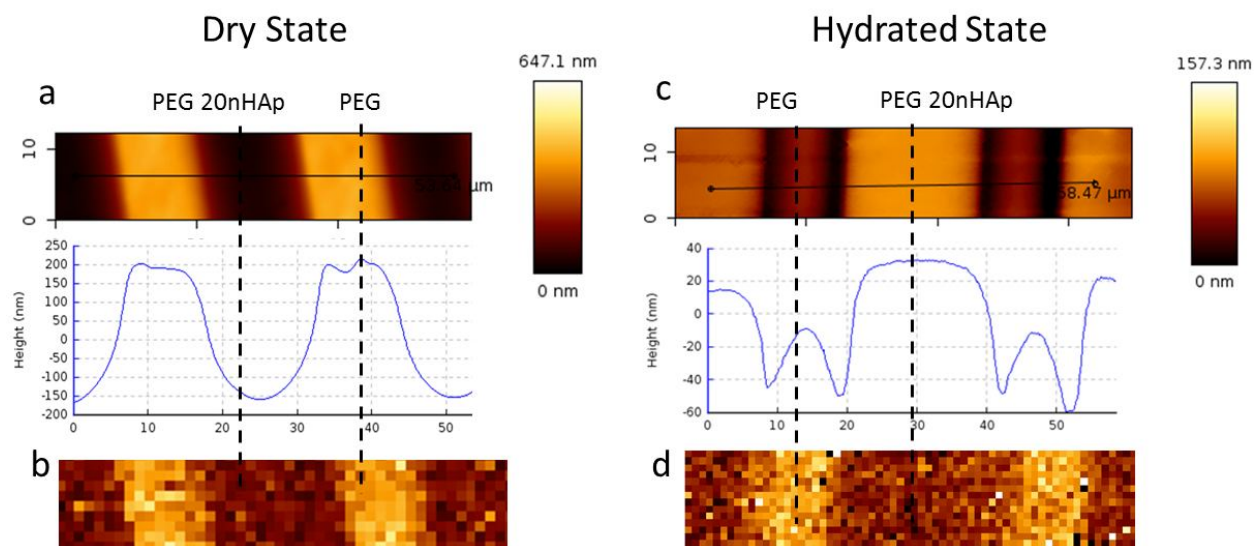
Figure 10: Topographical imaging of FIMIC platforms with PEG nHAp in dry (a) and hydrated state (c) with according force-maps (b/d), (if not differently stated, dimensions are in μm).

Since spatial control of cell-adhesion on biomaterials surface is essential, in this approach, locally controlled cell adhesion of two different kinds of cell-lines (I) osteoblasts (mouse osteoblast-like MC3T3-E1) and (II) fibroblasts (mouse fibroblasts L-929) is centered. Furthermore, it was intended to guide the cellular-adhesion along the FIMIC-structures containing HAp, since pure un-patterned PEG exhibits protein- and therefore cellular-repellent behavior.

In consequence of the data recorded during selective protein adsorption measurements, it was decided to investigate only those FIMIC platforms, which were fabricated with PEG nHAp due to the more homogeneous nature. Moreover, it was decided to work with two different kinds of cell lines, which exhibit different affinity towards calcium phosphates in order to elucidate the effectiveness of chemical patterning of the FIMIC substrates.

In order to compare cellular adhesion behavior of both cell types, osteoblasts and fibroblasts were seeded on the FIMIC platforms for 48 h and subsequently imaged with optical microscopy (data not shown) and SEM (Figure 11). The observed adhesion behavior demonstrates the

potential to control spatially guided cell-substrate interaction elicited via chemical patterning with PEG nHAp. The highly spread morphology of the osteoblasts on the FIMIC patterns indicate strong cell-substrate interaction and hence strong cell adhesion (Figure 11a-c). Furthermore, it can be noticed that the osteoblasts elongate along the trenches functionalized with HAp; this can be explicitly well noted in Figure 11a, in which three single osteoblasts adhere in parallel along the FIMIC pattern. This in contrary to investigations conducted with fibroblasts, which do not restrict interaction along the patterning structure (Figure 11c) and moreover exhibit round morphology (Figure 11d) implying only little affinity to the HAp patterned FIMIC substrate.

That is very interesting to note, since areas containing HAp are softer (see force map in Figure 10d). Under the presumption that cells preferentially adhere to stiffer areas than to softer as shown by Discher and co-workers[83,84], those findings may imply the overruling of mechanical patterning by chemical cues. Moreover can be excluded that one may potentially explain the different response patterns by the varying affinity towards surface roughness, since Kunzler et al. demonstrated that fibroblasts show greater tendency of adherence on smooth substrates than osteoblasts even though the experimental setup was in micrometer-range[45].
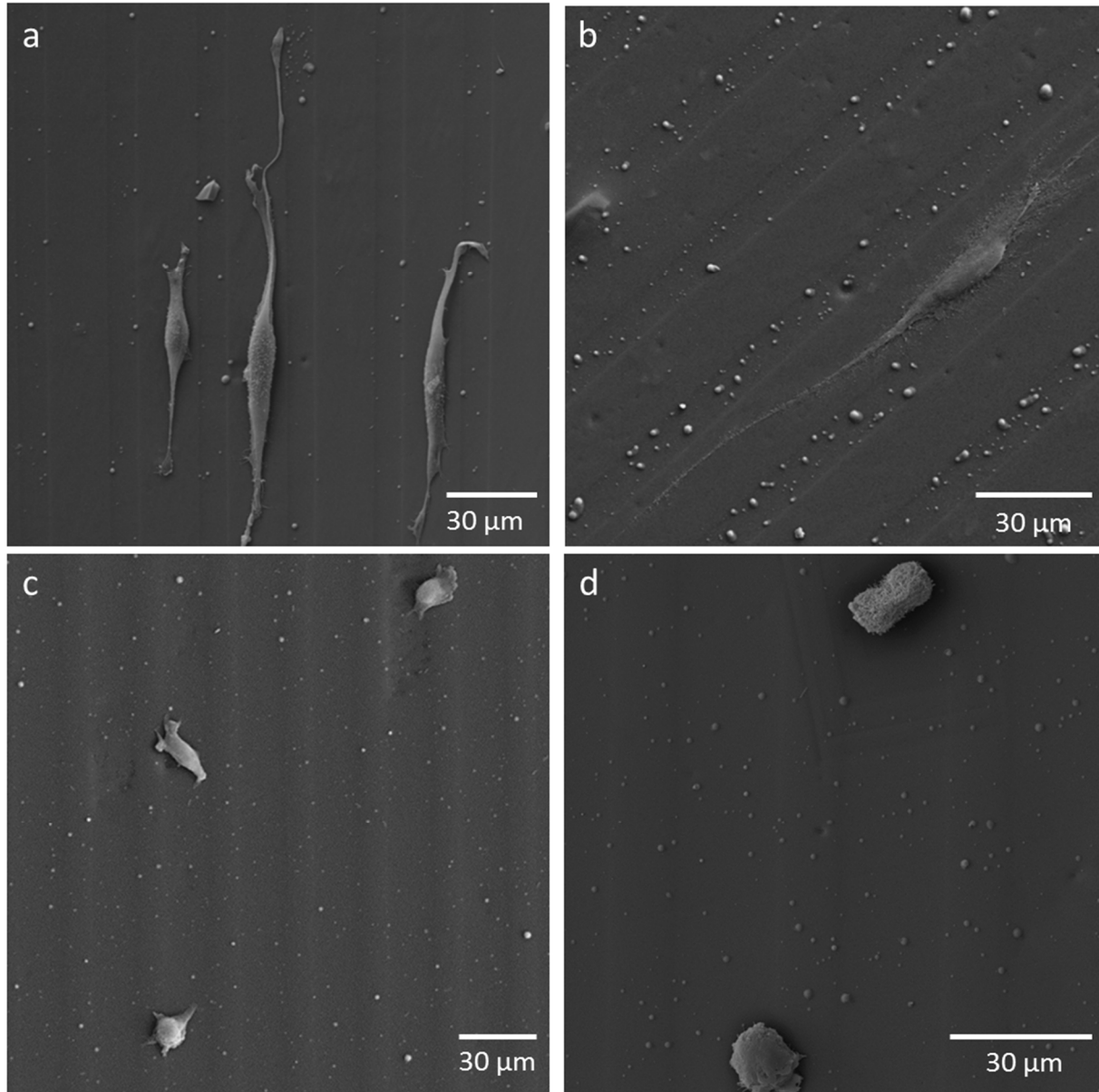
Figure 11: Scanning Electron Microscopy (SEM) images of osteoblast (a/b) and Fibroblast (c/d) –adhesion on FIMIC substrates containing chemically synthesized PEG-20nHAp composites. White globules are Sodium-phosphate (Na_3PO_4) from the nutrition solution during cell-culturing as determined via EDX analysis.

4.3.4 Summary

A new PEG - nHAp nanocomposite was successfully synthesized, characterized and micro-patterned with the recently developed soft lithographic Fillmolding In Capillaries (FIMIC) patterning method. In order to compare the effectiveness of chemical patterning, PEG nHAp was compared with a conventional, physically mixed hydrogel composite (PEG HAp NPs) regarding availability of HAp on the FIMIC surface, necessary for differential protein adsorption and localized control of post-fabrication functionalization with a HAp monolayer deposited from SBF. The spatial control over the HAp crystallite monolayer deposition creates an interesting tool for multiple-protein-affine materials enabling specific interface interaction. Furthermore, the ability to tune the deposited HAp concentration over time contributes to the precise control of the degree of surface functionality.

Ultimately, it could be shown, that osteoblasts and fibroblast display different adhesion behavior on the PEG nHAp FIMIC platforms. It could be demonstrated that osteoblasts, which display a high degree of affinity to calcium phosphates, adhere along the patterning structure of the FIMIC substrates and spread highly, while fibroblasts do not tend to align along the FIMIC pattern and show a rather round morphology, which can be attributed to weaker cell-substrate interaction.

It can be concluded, that the herein presented chemical hydrogel composite PEG nHAp possesses far superior potential to successfully introduce chemical patterning to biomaterials surfaces than the physically mixed PEG HAp NPs. This is due to its inherent homogenicity and processibility, which result in binary bioinert-bioactive PEG - PEG-HAp 2D patterns leading to differential cellular response depending on the cellular affinity towards HAp.

The author is convinced that the findings concerning the comparison between physical and chemical hydrogel composite materials may be generalized for many hybrid composite systems in biomaterials research, in particular in those in which precise control over surface properties and interfaces of biomaterials is a key issue.

Chapter 4.4

3D Patterned Reactive Mineralized Poly(ethylene glycol) Derived Hydrogels

Abstract

Providing decent replacement for bone or tendon defects remain one of the most challenging and demanding issues in the field of biomaterials research. In order to meet nowadays requirements, soft cytocompatible Poly(ethylene glycol) (PEG) based hydrogels with bioactive HAp were developed to fabricate porous and 3D patterned scaffolds with unique physicochemical and mechanical properties.

Post-gelation reactive 8armPEG based calcium phosphate nanocomposite hydrogels with homogeneously dispersed crystalline hydroxyapatite (HAp) nanodomains were fabricated via a novel in-situ synthesis procedure. Spontaneous gelation upon mixing of the Calcium and Phosphorous salt-solutions to the PEG-precursor solution indicate the formation of strong secondary bonding, yielding a novel self-assembly process responsible for the perfect homogenicity observed. In-situ Transmission Electron Microscopy (TEM) X-ray diffraction analysis revealed crystalline regions in the generally amorphous nature of the here presented composite system. Infrared- and RAMAN-spectroscopy as well as X-ray diffraction were conducted in order to verify the formation of HAp domains and to distinguish from other potential calcium phosphates. Ultraviolet (UV) radiation was applied in order to stabilize the formed nanocomposite hydrogel network under physiological conditions.

The strategy to synthesize well-defined nanocomposite biomaterials relies on the in-situ nucleation of varying amounts of HAp within the matrix of hydrogel precursors. The effect of HAp incorporation on as prepared PEG HAp hydrogel composite scaffolds were examined via compression testing and cell-testing, which were fabricated via freeze-drying and subsequent UV-radiation. Composite scaffolds exhibited interconnected 3D pore structures with pore-sizes

up to 500 micrometer allowing for vascularization and medium transport, decisive for successful tissue ingrowth.

Different amounts of HAp were incorporated in the PEG precursor matrix, from which hydrogel composites containing 20 wt% HAp (8PEG 20HAp) demonstrated to be most suitable for potential application in tissue engineering. They exhibit best structural properties, resulting in most appropriate mechanical performance and highest level of selective cellular response.

Attained data was gained in cooperation with the research group from Prof. Dr. Christian Rüssel of the Otto Schott Institute of the Friedrich-Schiller-University Jena, Germany (SEM images and EDX line Scan of Scaffolds) and the group of Prof. Su of the Department of Materials and Engineering of the Beijing Chemistry and Technology University, Beijing, China (optical microscopy of osteoblast adhesion on flat 8PEG 20HAp samples and according live-dead assay).

Loebus A+, Zhang Z+, Li Q, Strehmel C, Wisniewski W, Arafeh M, Rüssel C, Su Z, Lensen MC. 3D Patterned Reactive Mineralized Poly(ethylene glycol) Derived Hydrogels., *manuscript in preparation*

Incentives

Hydrogels are of great interest in various applications such as biotechnology, tissue-engineering and drug delivery due to their ability to take up water, porous structure and often found cytocompatible nature [86–91]. Among others, Poly(ethylene glycol)(PEG)-based hydrogels have been extensively explored as promising material for according applications [92–96]. However, despite the many advantages provided by PEG-based hydrogels they display insufficient mechanical rigidity and are therefore limited concerning an application as 3D matrix regarding tissue repair or scaffold in order to deliver cells or bioactive molecules [97]. Those drawbacks motivated in incorporation of a variety of nanoparticles (NPs), which aimed to improve the mechanical and biological properties such as laponite, hydroxyapatite (HAp) and silicate [98–101].

HAp NPs [53,55,102–105] and their bioactive characteristics[106–109] have been vastly investigated and are known to exert a strong impact on the final polymer-HAp composites systems, which find especial interest in hard tissue engineering related to bone or tendons [6,54,57,58,60].

In the herein presented approach, an in-situ nucleation process of HAp in a PEG-based hydrogel matrix exhibiting spontaneous gelation of a bioactive nanocomposite hydrogel is reported that not only overcomes the issue of homogeneous distribution of HAp NPs, which is a generally encountered problem[64], but also enables to precisely tune the mechanics, the cell response and the pore morphology.

Scaffolds fabrication and characterization have been in the focus of the hard-tissue engineering community for almost three decades. Modern scaffold design involves an entire library of novel requirements that are to be satisfied [110,111]. Porous interconnected structures support the diffusion of nutrients and waste as well as enable vascularization[112,113] . Such 3D fabricated devices offer an appropriate microenvironment for cells to adhere and proliferate or incorporate drugs to stimulate specific cellular responses[111,114–118] . However, major drawbacks encountered are inappropriate mechanical properties, toxic degradation products, ill-designed porous structure and insufficient biological performance. Several approaches of interpenetrating networks and composite hydrogels have been proposed in order to overcome

some of the limitations mentioned[99,115,119–124]. However, some of the material systems suggested are only poorly understood or only fulfill some but not all crucial requirements in a satisfactory manner [69].

In this study focus is laid on the fabrication of 3D macro-porous homogeneous nanocomposite hydrogels via an in-situ gelation process of hydroxyapatite (HAp)[53,55,102,105] domains utilizing PEG-based hydrogels matrix, which results in a materials system with precisely tunable properties in terms of bioactivity, elasticity and pore-structure. That routine avoids the common problem of agglomeration of HAp NPs[64] and furthermore enables the manufacture of scaffolds exhibiting large enough pore in order to allow for vascularization vital to successful 3D craft ingrowth [125,126].

Results and Discussion

4.4.1 Gel-formation

It was intended to fabricate 3D macro-porous, functionalizable homogeneous nanocomposite hydrogels via an in-situ gelation process of hydroxyapatite (HAp) domains utilizing Poly(ethylene glycol) (PEG)-based, namely 8PEG, hydrogel matrices. That results in a material system with precisely tunable properties in terms of pore-structure, elasticity, bioactivity, and post-gelation reactivity. Details to important material's properties are given in Figure 1.

material		Properties
Elastomer	**Star-shaped (8 arm)Poly-ethylene-glycol (8PEG)**	- hydrophilic - non-fouling - non-cytotoxic* **
Bio-mineral	**PEG-Hydroxy-apatite composite (8PEG-HAp)**	- patternable - UV-curable - non-cytotoxic** - cell-adhesive***

Figure 1: Materials properties of raw substances utilized in this project. Characteristics determined by following methods:* Colony forming assay (CFA), ** live dead assay, *** L-929 cells.

Successful 8PEG hydroxyapatite (8PEG HAp) nanocomposite gelformation was observed following the in-situ regime demonstrated in Figure 2. The salt solutions were given into reaction vessel and gelation was observed depending on the amount of NH_3 added. The obtained mineralized hydrogels were slightly opaque, almost transparent, easy processible and could be readily shaped to any desired form. As dipicted in Figure 2a, the pH value plays a critical role in the gelformation based on Michael type addition. It should be adjusted to around

9.8 in order to form stable hydrogel networks (more details of chemical principles are given in the PhD thesis of Zhenfang Zhang[2], a collaegue from the Lensen Lab). Hence, increased incorporation of HAp should also lead to accelerated gelformation, since the amount of injected NH_3 also augments. Nevertheless, this cannot be monitored, but it is rather observed that medium concentration of HAp and consequently NH_3 lead to quickest gelformation. That might implies the interference of HAp formation with Michael type addition chemistry (more detailed description of Michael type chemistry and reaction interpretation are stated in the PhD thesis of Zhenfang Zhang[2]). Proof for potential chealation of Ca^{2+} and PO_4^{2-} ions is not found, since neither the according FtIR- nor RAMAN-bands show any sign of shift. One can rather assume that the HAp nuclei form a sterical hindrance for the crosslinking points. The benefit of this reaction are on the one hand the reaction condition, allowing incorporation of biological cues, and on the other hand the avoidance of the common agglomeration problem, familiar to nanocomposites consisting of an inorganic and organic phase[64]. The in-situ nucleation of HAp domains in 8PEG leads to secondary interaction between both phases instead of pure mechanical entrapment of the inorganic filler phase in the polymer matrix.

Rheological measurements were conducted in order to access the gelation time in dependence of the HAp content (see table 1). Figure 2b depicts a representative example of a gelation time recording, which was determined as the crossover-point of the Storage Modulus (G′) and the Loss Modulus (G″). It was observed, that against intuition, there is no clear trend of gelation time with rising or falling HAp content. In contrast to expectations, 8PEG 20HAp (20 wt% HAp) showed the shortest gelation-time, which indicates strongest interaction between the salt solutions and the precursor 8PEG network. This is worth noticing, since the concentration of Calcium- or Phosphate-ions is considerably lower than in hydrogel composites containing 40 wt% HAp (8PEG 40HAp). It furthermore demonstrates that a minimum concentration of salt ions must be present in order to facilitate gelformation, since hydrogels with 10 wt% HAp (8PEG 10HAp) formed after approximately 18 h only, and were very soft in comparison to the other hydrogels with higher HAp content. Figure 2c sketches the proposed reaction scheme based on Michael type addition chemistry, in which HAp nucleates and matures in-situ, but does not play a vital role in the facilitation of hydrogel network formation.

Additional covalent binding of the model molecule SH-dye indicates the ability to bind chemical and biological cues posterior to network formation and processing via residual C=C bonds (proposed chemical mechanism can be found in PhD thesis of Zhenfang Zhang[2]).
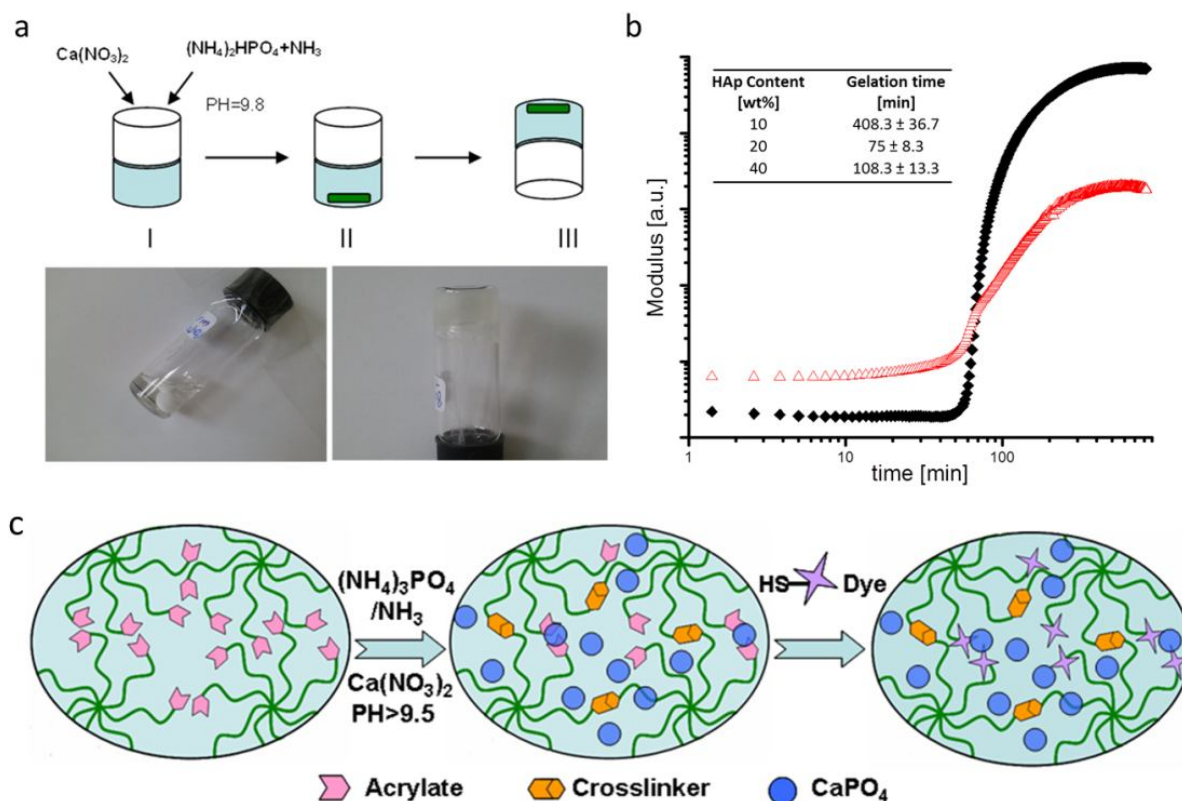
Figure 2: Gelformation process (a) gelformation during the reaction: (I) adding of Ca and P salts (II) maturation time under constant magnetic stirring (III) gelified 8PEG HAp composite hydrogel; (b) representative crossover recording of Storage and Loss Modulus during rheological measurement with according gelation times for the different 8PEG HAp hydrogel composites; (c) proposed gelation reaction scheme detailing the Michael type additon chemistry of the gelation reaction.

Chemical and morphological characterization was achieved via TEM, X-ray diffraction (XRD) and RAMAN spectroscopy (Figure 3).

In order to analyze the morphology of the as prepared nanocomposite gels, TEM imaging and in-situ electron diffraction was conducted (Figure 3a). One can clearly detect the crystallographic net-planes representing crystalline domains (white circle) of the composite. Electron diffraction helped identifying the corresponding net-planes assigned from the according Miller index reflections (002) and (211) and determining the respective net-plane distance to 2.84 Å and 3.41 Å [56].

XRD measurements (Figure 3b) can be ideally used in order to verify phase purity [56]. Here, it proved the presence of reflections typically assigned to HAp at 26 ° 2theta and 32 ° 2theta already ascertained via TEM diffraction verifying HAp presence in the nanocomposites. As shown, the intensity of the reflections increases with HAp content. As a consequence, 8PEG 10HAp is not depicted due to very small intensity of reflections in the according spectra. Furthermore, the spectra demonstrate that an increased incorporation of HAp also results in rising crystallinity of the HAp phase. However, for presented samples, XRD investigation imply very low crystallinity, untypical for HAp, as already indicated from in-situ TEM electron diffraction with only two reflections visible. Therefore, the Ca/P ration of the composite hydrogel was determined, which is generally considered a helpful tool discerning the different calcium phosphate phases. Hence, the observed low crystallinity of investigated composite hydrogel samples might be attributed to additional presence of Amorphous Calcium Phosphate (ACP). Energy Dispersive X-Ray diffraction (EDX) revealed a Ca/P ration of 1.35 ± 0.09 (n = 5) supporting the assumption of the presence of ACP, since ACP exhibits low Ca/P ration down to 1.18, as reviewed by Nancollas et al.[105] . This could be explained due to the fact that ACP is a precursor-phase for the formation of HAp during the nucleation process; moreover one should note that even calcium deficient HAp exhibits Ca/P values only down to 1.5.

Yet, final proof is delivered by RAMAN spectroscopy; bands existing at 965 cm^{-1} (attributed to HAp) and 1046 cm^{-1} (attributed to ACP) confirm the formation of HAp in 8PEG[56,62]. RAMAN spectroscopy enabled the identification of distinctive band peaks for HAp formation as depicted in Figure 3c. The recorded RAMAN spectra exhibit a rising peak at ca. 965 cm^{-1} with augmenting HAp content, which derives from a totally symmetric non-degenerated stretching mode of the

free tetrahedral phosphate ion. This is in agreement with literature, where this peak is widely recognized as identification site for HAp presence [56,61,62]. The spectrum of HAp NPs is additionally given for comparison. In addition, RAMAN spectroscopy allowed quantification of residual C=C double-bond (1636 cm^{-1}) decisive for post gelation reactivity (Figure 3d), revealing that for 8PEG 20HAp a 73 % of its initial amount of the C-double bonds are still accessible after gelation of the nanocomposite hydrogel. This demonstrates the superb potential to specifically tailor this unique nanocomposite material posterior to gelation.
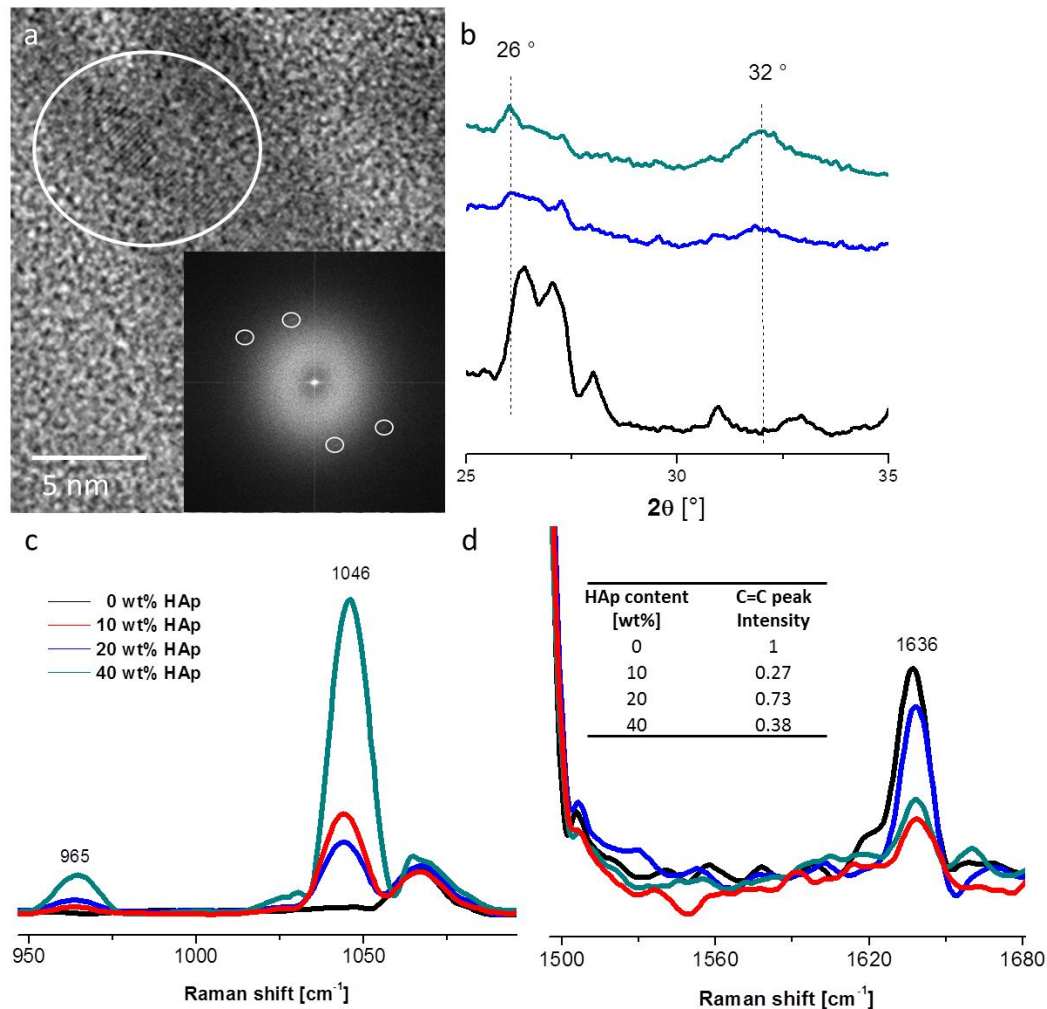
Figure 3: Chemical characterization of 8PEG HAp nanocomposites with varying composition. (a) TEM image of 8PEG 20HAp depicting crystalline areas (white circle) with corresponding-in-situ X-ray diffraction pattern; (b) Powder X-ray diffraction patterns displaying 8PEG 20HAp and 8PEG 40HAp; (c/d) RAMAN analysis of PEG HAp composite materials, demonstrating the existence of the HAp phase; Table in (d) states the residual quantities of C=C double bonds available for further post-gelation functionalization.

Thermogravimetric Analysis (TGA) (Figure 4) was primarily conducted in order to verify theoretically intended incorporated chemically bound HAp, but in addition revealed different amounts of physically and chemically bound water for varying HAp content (inset of Figure 3d).

Interestingly, 8PEG 20HAp exhibits the greatest amount of bound water and of residual mass after complete combustion at approximately 600 °C. This implies that composite hydrogels containing an optimum amount of HAp (8PEG 20HAp with 20 % HAp by weight) form the most homogeneous network, chemically binding the greatest amount of HAp. Surprisingly, 8PEG 40HAp theoretically designed with a stoichiometric amount 40 wt% HAp, exhibits a lower mass fraction of HAp after complete combustion than 8PEG 20HAp, which indicates an excess of Calcium and Phosphate in the salt solution interfering with hydrogel network formation of 8PEG. Otherwise, the residual HAp after complete combustion should be higher than that of 8PEG 20HAp. Apparently, no hydrogel network actively incorporating the entire amount of the Ca^{2+}- and PO_4^{2-}-ions could be established. The observed buckle at approximately 200 °C may be due to physical transitions such as vaporization or desorption of gaseous substances. The fact that 8PEG 20HAp displays the highest degree of mass loss at approximately 130 °C may be explained by the greatest degree of bound water. It is presumed that this is caused by the presence of HAp, which due to its inherent polar character can interact with molecular water and furthermore promote adsorption of physically bound water. This is supported by the absence of this buckle for pure 8PEG, only exhibiting polymer degradation. This assumption is further backed by the observation that for reduced presence of HAp (8PEG 10HAp) this buckle is hardly detectable. The monitored decline at 130 °C and leveling out at 600 °C is in coherence with the anticipated combustion process, since HAp presence is responsible for water binding and adsorption in the 8PEG network. TGA analysis supports RAMAN data, stating that 8PEG 20HAp seems to be the hydrogel composite exhibiting the greatest homogenicity and the highest degree of 8PEG - HAp interaction.
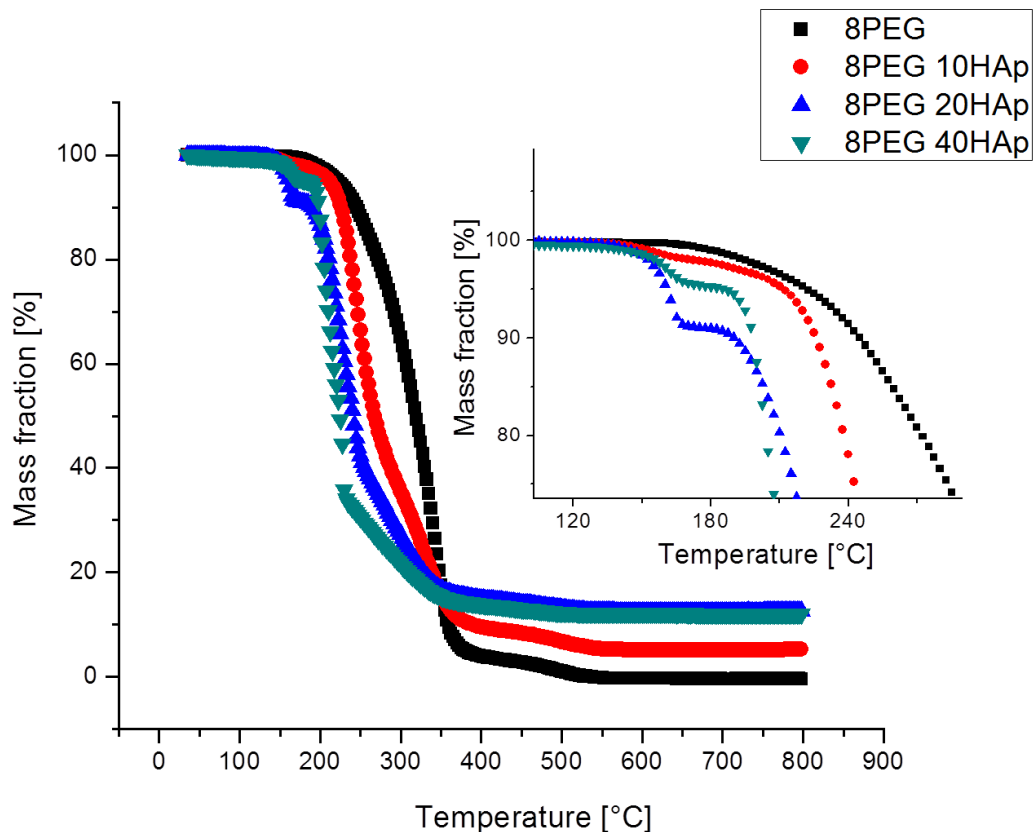
Figure 4: Thermogravimetric Analysis (TGA) measurements of 8PEG HAp hydrogel composites with varying HAp content.

In order to characterize the elemental distribution of Calcium and Phosphorus, Scanning Electron Microscopy (SEM) including EDX mapping was conducted as depicted in Figure 5. As a result, both elements were found largely homogeneously dispersed within the samples displaying areas of greater concentration (indicated by brighter colour, respectively) than in other areas. This was a little surprising, since perfectly homogeneous samples were expected. The observed result may be attributed to potential interactions between Ca^{2+} and PO_4^{2-} with the polymeric matrix during HAp maturation from ACP. However, no huge clusters or regions without Calcium and Phosphorus were detected. This is a characteristic, which underlines the novelty of the synthesis routine, preventing the clustering of the inorganic phase in hydrogel

composites produced, which is commonly observed in composites produced by the physical-mixing techniques[64].
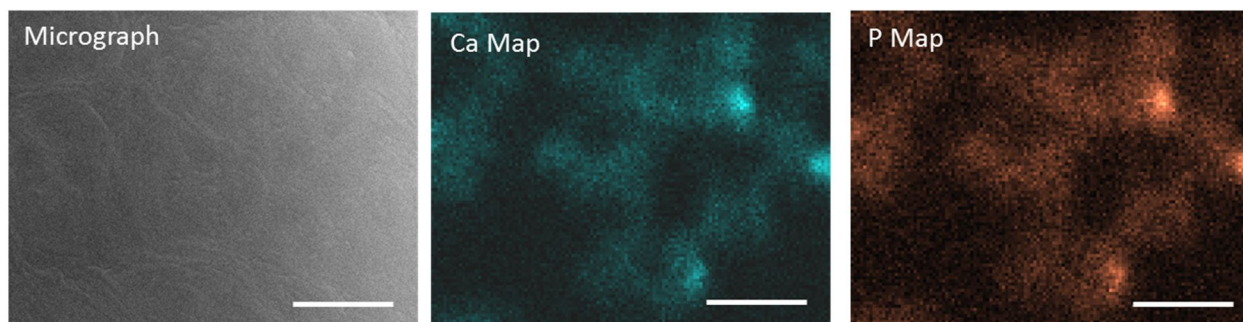

Figure 5: EDX Mapping of Calcium and Phosphorus demonstrates homogeneous distribution of HAp phase within the 8PEG matrix. (Scale bar 10 µm)

The readiness of incorporated HAp domains to chemically interact with the surface was tested and proven via the homogeneous adsorption of the model protein Bovine Serum Albumin (BSA) over the entire PEG 20HAp substrate surface (appendix SI 1). This supports the results from elemental mapping, since it was demonstrated that for PEG 20HAp a homogeneous elemental distribution of Ca and P over the entire sample could be monitored. This finding is in agreement with BSA adsorption experiments of PEG nHAp (see chapter 4.3 Figure 9.).

Mechanical characterization via tensile testing demonstrated increasing elasticity, strength and toughness (Table 1) with augmenting HAp incorporation. This finding may be explained by ionic interaction between the inorganic ions and the polymer matrix as well as higher NH_3 addition accompanying an increase of calcium phosphate addition.

Table 1: Summary of the main results of chemical and mechanical characterization of the various 8PEG HAp nanocomposites.

HAp Content [wt%]	Gelation Time [min]	Residual C=C double bonds [%]	Mechanical Characterization		
			Young's Modulus [MPa]	UTS [MPa]	Elongation at break [%]
0	n.d.	100*	n.d.	n.d.	n.d.
10	408.3 ± 36.7	27	0.24 ± 0.03	29 ± 1	58 ± 9
20	75 ± 8.3	73	0.41 ± 0.03	60 ± 2	32 ± 12
40	108.3 ± 13.3	38	0.51 ± 0.06	169 ± 10	67 ± 1

*theoretically normed

Concluding cytotoxicity tests were performed in order to demonstrate the cytocompatible nature of the here presented 8PEG HAp nanocomposite hydrogels (data not shown here, but in the PhD thesis of Christine Strehmel[3]).

4.4.2 3D Patterning of 8PEG HAp Hydrogel Composites

Porous, interconnected 3D scaffolds of reactive hydrogel composites were achieved via the freeze-drying technique. Optical microscopy revealed that different amounts of HAp enclosure yielded varying pore sizes and pore size structures, demonstrating precise tunability upon previous swelling and HAp content (Figure 6). Most promising results were attained for 8PEG 20HAp swollen for 15 min. Due to the time-dependent water uptake (data shown in appendix SI 2, details to experimental setup can be found in the PhD thesis of Zhenfang Zhang[2]), hydration was conducted in order to obtain homogeneous 3D interconnected structures. However, since water uptake properties for all presented hydrogel composites are in close resemblance, the monitored variations in the pore shapes with rising hydration time may be attributed exclusively to HAp content. Due to the bimodal pore pattern displaying pore dimensions

ranging around 300 μm and approximately 20 μm, vascularization and medium transport is enabled, necessary for tissue integration into the host, providing ideal ground for successful implant ingrowth.
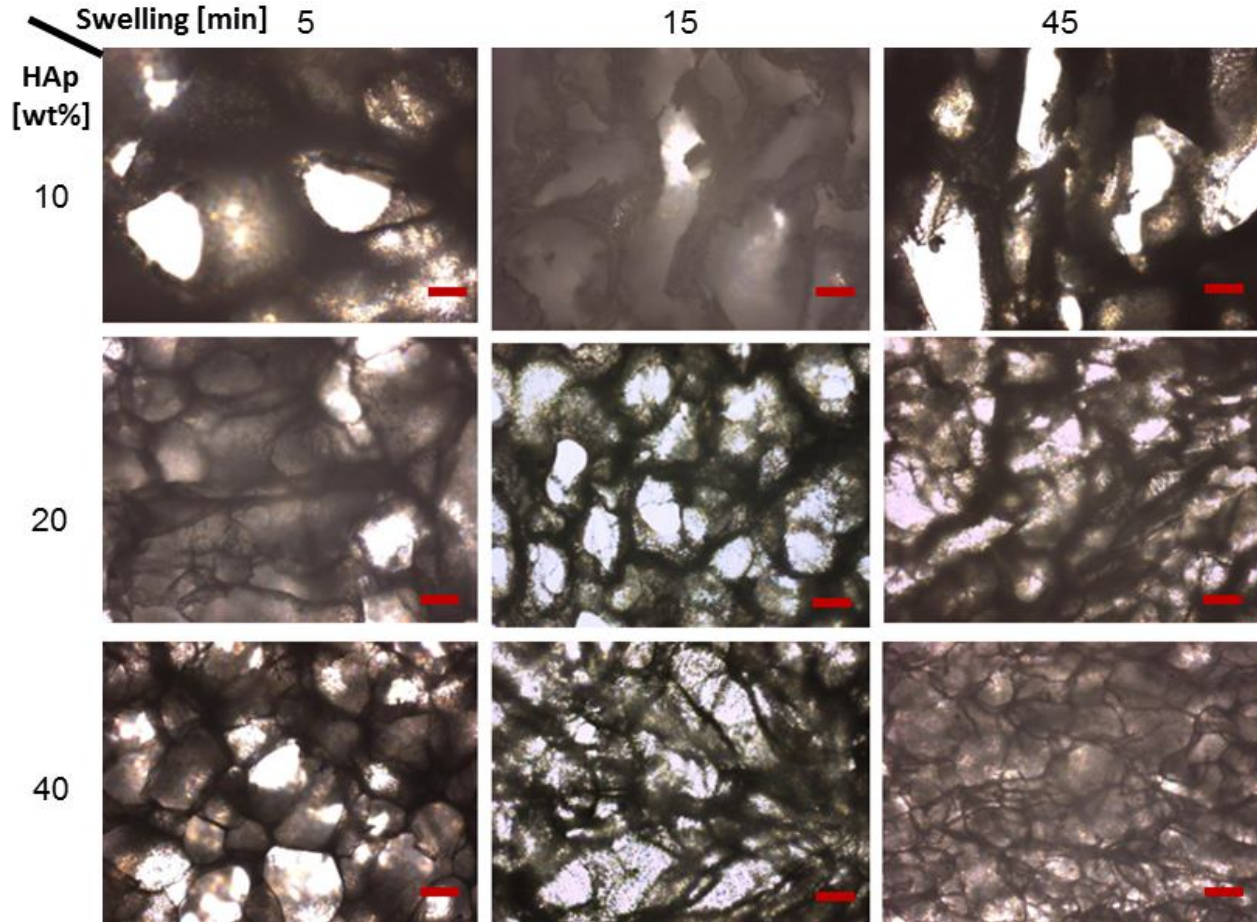
Figure 6: Optical images of a set of 3D scaffolds (fabricated via freeze-drying) with different amounts of incorporated HAp and different swelling times. (Scale bar 100 μm)

Patterned hydrogel composites exhibiting 15 min hydration time were investigated in more detail with SEM intending to identify the concrete pore shapes and sizes (Figure 7). Already observed bimodal interconnected pore structure for 8PEG 20HAp is verified as well as homogeneous round shaped bimodal pore shape structure (Figure 7c,d). The additional

detailed line scan EDX analysis for 8PEG 20HAp revealed varying intensities of Calcium and Phosphorus is depicted in Figure 7g, which is in agreement with EDX mapping of pure 8PEG samples (see Figure 5) (EDX line scan conducted by Dr. W. Wisnewski, FSU Jena). However, the persistent presence of both ions could be confirmed. Lower degree in regular pore shape implied by optical characterization (Figure 6) for 8PEG 10HAp, which exhibit rather oval shaped pore structures (Figure 7a,b) and irregular pore structure for 8PEG 40HAp (Figure 7e,f), respectively, is affirmed.
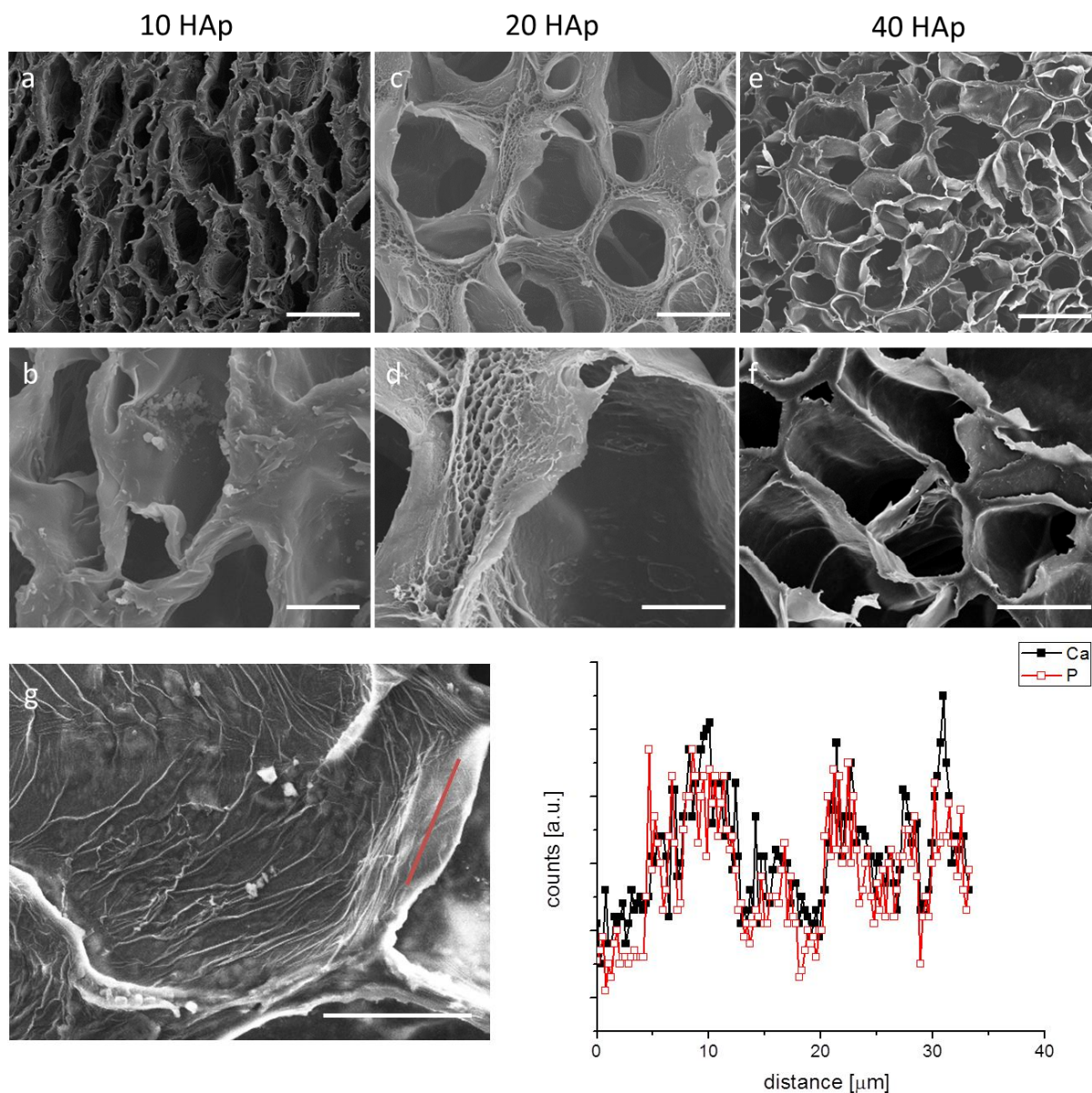
Figure 7: Scanning Electron Microscopy (SEM) images of 8PEG HAp composite scaffolds with varying HAp content and elemental scanning of Calcium (Ca) and Phosphorus (P). (a,b) porous structure of 8PEG 10HAp; (c,d) porous structure of 8PEG 20HAp; (e,f) porous structure of 8PEG; (g) Elemental line scan of Ca and P of 8PEG 20HAp. Scale bars (a),(c) and (e) 500 μm, (b),(d),(f) and (g) 50 μm, respectively.

In order to demonstrate the potential of post gelation reactivity of as fabricated composite scaffolds, a SH-dye as model molecule was employed, readily reacting with accessible C=C

double bonds from the 8PEG matrix (details to the chemical principles and an according chemical reaction scheme are given in the PhD thesis of the Lensen Lab colleague Zhenfang Zhang[2]). Figure 8 displays a 3D image (Figure 8a,b) with selected centering horizontal cross-section (Figure 8c-e), implying complete functionalization even in the interior (volume cross-section) indicating complete consumption of all residual C=C reaction sites. This proof of principle states that for any kind of functionality (e.g. biological or chemical cues), such 3D patterned hydrogel composites can be tailored precisely to the specific need. Furthermore, it can be claimed that the incorporation of inorganic ions do not interfere or impede with post-gelation functionalization. It should be noted, that the seemingly entire functionalization of the sample scaffold with the SH-dye demonstrates the interconnected nature of the pore structure, since medium transport facilitates the SH-dye transport and provides homogeneous distribution. Thus, SH-dye functionalization additionally serves as a model solution to illustrate potential biological medium transport in biological application.
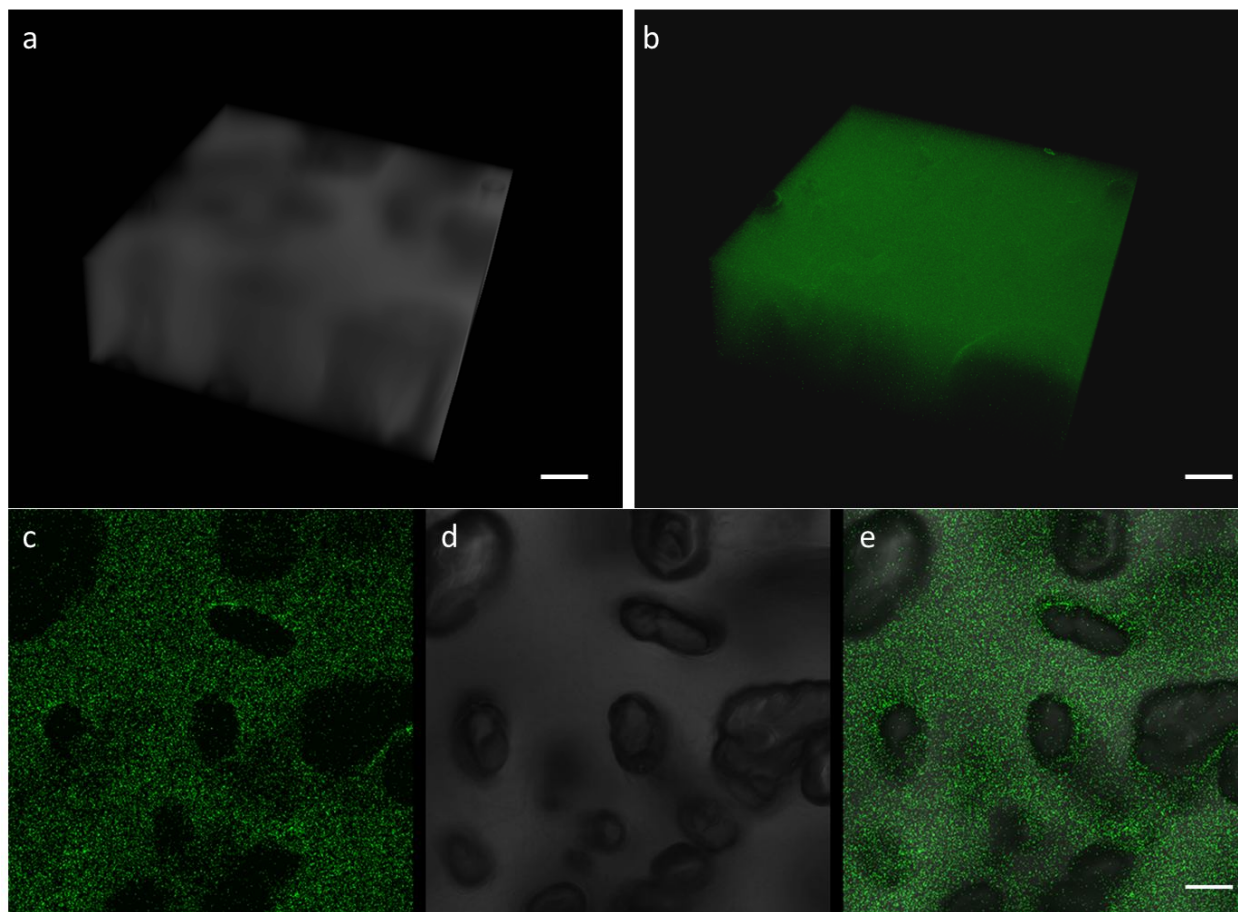
Figure 8: Confocal Scanning Laser Microscopy (CSLM) images (a,b 3D images, c-e volume cross-section) of a 3D patterned PEG 20HAp hydrogel composite, post-gelation functionalized with an SH-dye: (a) 3D optical image; (b) 3D fluorescent image; (c) cross section; (d) optical image; (e) overlay of fluorescent image and optical image. Scale bar 100 μm

As a consecutive step, it was investigated whether the model protein Bovine Serum Albumin (BSA) adsorbs on as prepared scaffolds (Figure 9). In consequence, it could be displayed that the composite hydrogel facilitates BSA adsorption, which is attributed to chemical interaction between Ca^{2+} (HAp surface) and COO^- (protein surface). Literature states in addition that BSA adsorption in particular is monitored when HAp exhibits amorphous characteristics [79,80] and beyond that may even impact HAp nucleation morphology[77]. The general idea of this experiment is to demonstrate the chemical accessibility of the HAp domains after scaffold formation, typical to chemical composites, in which the inorganic compound is not simply

entrapped within the polymer matrix, but rather covalently or electrostatically linked to the organic material.
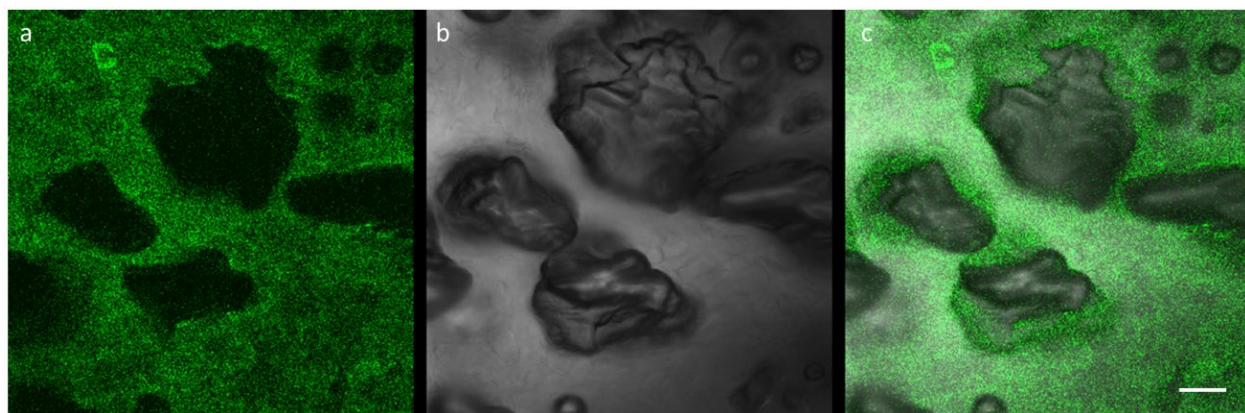

Figure 9: Confocal Scanning Laser Microscopy (CSLM) images of volume cross-section of Bovine Serum Albumin (BSA) adsorption in 8PEG 20HAp hydrogel composite scaffolds. (a) Fluorescence image; (b) Optical image; (c) overlay of Fluorescence image and Optical image. Scale bar 100 µm.

4.4.3 Chemically Cross-Linked 3D Interconnected Scaffolds

Radiation curing (e.g. UV radiation) represents another form of post gelation functionalization. In the course of this project, UV curing was conducted of as prepared 3D structured scaffolds. In consequence, 8PEG HAp scaffolds yield promising mechanical properties and resistance towards chemical degradation (e.g. hydrolysis). This leads to the formation of stable chemical crosslinks in the composite network, which durably stabilizes the system for application under physiological conditions (e.g. during cell experiments).

Mechanical testing in hydrated state of as prepared 8PEG HAp scaffolds was conducted via compression testing (Table 2). This method was chosen, since during potential application in tissue engineering, 3D structured crafts would most likely be exerted to compressive loading.

Although no significant distinction of the different examined 8PEG HAp composite hydrogels can be detected, still a clear trend towards strongest mechanical performance can be observed. That surprises, since enhanced amount of HAp incorporation was expected to lead to significant increase in mechanical strength and elasticity. However, it is still in agreement with water-uptake measurements (see appendix SI 3, experimental details, see PhD thesis of Zhenfang Zhang[2]), which demonstrate that 8PEG 20HAp exhibits the lowest degree of hydration with a pronounced plateau indicating an equilibrium hydration state after approximately 1.5 h. That supports the findings of compression testing, namely that out of the investigated 3D structures, 8PEG 20HAp scaffolds form the most homogeneous and robust hydrogel composite network. Hence, mechanical testing suggests that 8PEG 20HAp exhibits the tightest hydrogel network, which is in coherence with quantification of residual C=C double bonds by RAMAN spectroscopy (see Figure 3c,d).

Table 2: Compression testing of UV cured, fully hydrated 3D patterned hydrogel composite samples (n = 3).

HAp Content [wt%]	Young's Modulus [MPa]	Compression Strength [MPa]	Compression Strain [%]
10	2.94 ± 0.18	0.94 ± 0.07	39 ± 2
20	3.01 ± 0.08	1.23 ± 0.20	39 ± 3
40	2.13 ± 0.06	0.19 ± 0.04	49 ± 7

In conclusion of scaffold morphology characterization and mechanical investigation of UV cured 3D patterned 8PEG HAp hydrogel composite scaffolds, 8PEG 20 HAp was selected to ascertain the biological performance. Therefore, protein adsorption measurements with BSA and cellular investigation with different kinds of cell lines, namely osteoblasts (mouse osteoblast like MC3T3-E1) and fibroblasts (mouse fibroblasts L-929) were conducted. As expected, BSA adsorption still takes place homogeneously throughout the investigated scaffolds; however, some agglomerations of BSA occur and hence suggested HAp agglomerations are visible (Figure

10). One might assume that this observation is a result from molecular restructuring during the conversion from secondary interaction to covalent bonds during UV radiation (see appendix SI 4).
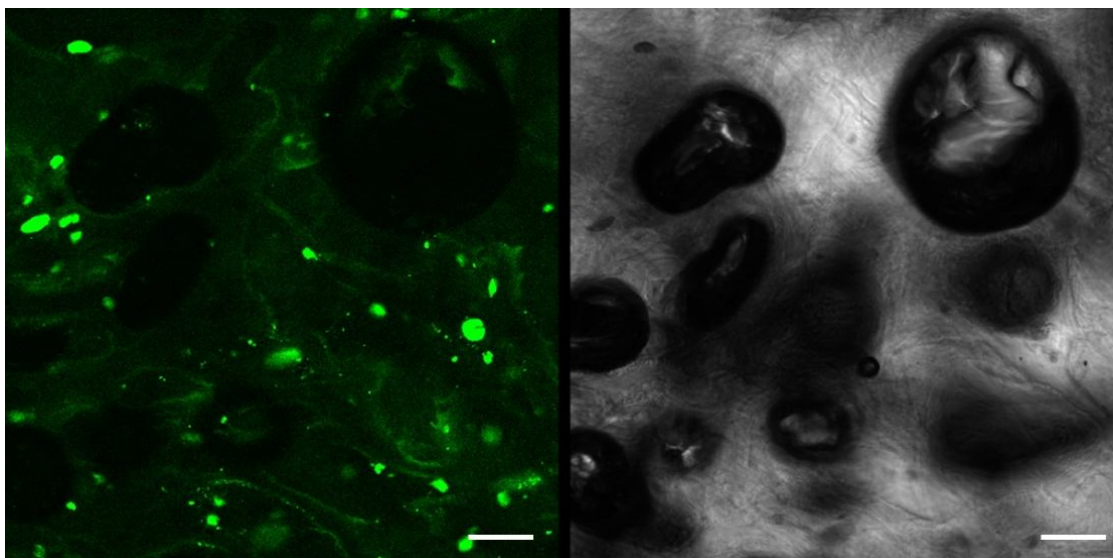

Figure 10: Confocal Scanning Laser Microscopy (CSLM) images of volume cross-section of Bovine Serum Albumin (BSA) adsorption in UV cured 8PEG 20HAp hydrogel composite scaffolds; (a) Fluorescence image; (b) Optical image. Scale bar 100 μm.

Preliminary to cellular investigation on UV-cured scaffolds, cellular adhesion measurements on flat, unpatterned 8PEG 20HAp samples were performed. The surface roughness of such samples was characterized via AFM (RMS 3.0 ± 0.7 nm over 160 μm^2 in fully hydrated state) in order to exclude topography as dominant cause for cellular adhesion. Investigation employing osteoblast-like cells as cell line for adhesion experiments (SI 5a) and cytotoxicity testing (SI 5b) via optical microscopy displayed a great number of spread cells over the entire sample, while only very few dead cells (dead cells are assigned in red in Figure SI 5b) after the live-dead assay could be monitored (viable cells are depicted in green in Figure SI 5b). This suggests strong adhesion of osteoblasts on 8PEG 20HAp substrates underlining the recognized bioactivity of

HAp as well as cytocompatibility of the here presented hydrogel composite (cell adhesion experiment cytotoxicity test conducted by the group of Prof. Su, China).

In order to show the differences of adhesion between different kinds of cell-lines exhibiting varying affinity towards calcium phosphates, fibroblasts and osteoblasts respective adhesion behavior and spreading pattern was monitored via SEM (Figure 12 and Figure 13 respectively). The general idea of this approach was to verify the feasibility of HAp incorporation into the 8PEG scaffolds. A significantly greater number of adhered osteoblasts were observed as shown in Figure 12. Almost carpet-like covering presented by osteoblasts (Figure 12a,b) is in contrast to distributed cluster-like appearance of fibroblasts (Figure 12c) on the 3D structured substrates.
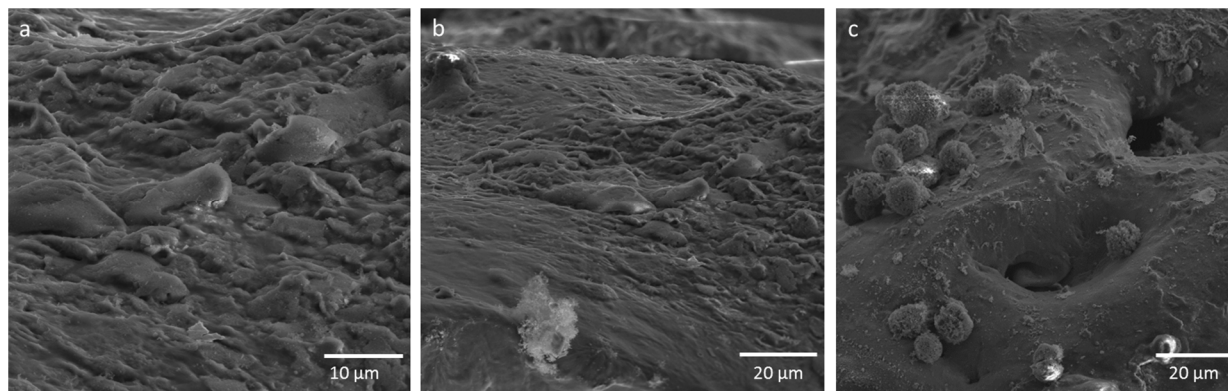
Figure 12: Adhesion characterization via Scanning Electron Microscopy (SEM) images of UV cured 3D patterned PEG 20HAp composite hydrogels with different cell types: (a,b) osteoblasts (mouse osteoblast like MC3T3-E1); (c) fibroblasts (mouse fibroblasts L-929).

It was revealed that osteoblasts exhibit a great degree of spreading characterized by the flat elongated morphology depicted in Figure 13a-c. Moreover, hardly any cell clustering can be observed. This relates to strong interaction between cell and substrate as well as to great affinity of the cells towards the scrutinized platform. Fibroblasts however do not exhibit the same degree of interaction, which is confirmed by the rather round morphology and apparent

tendency towards cell clustering (Figure 13 d-f). This can be explained by the widely recognized affinity of osteoblasts towards calcium phosphates. Thus, it could be displayed that chemical functionalization by HAp incorporation yields a direct effect on cellular reaction, demonstrating the feasibility of this approach and the potential for specific application in bone or tendon tissue engineering.

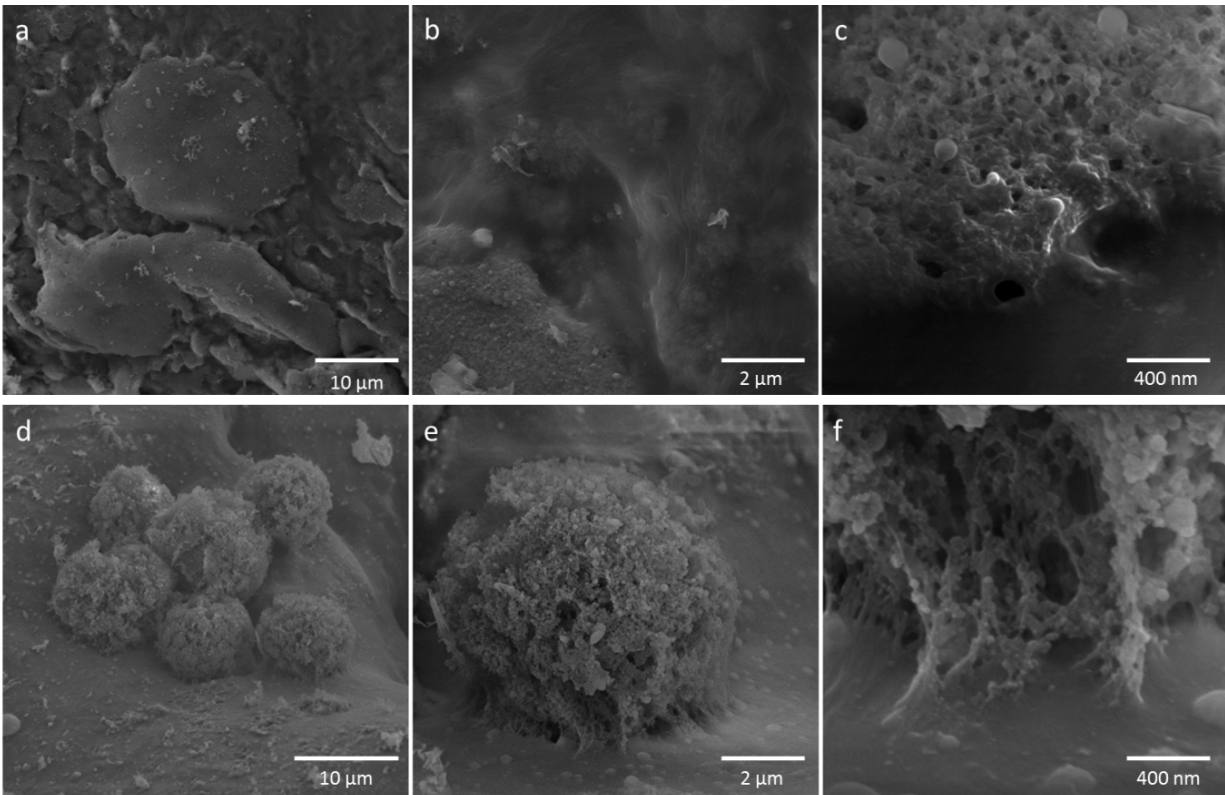Figure 13: Spreading analysis of osteoblasts (mouse osteoblast like MC3T3-E1) and fibroblasts (mouse fibroblasts L-929) via Scanning Electron Microscopy (SEM) imaging of UV cured 3D patterned PEG 20HAp composite hydrogels: (a-c) osteoblasts; (d-f) fibroblasts.

4.4.4 Summary

A new PEG – HAp nanocomposite was successfully synthesized, characterized and 3D patterned, designed for potential application in tissue engineering. The 3D structured post fabrication functionalizable star PEG HAp hydrogel composite (8PEG HAp) scaffolds were manufactured via freeze drying. The ability to be functionalized after gelformation yields the promising potential for the produced interconnected 3D structures to incorporate a wide range of biological or chemical cues for targeted applications. This was proven twofold; first, readiness of HAp accessibility via the adsorption of the model protein BSA and second, the cleavage of a model molecule in form of an SH-dye to residual $C=C$ double bonds verifying the ability of post-gelformation functionalization. That confirms that even after the formation of the porous crafts, 8PEG HAp hydrogel composite scaffolds maintain the post functionalization characteristic. The combination of novel chemical properties and processibility to a 3D design exhibiting pore structures necessary for vascularization and medium transport impart the potential of concerted application in tissue engineering. In addition can be stated that the clear distinction between observed adhesion patterns of osteoblasts and fibroblast demonstrate the successful chemical patterning with HAp as well as the ability of the herein presented scaffolds to distinguish between cell types possessing different affinities to calcium phosphates.

Chapter 5

Conclusion and Outlook

The general objective of this thesis marks the spatial control of cell - substrate interaction via concerted patterning strategies, and in consequence, to gain the ability of guided cell adhesion behavior on platforms for potential biomedical applications. In order to attain this purpose, two fundamentally different patterning approaches, namely surface patterning via a soft lithographic regime, Fillmolding In Capillaries (FIMIC) in chapters 4.1, 4.2 and 4.3 and 3D fabrication of scaffolds for potential tissue engineering in chapter 4.4 were employed. Nevertheless, both strategies have the same principal objective in common; controlled cellular interaction on specifically designed substrates, chemically patterned with calcium phosphates, which may favor osteoplastic cell type over fibroblastic ones. Chapter 4.3 and 4.4 demonstrate the successful achievement of these goals.

As main result of the FIMIC related research of this thesis, one should consider the controlled osteoblast adhesion on specifically designed FIMIC platform areas, while fibroblasts do not exhibit a notable pattern of interaction. The observed effect was solely obtained due to successful localized introduction of hydroxyapatite (HAp) nanodomains into the micropatterned systems. Two fundamentally different composite processing routes were applied and compared regarding homogenicity and accessibility of HAp eliciting increased osteoblast response for controlled cellular adhesion guidance. Those routes contained on the one hand the physical introduction of pre-prepared HAp nanoparticles (NPs) into linear Poly(ethylene glycol) (PEG) matrices (PEG HAp NPs) and on the other hand the production of a novel chemical PEG HAp hydrogel composite (PEG nHAp). It could be demonstrated that if both composite materials were incorporated in the FIMIC fabrication, PEG nHAp would, due to its inherent homogeneous nature, possess much greater potential to exert controlled cellular reaction than the physically mixed hydrogel composite PEG NPs HAp. Consequently, produced substrates exhibiting localized chemical functionalization were applied in cell studies with osteoblasts and fibroblasts demonstrating the potential of the fabricated FIMIC platforms to differentiate between distinct

cell types possessing varying affinities to calcium phosphates. This is underlined by the fact that to the best of the author's knowledge, topographic influence on cell adhesion patterns can be ruled out due to the leveled out physical nature of the presented FIMIC platform. Moreover, it could be shown that the post fabrication patterning ability of FIMIC samples patterned with PEG nHAp is far superior to those of PEG NPs HAp, proved via precise spatial control of HAp nucleation from Simulated Body Fluid resulting in sharp surface interfaces on prepared multiple-protein-affine substrates (substrates which exhibit areas with different degrees attractiveness adjacent to another), detailed in chapter 4.3.

The second part concentrates on the 3D fabrication of post fabrication functionalizable star PEG HAp hydrogel composite (8PEG HAp) scaffolds designed for potential tissue engineering application. The ability to be functionalized after gelformation yields the promising potential for the produced interconnected 3D structures to incorporate a wide range of biological or chemical cues for targeted applications. Even after the formation of the porous crafts via freeze drying, 8PEG HAp hydrogel composite scaffolds maintain the post functionalization characteristic. This conjuncture of novel chemical properties and processibility to a 3D design exhibiting pore structures necessary for vascularization and medium transport impart the potential of concerted application in tissue engineering. In addition can be stated that the clear distinction between observed adhesion patterns of osteoblasts and fibroblast demonstrate the successful chemical patterning with HAp as well as the ability of the herein presented scaffolds to distinguish between cell types possessing different affinities to calcium phosphates.

The FIMIC platforms still yield the problem of delamination in hydrated state, an issue that remains to be solved in order to make it a multifunctional device for any desired hydrogel combination. An inherent problem to patterned platforms via soft lithography remains the hydration characteristic of hydrogels, which may always differ to some extent leading e.g. for the same type of FIMIC to slight changes of topographies in nanometer range. Thus, regarding FIMIC substrates, careful characterization via AFM is generally recommended in order to exclude the topographic effect as driving force for cell - substrate interaction.

Scaffolds fabricated via freeze drying generally yield the disadvantage of unsuitability to minimal invasive therapies. However, the author is convinced that the system of 8PEG HAp possesses the potential to form 3D crafts with precisely controllable physical and mechanical properties after syringe ejection.

A concluding experiment for both presented strategies might be the joint seeding of osteoblast and fibroblast, which may demonstrate the dominant adhesion pattern of osteoblasts, or at best over time, display an expulsion process of fibroblast due to a lower degree of interaction with the substrate.

References

1.   Dunlop, J. W. C. & Fratzl, P. Biological Composites. *Annual Review of Materials Research* **40**, 1–24 (2010).

2.   Zhang, Z. Synthesis and Properties of Eight-arm Poly(ethylene glycol) Based Hydrogel for Biomaterial Research. (2013).

3.   Strehmel, C. title to be determined. (2013).

4.   Williams, D. F. *Definitions Biomaterials*. **242**, 72 (Elsevier: Amsterdam, 1987).

5.   Wintermantel, E. & Ha, S.-W. *Medizintechnik Life Science Engineering*. *Science* **5. Auflage**, (Springer-Verlag: 2009).

6.   Ratner, B. D., Hoffman, A. S., Schoen, F. J. & Lemons, J. E. *Biomaterials Science: An Introduction to Materials in Medicine*. *Journal of Clinical Engineering* **22**, (Elsevier Academic Press: 2012).

7.   Alves, N. M., Pashkuleva, I., Reis, R. L. & Mano, J. F. Controlling cell behavior through the design of polymer surfaces. *Small* **6**, 2208–20 (2010).

8.   Wheeldon, I., Farhadi, A., Bick, A. G., Jabbari, E. & Khademhosseini, A. Nanoscale tissue engineering: spatial control over cell-materials interactions. *Nanotechnology* **22**, 212001 (2011).

9.   Diez, M., Schulte, V. A., Etti, P. A., Ventre, M. & Lensen, M. C. Molding Micropatterns of Elasticity on PEG-based Hydrogels to Control Cell Adhesion and Migration. *Advanced Engineering Materials* **13**, B395–B404 (2011).

10.   Kloxin, A. M., Kloxin, C. J., Bowman, C. N. & Anseth, K. S. Mechanical properties of cellularly responsive hydrogels and their experimental determination. *Advanced Materials* **22**, 3484–94 (2010).

11.   Xia, Y. & Whitesides, G. M. Soft Lithography. *Annual Review of Materials Science* **28**, 153–184 (1998).

12.   Meldrum, F. C. & Cölfen, H. Controlling Mineral Morphologies and Structures in Biological and Synthetic Systems. *Chemical Reviews* 4332–4432 (2008).

13. Palmer, L. C., Newcomb, C. J., Kaltz, S. R., Spoerke, E. D. & Stupp, S. I. Biomimetic Systems for Hydroxyapatite Mineralization Inspired By Bone and Enamel. *Chemical Reviews* 4754–4783 (2008).

14. Gross, K. A. & Berndt, C. C. Thermal processing of hydroxyapatite for coating production. *Journal of Biomedical Materials Research* **39**, 580–7 (1998).

15. Bigi, a., Boanini, E. & Rubini, K. Hydroxyapatite gels and nanocrystals prepared through a sol–gel process. *Journal of Solid State Chemistry* **177**, 3092–3098 (2004).

16. Boccaccini, A. R., Minay, E. J. & Krause, D. Bioglass® Coatings on Superelastic NiTi Wires by Electrophoretic Deposition (EPD). *Key Engineering Materials* **314**, 219–224 (2006).

17. Kmita, G., Stoch, J., Jastrze, W., Stoch, A. & Broz, A. Electrophoretic coating of hydroxyapatite on titanium implants. *Journal of Molecular Structure* **596**, 191–200 (2001).

18. Abe, Y., Kokubo, T. & Yamamuro, T. Apatite coating on ceramics , metals and polymers utilizing a biological process. *Journal of Materials Science: Materials in Medicine* **1**, 233–238 (1990).

19. Stigter, M., De Groot, K. & Layrolle, P. Incorporation of tobramycin into biomimetic hydroxyapatite coating on titanium. *Biomaterials* **23**, 4143–53 (2002).

20. Liu, Y., Hunziker, E. B., Randall, N. X., De Groot, K. & Layrolle, P. Proteins incorporated into biomimetically prepared calcium phosphate coatings modulate their mechanical strength and dissolution rate. *Biomaterials* **24**, 65–70 (2003).

21. Zhu, P., Masuda, Y. & Koumoto, K. The effect of surface charge on hydroxyapatite nucleation. *Biomaterials* **25**, 3915–21 (2004).

22. Luz, G. M., Boesel, L., Del Campo, A. & Mano, J. F. Micropatterning of bioactive glass nanoparticles on chitosan membranes for spatial controlled biomineralization. *Langmuir* **28**, 6970–7 (2012).

23. Matsumoto, T., Ozawa, N. & Yao, T. Micropatterning of Apatite by Using $CaO-SiO_2$ Based Glass Powder Dispersed Solution. *Key Engineering Materials* **254-256**, 911–914 (2004).

24. Okada, H., Yamaguchi, S., Hasegawa, S., Neo, M. & Nakamura, T. Development of Apatite Micropattern Test Specimen for Cell Operation. *Key Engineering Materials* **309-311**, 663–666 (2006).

25. Ozawa, N. & Yao, T. Micropattern formation of apatite by combination of a biomimetic process and transcription of resist pattern. *Journal of Biomedical Materials Research* **62**, 579–86 (2002).

26. Shi, J., Alves, N. M. & Mano, J. F. Thermally Responsive Biomineralization on Biodegradable Substrates. *Advanced Functional Materials* **17**, 3312–3318 (2007).

27. Pittrof, A., Bauer, S. & Schmuki, P. Micropatterned TiO_2 nanotube surfaces for site-selective nucleation of hydroxyapatite from simulated body fluid. *Acta Biomaterialia* **7**, 424–431 (2011).

28. Farshchian, B., Choi, J., Amirsadeghi, A., Lee, J. & Park, S. 3D nanomolding for lab-on-a-chip applications. *Lab on a Chip* **12**, 4764–71 (2012).

29. Tekin, H., Sanchez, J., Landeros, C., Langer, R. & Khademhosseini, A. Controlling spatial organization of multiple cell types in defined 3D geometries. *Advanced Materials* **24**, 5543–7, 5542 (2012).

30. Roach, P., Eglin, D., Rohde, K. & Perry, C. C. Modern biomaterials: a review - bulk properties and implications of surface modifications. *Journal of Materials Science. Materials in Medicine* **18**, 1263–77 (2007).

31. Pezron, E. & Magny, B. Modeling of UV oligomers properties. *European Coating Journal* **9**, 602–606 (1996).

32. Zhou, F., Zheng, Z., Yu, B., Liu, W. & Huck, W. T. S. Multicomponent polymer brushes. *Journal of the American Chemical Society* **128**, 16253–8 (2006).

33. Shahin, V., Ludwig, Y., Schafer, C., Nikova, D. & Oberleithner, H. Glucocorticoids remodel nuclear envelope structure and permeability. *Journal of Cell Science* **118**, 2881–2889 (2005).

34. Müller, L. & Müller, F. A. Preparation of SBF with different HCO3- content and its influence on the composition of biomimetic apatites. *Acta Biomaterialia* **2**, 181–189 (2006).

35. Flory, P. J. *Principles of Polymer Chemistry.* (University Press: Cornell, 1953).

36. Bilodeau, G. Regular pyramid punch problem. *Journal of Applied Mechancis* **59**, 519–23 (1992).

37. Buxboim, A., Rajagopal, K., Brown, A. E. X. & Dennis, E. How deeply cells feel: methods for thin gels. *J. Phys. Condens. Matter.* **22**, (2011).

38. Kuo, C.-H. R., Xian, J., Brenton, J. D., Franze, K. & Sivaniah, E. Complex stiffness gradient substrates for studying mechanotactic cell migration. *Advanced Materials* **24**, 6059–64 (2012).

39. Maloney, J., Walton, E., Bruce, C. & Van Vliet, K. Influence of finite thickness and stiffness on cellular adhesion-induced deformation of compliant substrata. *Physical Review E* **78**, 041923 (2008).

40. Cortese, B., Gigli, G. & Riehle, M. Mechanical Gradient Cues for Guided Cell Motility and Control of Cell Behavior on Uniform Substrates. *Advanced Functional Materials* **19**, 2961–2968 (2009).

41. Sen, S., Engler, A. & Discher, D. Matrix strains induced by cells: Computing how far cells can feel. *Cell. Mol. Bioeng.* **2**, 39–48 (2010).

42. Buxboim, A., Ivanovska, I. L. & Discher, D. E. Matrix elasticity, cytoskeletal forces and physics of the nucleus: how deeply do cells "feel" outside and in? *Journal of Cell Science* **123**, 297–308 (2010).

43. Ball, M., Grant, D. M., Lo, W.-J. & Scotchford, C. A. The effect of different surface morphology and roughness on osteoblast-like cells. *Journal of Biomedical Materials Research. Part A* **86**, 637–47 (2008).

44. Curtis, a & Wilkinson, C. Topographical control of cells. *Biomaterials* **18**, 1573–83 (1997).

45. Kunzler, T. P., Drobek, T., Schuler, M. & Spencer, N. D. Systematic study of osteoblast and fibroblast response to roughness by means of surface-morphology gradients. *Biomaterials* **28**, 2175–82 (2007).

46. Geblinger, D., Addadi, L. & Geiger, B. Nano-topography sensing by osteoclasts. *Journal of Cell Science* **123**, 1814–1814 (2010).

47. Bartneck, M., Schulte, V. A., Diez, M., Lensen, M. C. & Zwadlo-Klarwasser, G. Induction of specific macrophage subtypes by defined micro-patterned structures. *Acta Biomaterialia* **6**, 3864–3872 (2010).

48. Lensen, M. C., Schulte, V. A., Salber, J. & Möller, M. Cellular responses to novel, micropatterned biomaterials. *Pure and Applied Chemistry* **80**, 2479–2487 (2008).

49. Lim, J. Y. & Donahue, H. J. Cell sensing and response to micro- and nanostructured surfaces produced by chemical and topographic patterning. *Tissue Engineering* **13**, 1879–91 (2007).

50. Williams, D. F. On the mechanisms of biocompatibility. *Biomaterials* **29**, 2941–2953 (2008).

51. Schulte, V. A., Diez, M., Hu, Y., Möller, M. & Lensen, M. C. Combined influence of substrate stiffness and surface topography on the antiadhesive properties of Acr-sP(EO-stat-PO) hydrogels. *Biomacromolecules* **11**, 3375–3383 (2010).

52. Nemir, S., Hayenga, H. N. & West, J. L. PEGDA hydrogels with patterned elasticity: Novel tools for the study of cell response to substrate rigidity. *Biotechnology and Bioengineering* **105**, 636–44 (2010).

53. Cazalbou, S., Combes, C., Eichert, D. & Rey, C. Adaptative physico-chemistry of bio-related calcium phosphates. *Journal of Materials Chemistry* **14**, 2148 (2004).

54. Neffe, A. T., Loebus, A., Zaupa, A., Müller, F. A. & Lendlein, A. Gelatin functionalization with tyrosine derived moieties to increase the interaction with hydroxyapatite fillers. *Acta Biomaterialia* **7**, 1693–701 (2011).

55. Vallet-Regi, M. Calcium phosphates as substitution of bone tissues. *Progress in Solid State Chemistry* **32**, 1–31 (2004).

56. Uskokovic, D. P. Review Nanosized hydroxyapatite and other calcium phosphates : Chemistry of formation and application as drug and gene delivery agents. *Tissue Engineering* (2010).

57. Paxton, J. Z., Donnelly, K., Keatch, R. P. & Baar, K. Engineering the Bone-Ligament interface using Polyethylene Glycol Diacrylate incorporated with Hydroxyapatite. *Tissue Eng Part A.* **15**, 1201–1209 (2009).

58. Zhou, Z., Ren, Y., Yang, D. & Nie, J. Performance improvement of injectable poly(ethylene glycol) dimethacrylate-based hydrogels with finely dispersed hydroxyapatite. *Biomedical materials (Bristol, England)* **4**, 035007 (2009).

59. Zhou, Z., Yang, D., Nie, J., Ren, Y. & Cui, F. Injectable Poly(ethylene glycol) Dimethacrylate-based Hydrogels with Hydroxyapatite. *Journal of Bioactive and Compatible Polymers* **24**, 405–423 (2009).

60. Fu, S., Guo, G., Gong, C., Wei, Y. & Qian, Z. Injectable biodegradable thermosensitive hydrogel composite for orthopedic tissue engineering. 1. Preparation and characterization of nanohydroxyapatite/poly(ethylene glycol)-poly(epsilon-caprolactone)-poly(ethylene glycol) hydrogel nanocomposites. *The Journal of Physical Chemistry. B* **113**, 16518–25 (2009).

61. Muller, F., Muller, L., Caillard, D. & Conforto, E. Preferred growth orientation of biomimetic apatite crystals. *Journal of Crystal Growth* **304**, 464–471 (2007).

62. Seah, R. K. H., Garland, M., Loo, J. S. C. & Widjaja, E. Use of Raman Microscopy and Multivariate Data Analysis to Observe the Biomimetic Growth of Carbonated Hydroxyapatite on Bioactive Glass. *Analytical Chemistry* **81**, 1442–1449 (2009).

63. Rietveld, H. M. & Loopstra, B. O. The Structure of Some Alkaline-Earth Metal Uranates. *Acta Crystallographica* **B25**, 787–91 (1969).

64. Supová, M. Problem of hydroxyapatite dispersion in polymer matrices: a review. *Journal of Materials Science. Materials in Mgedicine* **20**, 1201–13 (2009).

65. Halvorson, R. H., Erickson, R. L. & Davidson, C. L. The effect of filler and silane content on conversion of resin-based composite. *Dental Materials* **19**, 327–33 (2003).

66. Howard, B., Wilson, N., Newman, S., Pfeifer, C. & Stansbury, J. Relationships between Conversion, Temperature and Optical Properties during Composite Photopolymerization. *Acta Biomaterialia* **6**, 2053–2059 (2011).

67. Yang, J., Han, C.-R., Duan, J.-F., Xu, F. & Sun, R.-C. Mechanical and viscoelastic properties of cellulose nanocrystals reinforced poly(ethylene glycol) nanocomposite hydrogels. *ACS Applied Materials & Interfaces* **5**, 3199–207 (2013).

68. Moraes, R., Grarcia, J., Barros, D., Liu, J. & Stansbury, J. Control of polymerization shrinkage and stress in nanogelmodified monomer and composite materials. *Dental Materials* **27**, 509–519 (2012).

69. Gaharwar, A. K., Dammu, S. a, Canter, J. M., Wu, C.-J. & Schmidt, G. Highly extensible, tough, and elastomeric nanocomposite hydrogels from poly(ethylene glycol) and hydroxyapatite nanoparticles. *Biomacromolecules* **12**, 1641–50 (2011).

70. Fu, S., Wang, X., Guo, G., Wei, Y. & Qian, Z. Preparation and Characterization of Nano-Hydroxyapatite-Poly(ε-caprolactone)-Poly(ethylene glycol)-Poly(ε-caprolactone) Composite Fibers for Tisue Engineering. *Journal of Physical Chemistry C* **114**, 18372–18378 (2010).

71. Pielichowska, K. & Blazewicz, S. Bioactive Polymer / Hydroxyapatite (Nano) composites for Bone Tissue Regeneration. *Advances in Polymer Science* 97–207 (2010).

72. Vural, S., Dikovics, K. B. & Kalyon, D. M. Cross-link density, viscoelasticity and swelling of hydrogels as affected by dispersion of multi-walled carbon nanotubes. *Soft Matter* **6**, 3870 (2010).

73. Xiao, Q. & Zhang, L. C. Effective separation and alignment of long entangled carbon nanotubes in epoxy. *Journal of Materials Science* **40**, 6513–6516 (2005).

74. Huang, H. H., Ho, C. T., Lee, T. L., Liao, K. . & Chen, F. L. Effect of surface roughness of ground titanium on initial cell adhesion. *Biomolecular Engineering* **21**, 93–97 (2004).

75. Cha, C., Kim, E.-S., Kim, I. W. & Kong, H. Integrative design of a poly(ethylene glycol)-poly(propylene glycol)-alginate hydrogel to control three dimensional biomineralization. *Biomaterials* **32**, 2695–703 (2011).

76. Shkilnyy, A., Gräf, R., Neffe, A. T., Hartmann, J. & Taubert, A. Unprecedented, low cytotoxicity of spongelike calcium phosphate/poly(ethylene imine) hydrogel composites. *Macromolecular Bioscience* **9**, 179–86 (2009).

77. Luong, L. N., Hong, S. I., Patel, R. J., Outslay, M. E. & Kohn, D. H. Spatial control of protein within biomimetically nucleated mineral. *Biomaterials* **27**, 1175–86 (2006).

78. Hofmann, I., Müller, L., Greil, P. & Müller, F. A. Precipitation of Carbonated Calcium Phosphate Powders from a Highly Supersaturated SBF Solution. *Key Engineering Materials* **330-332**, 59–62 (2007).

79. Mavropoulos, E., Costa, A. M., Costa, L. T., Granjeiro, J. M. & Rossi, A. M. Adsorption and bioactivity studies of albumin onto hydroxyapatite surface. *Colloids and Surfaces. B, Biointerfaces* **83**, 1–9 (2011).

80. Lee, W.-H., Zavgorodniy, A. V, Loo, C.-Y. & Rohanizadeh, R. Synthesis and characterization of hydroxyapatite with different crystallinity: effects on protein adsorption and release. *Journal of Biomedical Materials Research. Part A* **100**, 1539–49 (2012).

81. Suh, K. Y., Seong, J., Khademhosseini, A., Laibinis, P. E. & Langer, R. A simple soft lithographic route to fabrication of poly(ethylene glycol) microstructures for protein and cell patterning. *Biomaterials* **25**, 557–563 (2004).

82. Pelham, R. J. & Wang, Y. L. Cell locomotion and focal adhesions are regulated by the mechanical properties of the substrate. *The Biological Bulletin* **194**, 348–50 (1998).

83. Engler, A. J., Sen, S., Sweeney, H. L. & Discher, D. E. Matrix elasticity directs stem cell lineage specification. *Cell* **126**, 677–89 (2006).

84. Discher, D. E., Janmey, P. & Wang, Y. Tissue Cells Feel and Respond to the Stiffness of Their Substrate. *Science* **1139**, (2012).

85. Britland, S., Perridge, C., Denyer, M., Curtis, A. & Wilkinson, C. Morphogenetic guidance cues can interact synergistically and hierarchically in steering nerve cell growth. *Experimental Biology Online - EBO* **1**, 1–15 (1996).

86. Hoffman, A S. Hydrogels for biomedical applications. *Annals of the New York Academy of Sciences* **944**, 62–73 (2001).

87. Peppas, N. A., Hilt, J. Z., Khademhosseini, a. & Langer, R. Hydrogels in Biology and Medicine: From Molecular Principles to Bionanotechnology. *Advanced Materials* **18**, 1345–1360 (2006).

88. Khademhosseini, A., Langer, R., Borenstein, J. & Vacanti, J. P. Microscale technologies for tissue engineering and biology. *Proceedings of the National Academy of Sciences of the United States of America* **103**, 2480–7 (2006).

89. Lee, K. Y. & Mooney, D. J. Hydrogels for Tissue Engineering. *Surgery* **101**, (2001).

90. Sant, S., Hancock, M. J., Donnelly, J. P., Iyer, D. & Khademhosseini, A. Biomimetic Gradient Hydrogels for Tissue Engineering. *The Canadian Journal of Chemical Engineering* **88**, 899–911 (2010).

91. West, J. L. & Hubbell, J. A. Reactive polymers Photopolymerized hydrogel materials for drug delivery applications. *Science* **25**, 139–147 (1995).

92. Iza, M., Stoianovici, G., Viora, L., Grossiord, J. L. & Couarraze, G. Hydrogels of poly(ethylene glycol): mechanical characterization and release of a model drug. *Journal of controlled release : official journal of the Controlled Release Society* **52**, 41–51 (1998).

93. Harris, J. *Poly(Ethylene Glycol) Chemistry: Biotechnical and Biomedical Applications.* (Plenum Press: New York and London, 1992).

94. Kim, B. & Peppas, N. A. Poly (ethylene glycol) -containing Hydrogels for Oral Protein Delivery Applications. *Drug Delivery* 333–341 (2003).

95. Schulte, V., Diez, M., Moeller, M. & Lensen, M. Surface Topography Induces Fibroblast Adhesion on Intrinsically Nonadhesive Poly (ethylene glycol) Substrates. *Biomacromolecules* 2795–2801 (2009).

96. Peppas, N. a, Keys, K. B., Torres-Lugo, M. & Lowman, a M. Poly(ethylene glycol)-containing hydrogels in drug delivery. *Journal of controlled release : official journal of the Controlled Release Society* **62**, 81–7 (1999).

97. Kopecek, J. Hydrogel Biomaterials: A smart Future? *Biomaterials* **28**, 5185–5192 (2008).

98. Haraguchi, K. Synthesis and properties of soft nanocomposite materials with novel organic/inorganic network structures. *Polymer Journal* **43**, 223–241 (2011).

99. Gaharwar, A. K., Rivera, C. P., Wu, C.-J. & Schmidt, G. Transparent, elastomeric and tough hydrogels from poly(ethylene glycol) and silicate nanoparticles. *Acta Biomaterialia* **7**, 4139–48 (2011).

100. Schexnailder, P. & Schmidt, G. Nanocomposite polymer hydrogels. *Colloid and Polymer Science* **287**, 1–11 (2008).

101. Wu, C.-J., Gaharwar, A. K., Schexnailder, P. J. & Schmidt, G. Development of Biomedical Polymer-Silicate Nanocomposites: A Materials Science Perspective. *Materials* **3**, 2986–3005 (2010).

102. Gupta, H. S. & Guitia, F. An Effective Morphology Control of Hydroxyapatite Crystals. *Crystal Growth & Design* (2009).

103. Loo, S. C. J., Siew, Y. E., Ho, S., Boey, F. Y. C. & Ma, J. Synthesis and hydrothermal treatment of nanostructured hydroxyapatite of controllable sizes. *Journal of Materials Science: Materials in Medicine* **19**, 1389–1397 (2008).

104. Padilla, S., Izquierdo-Barba, I. & Vallet-Regi, M. High Specific Surface Area in Nanometric Carbonated Hydroxyapatite. *Chem. Mater.* **20**, 5942–5944 (2008).

105. Wang, L. & Nancollas, G. H. Calcium orthophosphates: crystallization and dissolution. *Chemical Reviews* **108**, 4628–69 (2008).

106. Lu, Z., Roohani-Esfahani, S., Kwok, P. & Zreiqat, H. Osteoblasts on rod shaped hydroxyapatite nanoparticles incorporated PCL Film provide an optimal osteogenic niche for stem cell differentiation. **Jun**, 1651–61 (2011).

107. Tsurushima, H., Marushima, A., Nakamura, K., Matsumura, A. & Ito, A. Enhanced bone formation using hydroxyapatite ceramic coated with fibroblast growth factor-2. *Acta Biomaterialia* **6**, 2751–9 (2010).

108. Kaito, T., Myoui, A., Takaoka, K., Tamai, N. & Yoshikawa, H. Potentiation of the activity of bone morphogenetic protein-2 in bone regeneration by a PLA-PEG/hydroxyapatite composite. *Biomaterials* **26**, 73–9 (2005).

109. Cai, L., Guinn, A. S. & Wang, S. Exposed hydroxyapatite particles on the surface of photo-crosslinked nanocomposites for promoting MC3T3 cell proliferation and differentiation. *Acta biomaterialia* **7**, 2185–99 (2011).

110. Sachlos, E. & Czernuszka, J. T. Making tissue engineering scaffolds work. Review: the application of solid freeform fabrication technology to the production of tissue engineering scaffolds. *European cells & materials* **5**, 29–39; discussion 39–40 (2003).

111. Freed, L. E., Novakovic, G. V., Biron, R. J., Barlow, S. K. & Langer, R. Biodegradable Polymer Scaffolds for Tissue Engineering. *Nature* **12**, 689–693 (1994).

112. Drury, J. L. & Mooney, D. J. Hydrogels for tissue engineering: scaffold design variables and applications. *Biomaterials* **24**, 4337–4351 (2003).

113. Hollister, S. J. Porous scaffold design for tissue engineering. *Nature Materials* **4**, 518–24 (2005).

114. Cukierman, E., Pankov, R., Stevens, D. R. & Yamada, K. M. Taking cell-matrix adhesions to the third dimension. *Science* **294**, 1708–12 (2001).

115. Lee, J., Cuddihy, M. J. & Kotov, N. A. Three-Dimensional Cell Culture Matrices: State of the Art. *Tissue Engineering Part B: Reviews* **14**, 61–86 (2008).

116. Abbott, A. Biology ' s new dimension. *Nature* **424**, (2003).

117. Cushing, M. C. & Anseth, K. S. Hydrogel Cell Cultures. *Science* **316**, 1133–1134 (2007).

118. Kretlow, J. D., Klouda, L. & Mikos, A. G. Injectable matrices and scaffolds for drug delivery in tissue engineering. *Advanced Drug Delivery Reviews* **59**, 263–273 (2007).

119. Haraguchi, K. & Takehisa, T. Nanocomposite Hydrogels : A Unique Organic Inorganic Network Structure with Extraordinary mechanical, optical and swelling/deswelling properties. *Advanced Materials* 1120–1124 (2002).

120. Moutos, F. T., Freed, L. E. & Guilak, F. A biomimetic three-dimensional woven composite scaffold for functional tissue engineering of cartilage. *Nature Materials* **6**, 162–7 (2007).

121. Yu, L. & Ding, J. Injectable hydrogels as unique biomedical materials. *Chemical Society Reviews* **37**, 1473–81 (2008).

122. Podsiadlo, P., Kaushik, A. K., Lahann, J., Ramamoorthy, A. & Kotov, N. a Ultrastrong and stiff layered polymer nanocomposites. *Science* **318**, 80–3 (2007).

123. Wang, Q., Mynar, J. L., Yoshida, M., Kinbara, K. & Aida, T. High-water-content mouldable hydrogels by mixing clay and a dendritic molecular binder. *Nature* **463**, 339–43 (2010).

124. Capadona, J. R., Shanmuganathan, K., Tyler, D. J., Rowan, S. J. & Weder, C. Stimuli-responsive polymer nanocomposites inspired by the sea cucumber dermis. *Science* **319**, 1370–4 (2008).

125. Klenke, F. M., Liu, Y., Hunziker, E. B., Siebenrock, K. a & Hofstetter, W. Impact of pore size on the vascularization and osseointegration of ceramic bone substitutes in vivo. *Journal of Biomedical Materials Research. Part A* **85**, 777–86 (2008).

126. Hing, K., Best, S. M., Tanner, K. E., Bonfield, W. & Revell, P. a Mediation of bone ingrowth in porous hydroxyapatite bone graft substitutes. *Journal of Bomedical Materials Research. Part A* **68**, 187–200 (2004).

Abstract

This thesis comprises two fundamentally different approaches, namely the soft lithographic surface patterning Fillmolding In Capillaries (FIMIC) technique and the fabrication of 3D crafts in order to pursue the same goal; controlled cellular adhesion behavior on the basis of localized chemical functionalization. It is commonly accepted that the understanding of protein adsorption and cell adhesion behavior on engineered surfaces and interfaces is essential for the successful development of novel biomaterials. In the course of this thesis, chemical functionalization with calcium phosphates, in particular hydroxyapatite (HAp), were conducted. The intention to compare cellular response of different cell types, namely osteoblasts (mouse osteoblast like MC3T3-E1) and fibroblasts (mouse fibroblasts L-929) in order to reveal guided osteoblast adhesion on specifically chemically patterned hydrogel substrates. Therefore, Poly(ethylene glycol) (PEG) based hydrogels and HAp were utilized in order to form various polymer-inorganic hybrid composites. The overall objective was to exploit the intrinsic protein repellent behavior of PEG-based hydrogels and the protein attractive properties of HAp-based ceramics in order to produce surface patterns of adjacent bioactive and bioinert properties. Thus, it could be demonstrated that spatially controlled introduction of HAp on micropatterned surfaces can determine the adhesion pattern of HAp affine osteoblasts. This stands in opposite to fibroblast, where the aforementioned effect could not be observed. In consequence, it displays the potential of this approach to promote specific cell-substrate interaction of desired cell phenotypes and to distinguish between several cell lines exhibiting varying affinity to a particular chemical pattern.

In the first part of this thesis, the soft lithographic FIMIC method was utilized in the first place to demonstrate that targeted surface patterning with HAp may control adhesion pattern and site of osteoblast adhesion, but in contrast does not show the same effect for fibroblast. Therefore, physically mixed (PEG HAp NPs) and chemically synthesized (PEG nHAp) PEG HAp hydrogel composites fabricated via a precipitation reaction were produced and compared. It was revealed via protein adsorption experiments with the model protein Bovine Serum Albumin

(BSA), that PEG nHAp, in consequence of their inherent higher homogenicity, reaches a far greater bioactivity than PEG HAp NPs. This verifies the principle, in which successful chemical patterning for a specific cell type is desired, yielding control over cellular response due to cell substrate interaction. In this project, Atomic Force Microscopy (AFM) was applied for the physical and mechanical characterization of as prepared FIMIC platforms in dry and hydrated state; a necessary requirement for in-situ investigation in biological application as well as to scrutinize whether topography represents the dominant factor for adhesion. Post fabrication patternability with spatial and chronological resolution of HAp nucleation from Simulated Body Fluid (SBF) over a time-span of 10 days was carried out as concluding step in the comparison between PEG HAp NPs and PEG nHAp. It could be revealed that PEG nHAp allows precise control regarding site and density of HAp nuclei deposition in opposite to PEG HAp NPs. The herein presented comparison of physical and chemical hydrogel composites may serve as a model system to demonstrate the necessity and feasibility of chemical inorganic-organic composites towards their physical counterparts.

In the second part, porous scaffolds made of chemically synthesized star-shaped PEG HAp (8PEG HAp) hydrogel composites via precipitation reaction and subsequent freeze-drying were produced, which combine readiness of functionalization of biological or chemical cues with physical and mechanical suitability for tissue replacement. The general idea was to fabricate 3D interconnected structures, which possess post fabrication functionalization ability via residual carbon double bonds and chemically active HAp. This was proven via the successful cleavage of a model molecule in form of a SH dye and the homogeneous adsorption of the HAp reactive model protein Bovine Serum Albumin (BSA). In conclusion, fibroblast and osteoblast displayed distinct adhesion patterns regarding number of adhered cells and cell morphology. In contrast to fibroblasts, osteoblasts covered almost the entire craft and showed strong spreading, which is generally related to strong cell-substrate interaction. Moreover could be monitored that scaffolds exhibited a pore size structure suitable for vascularization and medium transport, which is indispensable for function and the successful quick ingrowth to the host, an essential need, considering potential replacements in tissue engineering.

Zusammenfassung

Die vorgelegte Arbeit beinhaltet zwei fundamental unterschiedliche Herangehensweisen, Soft Lithographie in Form von Fillmolding In Capillaries (FIMIC) und die Fabrikation von 3D Werkzeugen um kontrolliertes Zelladhäsionsverhalten durch gezielte chemische Strukturierung zu erreichen. Es ist weithin akzeptiert, dass das Verständnis für Proteinadsorption und Zelladhäsionsverhalten auf Oberflächen und Grenzflächen für die Entwicklung zeitgemäßer Biomaterialien von großer Bedeutung ist. Deshalb wurden in dieser Thesis Kalziumphosphate, insbesondere Hydroxylapatit (HAp) mit dem Ziel verwendet unterschiedlich HAp-responsive Zelltypen, Osteoblasten (Maus-Osteoblasten ähnlich MC3T3-E1) und Fibroblasten (Maus-Fibroblasten L-929), auf chemisch strukturierten Hydrogel Oberflächen anzusiedeln und vergleichend zu untersuchen. Daher wurden Poly(ethylen glykol) basierte Hydrogele und HAp eingesetzt um verschiedene inorganisch-organische Hydrogel Komposite zu formen. Dabei war es Ziel, das intrinsische proteinabweisende Verhalten von PEG basierten Hydrogelen und die proteinanziehenden Eigenschaften von HAp basierten Keramiken auszunutzen um mikrostrukturierte Oberflächen zu designen, in denen bioinerte und bioaktive Areale direkt einander angrenzen. Auf diese Weise konnte gezeigt werden, dass die örtlich kontrollierte Einbringung von HAp das Adhäsionsverhalten von HAp affinen Osteoblasten bestimmt. Das steht im Gegensatz zu Fibroblasten, wo dieser Effekt nicht beobachtet werden konnte und demonstriert das Potential dieses Ansatzes, gewünschte spezifische Zell-Substrat Wechselwirkung zu fördern und zwischen unterschiedliche Zelltypen mit variiernder Affinität zu chemischen Substanzen zu selektieren.

Im ersten Teil dieser Arbeit wurde die soft lithographische FIMIC Methode in erster Linie dafür eingesetzt um das lokal kontrollierte Adhäsionsverhalten von Osteoblasten zu zeigen, ein Effekt der für Fibroblasten nicht nachgewiesen werden konnte. Dafür wurden aus linearem PEG und entsprechenden Salzlösungen mittels Abscheidungsreaktion physikalisch gemischte (PEG HAp NPs) und chemisch synthetisierte (PEG nHAp) PEG HAp Hydrogel Komposite produziert und verglichen. Es stellte sich durch Experimente zur Proteinadsorption mit dem Modell-Protein

Bovine Serum Albumin (BSA) heraus, dass aufgrund der inherenten überlegenen Homogenität von PEG nHAp eine weitaus höhere Bioaktivität erreicht wird als bei PEG HAp NPs. Dabei wird das Prinzip bestätigt, in welchem durch erfolgreiche chemische Oberflächenstrukturierung für gezielte Zellarten Kontrolle über die Zell-Substrat Interaktion gewonnen werden kann. In diesem Rahmen wurde Rasterkraftmikoskopie (AFM) zur physischen und mechanischen Untersuchung der erzeugten FIMIC Plattformen in trockenem und hydratisierten Zustand eingesetzt, da dies eine absolut notwendige in-situ Charakterisierungmethode für biologische Anwendung darstellt. Darüber hinaus untersucht diese Methode, dass Adhäsionsmuster der Zellen nicht durch topographische Eigenschaften des Substrates dominiert werden. Die weitergehende Strukturierung von FIMIC Plattformen mit örtlich und zeitlich kontrollierter HAp Disposition von Simulated Body Fluid (SBF) über eine Zeitspanne von 10 Tagen war der abschließende Schritt in dem Vergleich zwischen PEG nHAp und PEG HAp NPs. Es zeigte sich, dass PEG nHAp im Gegensatz zu PEG HAp NPs sich ausgezeichnet eignet um HAp lokal gezielt und zeitlich kontrolliert nukleieren zu lassen. Der hierin präsentierte Vergleich physikalischer und chemischer Hydrogel-basierter Verbundwerkstoffe könnte als Modellsystem dienen um die Notwendigkeit zu demonstrieren, chemische inorganische-organische Komposite entsprechenden Physikalischen vorzuziehen.

Im zweiten Teil dieser Arbeit wurden poröse Gerüste (scaffolds) aus chemisch synthetisierte PEG HAp (8PEG HAp) Hydrogel Komposite aus sternartigem PEG sowie entsprechender Salzlösungen mittels Abscheidungsreaktion und darauffolgender Gefriertrocknung hergestellt. Diese besitzen die Fähigkeit der Funktionalisierung mit biologischen und chemischen Reaktanten nach der Gerüstformung sowie die nötigen physikalischen und mechanischen Eigenschaften für den Einsatz als Gewebeersatzwerkstoff. Die generelle Idee war es 3D Strukturen zu fertigen, die auf der einen Seite nach der Formgebung noch weiter chemisch funktionalisierbar sind und des weiteren über aktive HAp Domänen an der Oberfläche verfügen. Dies wurde durch die demonstrierte Anbindung eines Modellmoleküles in Form eines Modellmoleküls eines SH dye sowie die erfolgreiche homogene Adsorption des HAp reaktiven Modelproteins Bovine Serum Albumin (BSA) erreicht. Im Anschluss zeigten Fibroblasten und Osteoblasten unterschiedliche Adhäsionmuster in Hinsicht auf Anzahl der adhärierten Zellen

und Zellmorphologie. Im Kontrast zu Fibroblasten bedeckten Osteoblasten beinahe das gesamte Substrat bei starker Zellspreitung, was gemeinhin als Zeichen starker Zell-Oberflächen Wechselwirkung angesehen wird. Zudem verfügen die produzierten 3D Strukturen über Porgrößen von über 100 µm, welche für Vaskularisation und Mediumtransport notwendig sind um somit Funktion und schnelles Einwachsen bei potentieller Anwendung als Gewebeersatz zu garantieren.

Acknowledgements

I would like to thank Prof. Marga C. Lensen for giving me the opportunity to carry out my doctoral thesis in her research group. I want express my gratitude to her guidance, supervision, time and patience throughout the past three years.

Special gratitude goes in particular to Zhenfang Zhang, with whom I conducted basically every single project in cooperation. This cooperation is the main source of to the herein presented results.

Furthermore, I owe gratitude to Christine Strehmel and Gonzalo de Vicente Lucas for working with me directly in the lab and conducting experiments, which I would have not been able to conduct myself. Moreover do I want thank them for their advice and many inspiring conversations.

In addition, I wish to thank the rest of the group for the nice working atmosphere throughout the time that I spend at the TU Berlin

Beyond that, I want to express my gratitude to the persons, who helped in several instrumental analyses conducted during the course of this thesis.

I am indebted to my family for their support, patience and empathy in the past three years.

List of Publications

Publications employed in this thesis

Kelleher S, Jongerius A, **Loebus A**, Strehmel C, Zhang Z, Lensen MC.; AFM Characterization of Elastically Micropatterned Surfaces Fabricated by Fill-Molding In Capillaries (FIMIC) and Investigation of the Topographical Influence on Cell Adhesion to the Patterns.; *Advanced Engineering Materials, **14**, B56–B66 (2012).*

Publication-Manuscripts employed in this thesis

Kelleher S, Zhang Z, **Loebus A**, Strehmel C, Lensen MC.; Blending Poly(ethylene glycol) (PEG)-based Polymers in order to Obtain a Library of new Biomaterials and their Application in Surface-micro-patterning by the Fillmolding In Capillaries (FIMIC) Method. *Submitted to Soft Matter*

Loebus A+, Zhang Z+, Strehmel S, de Vicente Lucas G, Lensen M C. Soft lithographic surface patterning of physically and chemically mineralized Poly(ethylene glycol) hydrogels for selective interface interaction. *To be submitted.*

Loebus A+, Zhang Z+, Li Q, Strehmel C, Wisniewski W, Arafeh M, Rüssel C, Su Z, Lensen MC. 3D Patterned Reactive Mineralized Poly(ethylene glycol) Derived Hydrogels., *manuscript in preparation*

Additional publications and manuscripts

Zhang Z, **Loebus A**, de Vicente Lucas G, Manar Arafeh M, Lensen MC. In situ formation of novel Poly(ethyleneglycol)-based Hydrogels via Amine-Michael Type Addition with Tunable Mechanics and Chemical Functionality. *Submitted to Angew. Chem.*

Zhang Z+, **Loebus A**+, Li Q, Strehmel C, Wang J, Su Z, Lensen MC. Calciumphosphate Incorporation into Chemically Crosslinked Poly(ethylene glycol) based Composite Hydrogels for Bone Tisse Engineering. *Manuscript in preparation*

Zhang Z, Kelleher S, Steinhilber D, **Loebus A,** de Vicente G, Strehmel C, Haag R, Lensen MC. Click Chemistry as a Crosslinking Method in the Fabrication of Hydrogels with Tuneable Degradation Properties from star-shaped and Hyperbranched Polyether Macromonomers. *Manuscript in preparation*

Li Q+, Zhang Z+, Zhang X, **Loebus A,** Wang J, Ouyang Z, Su Z, Lensen MC. Chemically cross-linked PEG-based hydrogel with Crystalline Domains in long-range Ordering. *Manuscript in preparation*

Strehmel C, Perez-Hernandez H, Zhang Z, **Loebus A,** Werner C, Lasagni AF, Lensen MC. Controlling Cell Alignment and Spreading by Poly(ethylene glycol) and Ormocomp® Microstructures on Polymer Surfaces. *Manuscript in preparation.*

Li Q+, Zhang Z+, Zhang X, **Loebus A,** Wang J, Ouyang Z, Su Z, Lensen MC. Electrospinning Fibers through 8armPEG Hydrogel Formation Process. *Manuscript* i*n preparation*

Chen J, Arafeh M, Guillet A, Felkel D, Loebus A, Kelleher S, Fischer A, Lensen MC. Hybrid Hierarchical Patterns of Gold Nanoparticles and Poly(Ethylene Glycol) Microstructures. *Submitted to Journal of Materials Chemistry C*

Contribution to Scientific Conferences

Poster contributions

Micro- and Nanofabrication Methods to create patterned PEG Hydrogels for Nano-Biotechnological Applications. Axel Loebus, Susan Kelleher, Zhenfang Zhang, Marga C. Lensen. EuroBiomat 2011, **First Posterprice**

Micro- and Nano- surface patterning of PEG-Nanocomposites Hydrogels for Biomedical Applications. Axel Loebus, Zhenfang Zhang, Christine Strehmel, Marga C. Lensen. Nanomaterials for Biomedical Technologies 2012, Frankfurt/Main

Micro- and Nano- surface patterning of PEG-Nanocomposites Hydrogels for Biomedical Applications. Axel Loebus, Zhenfang Zhang, Christine Strehmel, Marga C. Lensen. Jahrestagung der Deutschen Gesellschaft für Biomaterialien 2012, Hamburg

Appendix

In this "Appendix" the reader will find all auxiliary information. All data shown here are referred to in the main text of the thesis and is ordered according to the respective chapter. In general, the reader will find results of experimental processing conducted by a colleague or where the intellectual effort is attributed to someone else. In some cases however, figures serve to support a statement made in the main text body, but are not of essential importance for the thesis itself.

Chapter 4.1

Acrylation procedure

PPEG-b-PPG-b-PEG (4400 Da, Sigma Aldrich) and K_2CO_3 were dried in a vacuum oven at 100 °C for 4 hr. PEG-b-PPG-b-PEG (5 g) and K_2CO_3 (20 g) were dissolved in dry CH_2Cl_2 (50 mL) under N_2. The solution was then cooled to 0 °C and acryloyl chloride (15 g) was added dropwise. The mixture was stirred at 50 °C for 2 days. The solution was filtered and poured into petroleum ether cooled to -196 °C. The solution was stirred for 10 min and the ether decanted, leaving behind a crude product. This crude product was dissolved in 50 mL CH_2Cl_2 and then washed 3 times with saturated NaCl solution 3 times. The organic layer was collected, dried with $MgSO_4$, filtered and the solvent was removed under reduced pressure resulting in a colourless liquid. A typical yield from this procedure was 60 %. ^{1}H NMR ($OCH_2CHC\mathbf{H_3}$O 1.12 ppm, $OCH_2C\mathbf{H}CH_3$O 3.38 ppm, $OC\mathbf{H_2}CHCH_3$O 3.52 ppm, $OC\mathbf{H_2}C\mathbf{H_2}$O 3.63 ppm, (C=O)OC$\mathbf{H_2}$ 4.30 ppm$\mathbf{,}$ =C-$\mathbf{H}$ trans 5.83 ppm, C$\mathbf{H}$=C 6.15 ppm, =C-$\mathbf{H}$ cis 6.42 ppm).
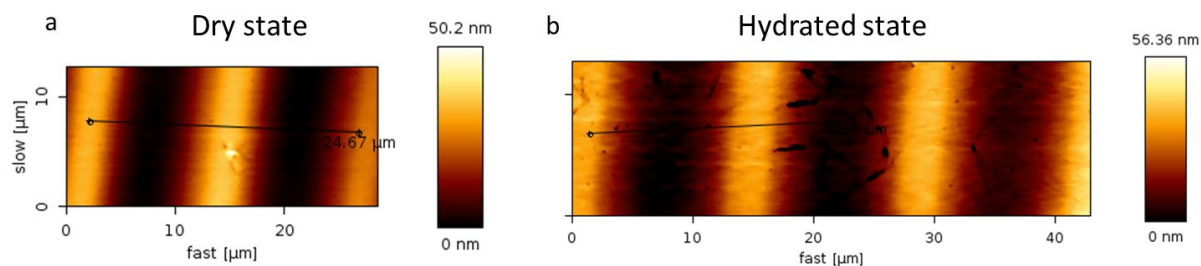
Figure 1: Atomic Force Microscopy (AFM) topographic images of PEG_{575} in PEG_{575} containing 1 % PI and 5 % CL in the mold and filler likewise. (a) dry state; (b) hydrated state.

Chapter 4.2

Acrylation-procedure for 8arm PEG:

At first, 8arms PEG-OH (15 kDa) and K_2CO_3 was dried in a vacuum oven at 100 $^\circ$C for 4 h. Then, 8arms PEG (5g) and K_2CO_3 (30 times) were dissolved in 50 mL CH_2Cl_2 under N_2 -condition. Acryloyl Chloride (20 times) was added dropwise in a water-ice bath. The mixture was stirred at 60 $^\circ$C for 4 days. The solution was filtered, and then poured into the cold petroleum ether (cooled by water-ice). The solution was stirred for 10 min, and then separated to get the crude product. The crude product was dissolved in 50 mL DCM and then extracted with saturated NaCl solution for 3 times. The organic layer was collected. The solution was dried by magnesium-sulfate overnight, then filtered to remove $MgSO_4$ and subsequently the solvent was removed under reduced pressure to get the final product. (white solid) Isolated yield (72 %)^{1}HNMR(OCH_2CH_2O 3.64 ppm(1496H), (C=O)OCH_2 4.31 ppm(16H), =C-**H** trans 5.83 ppm(8H), C**H**=C 6.15 ppm(8H), =C-**H** cis 6.42 ppm(8H)).

Processing of pure polymers:

In order to process the polymers into mouldable gels, one must ensure they are 1) in a liquid state and 2) homogenously mixed with the photoinitiator (PI) (1% PI). In the case of the two liquid polymers (PEG1 and 3BC1), the PI is evenly dispersed throughout the mix using a small

amount of acetone, which is removed after mixing. Solid polymers, on the other hand, require additional treatments for them to become processible.

Dissolving the solid polymers (PEG2, 3BC2 and 8PEG) and the PI in water allows for the formation of very soft but strong hydrogels, depending of the amount of water used in the process. However, the FIMIC process is not compatible with water-based gels at present, due to either rapid dehydration of highly hydrated molds during the filling step or indeed hydration of non-hydrated molds being filled with water-based polymer solution, both phenomena that are followed by curling off of the molds from surface, so one has to avoid using water in our system. For this reason solids were heated above their Glass Transition Temperature (T_g) to yield melted polymers and to allow to handle them in liquid form and therefore enable the molding of these materials without any solvent.

The window of processing time for this liquid processing is less than five minutes, after which time precursors begin to solidify. Polymers that were heated to the correct temperature (above their T_g) and were rapidly cast into molds and resulting transparent, homogenous samples. Analysis using optical microscopy and Atomic Force Microscopy (AFM) confirmed the homogeneity of the samples (results not shown). Highly crystalline polymers, e.g. PEG2, were the most difficult to make into a transparent, homogeneous gel sometimes showing the formation of spherulites upon molding (and concurrent crystallisation). This can be avoided by working quickly with the melt and warming the molds and glassware used in the casting.

The hydrogels are easy to handle, flexible and transparent and thus ideal for using in the eventual cell studies. After fabricating samples from five pure polymers, the swelling degree (SD) was calculated of each sample after 24 hours in deionised water at 37 °C (SI 1).

Table 1 – The characteristics of the pure polymers and how well they formed transparent, homogenous gels (+++ = very well, + = not very well).

Polymer	Tg (or Mp) °C	SD (%)	Chain length (kDa)	Gel formation
PEG1	12-17	28	0.6	+++
PEG2	58-65	179	3.4	+++
8PEG	~ 50	157	~ 2	+++
3BC1	5	6	4.4	+
3BC2	~ 52	204	8.4	++

Of the pure PEG-based gels, PEG2 swells the most after 24 hours. This can be explained by the longer chain length compared to the other two derivatives (PEG1 and 8PEG) and therefore the cross-linking points that are further apart. The swelling ability of the block co-polymer 3BC1 is significantly poorer than the pure PEG counterparts, due to the chemistry of the block copolymer, with a large section of the polymer consisting of the hydrophobic PPG. In addition, the relatively short chains mean that 3BC1 hardly swells at all in water. Interestingly, on the other hand, the block co-polymer 3BC2 has the highest swelling degree of all the gels, showing that despite the presence of the PPG moieties, the longer chain length produces, upon crosslinking, a "loose" network that is capable of taking up more water.

The swelling data is vital for the understanding the swelling degree of the hydrogels used in order to manipulate the topography produced in the FIMIC samples and subsequently levelling out of respective samples. From Table 1 it becomes clear that based on their large swelling ability, 3BC2 and 8PEG are the most promising candidates to use in the strategy of employing a filler material that swells more than the mold. Nevertheless, these two derivatives are also the most challenging to make processible.

Moreover, the chemistry of these two polymers is quite different; 3BC2 contains 20% PPG whereas 8PEG contains only PEG. In order to rule-out any chemistry differences on FIMIC samples, two similar polymers for blending for the use in the FIMIC process are paired. Blending building blocks give more versatility in tuning the properties of the resulting gels; the physicochemical properties such as swelling degree lie in between those of the gels formed from the pure constituent. By adding different amounts of crosslinker (CL), one can keep the chemistry of two gels the same, while adjusting the stiffness. Samples of homogenous gels with different levels of cross-linker (0 %, 5 % and 10 %) and therefore, tuneable physicochemical properties, were fabricated.

Blending:

Blending the two liquid pre-polymers (i.e. PEG1 and 3BC1) was thought to be the least complicated combination to physically mix. Yet, attempting to blend the two polymers in different ratios showed that the homogenous blending reached a limit (SI 2a). Gels with a smaller ratio of PEG1:3BC1 were better able to form a homogenous gel, with mixes containing a higher percentage of 3BC1 were shown to form a phase-separated material. This phase-separated material was recognised by the naked eye by its opaqueness, and optical microscopy confirmed the presence of micrometer-sized droplets (around 50-100 μm in size; SI 2b). Nevertheless, when the % PEG1 was smaller than approximately 40 % (3BC1 was approximately 60 % or more) the formation of a homogenous, transparent hydrogel could be observed (SI 2c).

a PEG1 %	3BC1 %	Homogenous gel
17	83	+
33	66	+
50	50	-
70	30	-

SI 1: (a) Successful formation of good hydrogels depends on the ratio of PEG1:3BC1; (b) phase

separation gel formed from a mixture of PEG1:3BC1 (50:50); (c) a mixing ratio of PEG1: 3BC1 (33:66) gives a transparent gel (the limit for the transparency lies at approximately 40% PEG1).

The swelling degrees of the successful, homogenous blends (i.e. PEG1:3BC1 in mixing ratios below 40:60) as well as the swelling degree after 24 hours of the pure polymer gels were measured (SI 3). The more PEG1 and/or less crosslinker (CL) present in the gel, the more it swells. This graph shows that by altering these two factors one can fabricate gels within a wide range of swelling degrees. The liquid PEG-based hydrogels have a maximum swelling ratio of about 30%.
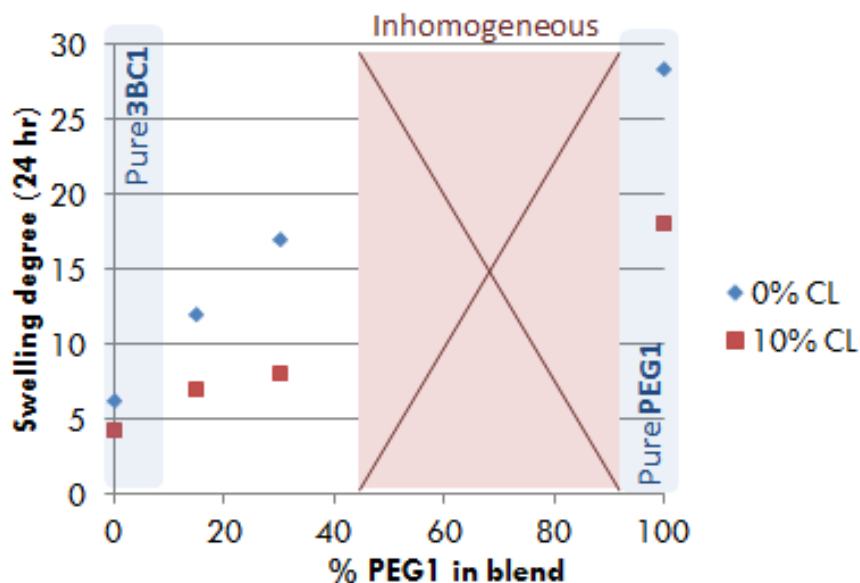
SI 2: The swelling degrees of pure PEG1, 3BC1 and the homogenous blend gels (described in terms of their PEG1 content). Higher amounts of crosslinker (CL) reduce the swelling ability of the hydrogels.

Although it is able to process the individual solid PEG polymers (3BC2, PEG2 or 8PEG) to get transparent, homogenous gels, blending of two solid PEG polymers by heating and mixing was unsuccessful. Therefore, to add fluidity to the mixtures of solid polymers, solid PEG-derivative with a liquid one, namely with PEG1 or 3BC1 were mixed.

SI 4 summarizes the combinations of liquid polymer with solid polymer that resulted in the formation of homogenous, transparent gels. The best (i.e. the easiest to form, most

homogenous/transparent and stable within the time frame of processing) liquid/solid blends that were fabricated involved the PEG1 liquid polymer. Mixing melts of each 3BC2 and 8PEG with liquid PEG1 easily gave gels that were homogenous and transparent upon curing (entries 1 and 2). On the other hand, the blending of PEG1 with the solid, longer chain PEG2 was unsuccessful in the formation of a homogenous gel as the PEG2 recrystallizes upon mixing with the PEG1 leading to opaque gels full of crystals (entry 3). Finally, the blending of liquid 3BC1 with the two solid, pure PEG-polymers (PEG2 and 8PEG) did not result in any homogenous gel formation as they were immiscible (entries 4 and 5).

Thus, the successful blending of the combinations of both the liquid/liquid blend PEG1/3BC2 and the liquid/solid blends of pure PEG, i.e. PEG2/8PEG or PEG1/8PEG, yielded a range of gels with different swelling ratios. In particular, the swelling degree and crosslinking variation of the PEG1/8PEG gels show promise in being an excellent candidate for use in the levelling out experiment, since 8PEG itself swells more than PEG1, and the blends therefore combine good processibility with a larger swelling range than the pure constituents. SI 4b shows the swelling degree (SD) of blends of three different ratios of PEG1/8PEG; obviously, the more 8PEG in the blend, the more the gel swells.
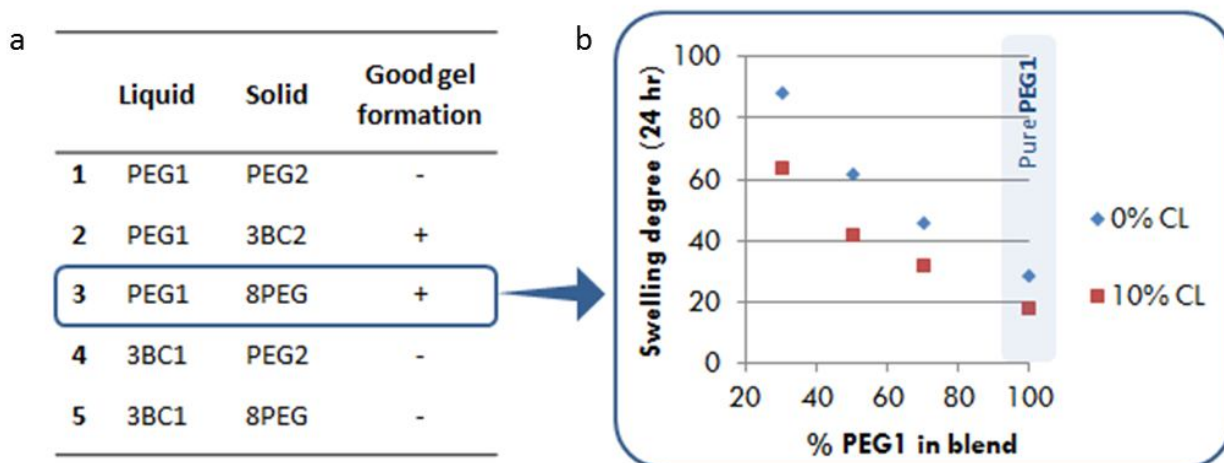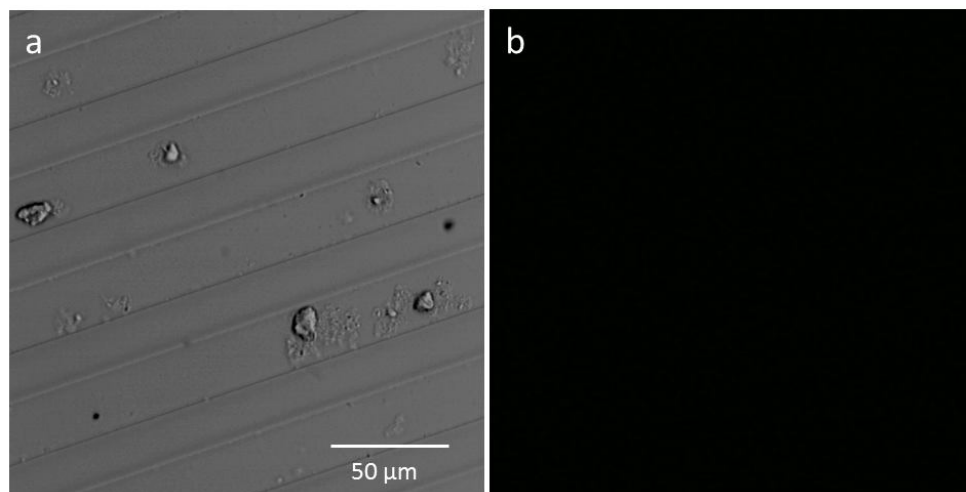

SI 3: (a) Table - The outcome of blending liquid/solid pre-polymers aiming to fabricate a homogenous blend; (b) Chart - the swelling degrees of the PEG1/8PEG blends as a function of their composition and amount of crosslinker (CL).
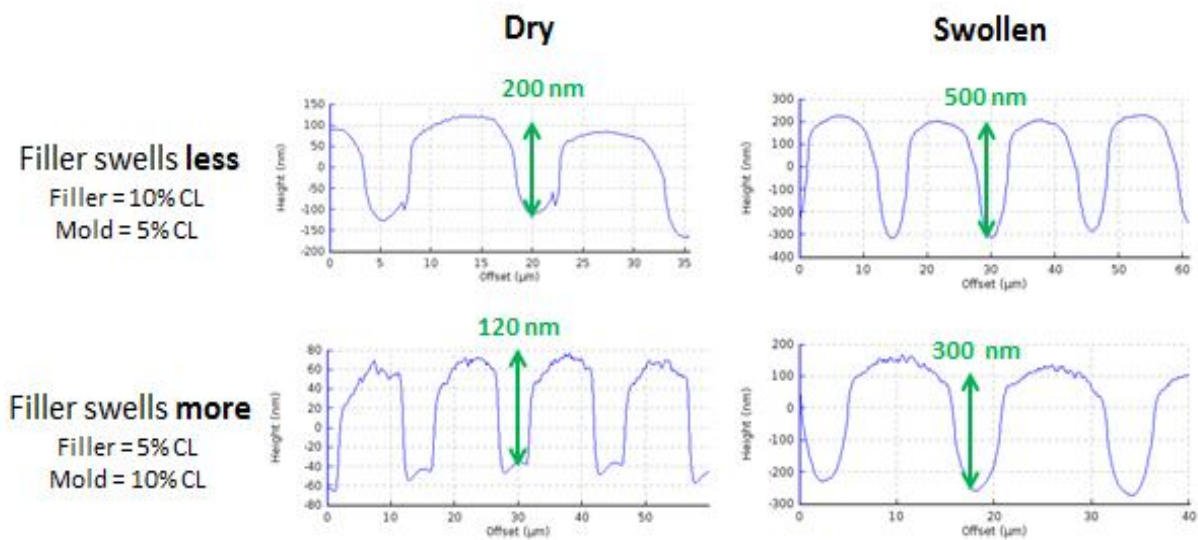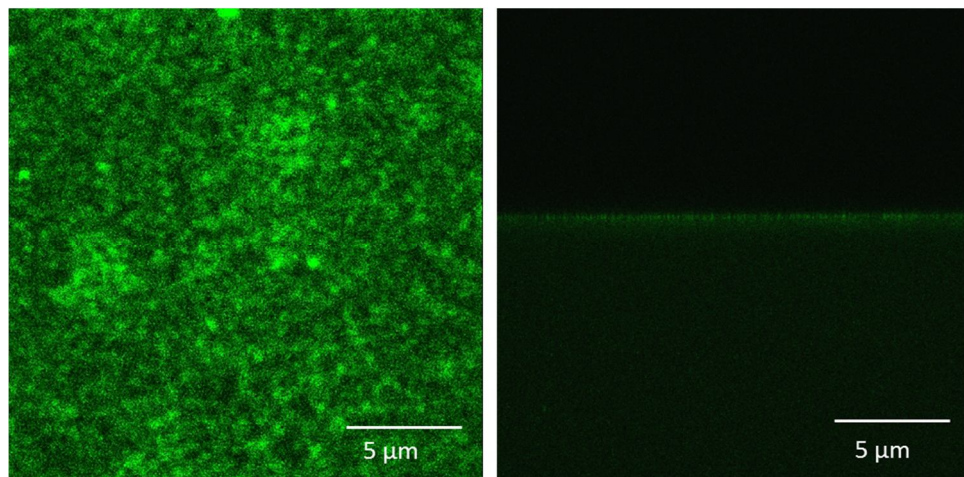
SI 4: Topography of FIMICs with blends of PEG and 3BC with varying amounts of crosslinker (CL) in mold and filler.
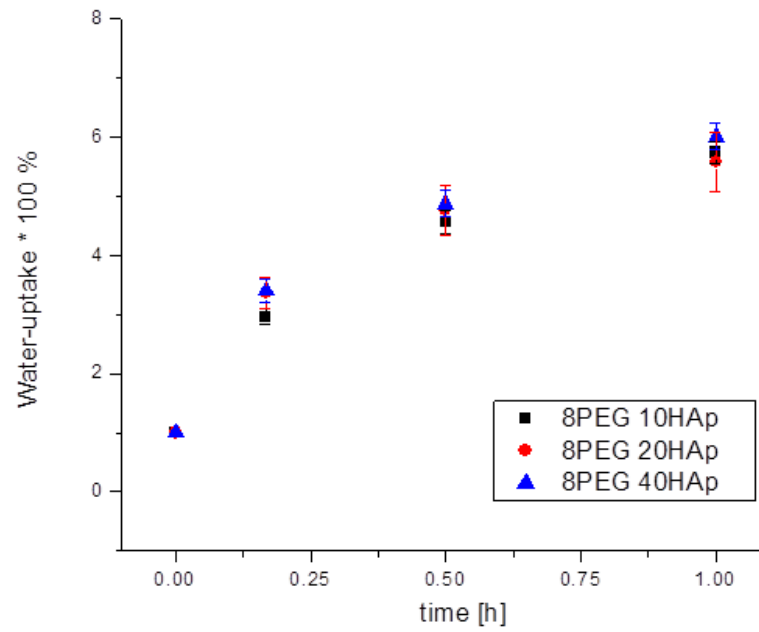
Chapter 4.3.3

SI 1: Enlarged depiction of Figure 7f. CLSM optical and fluorescent images (a) optical image, (b) fluorescent image.
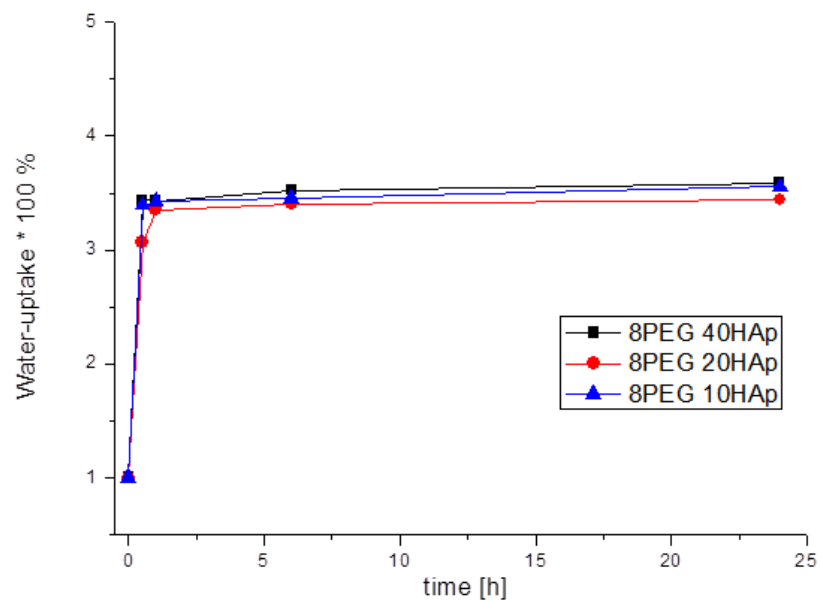
Chapter 4.4.1

SI 1: CLSM fluorescent images of Bovine Serum Albumin (BSA) adsorption on a representative non-UV cured flat 8PEG 20HAp sample.(a) topview; (b) cross-section.
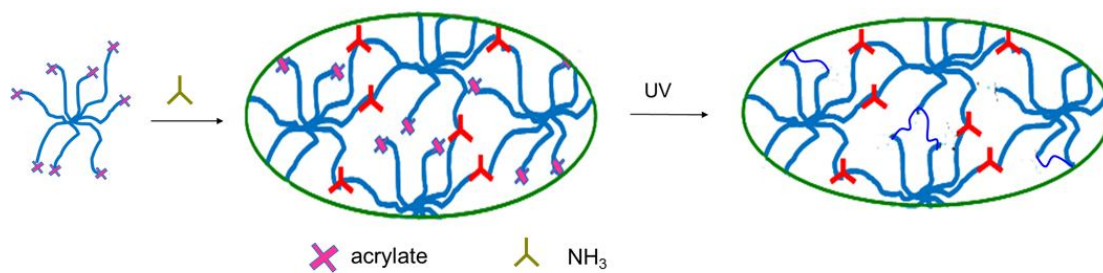
Chapter 4.4.2

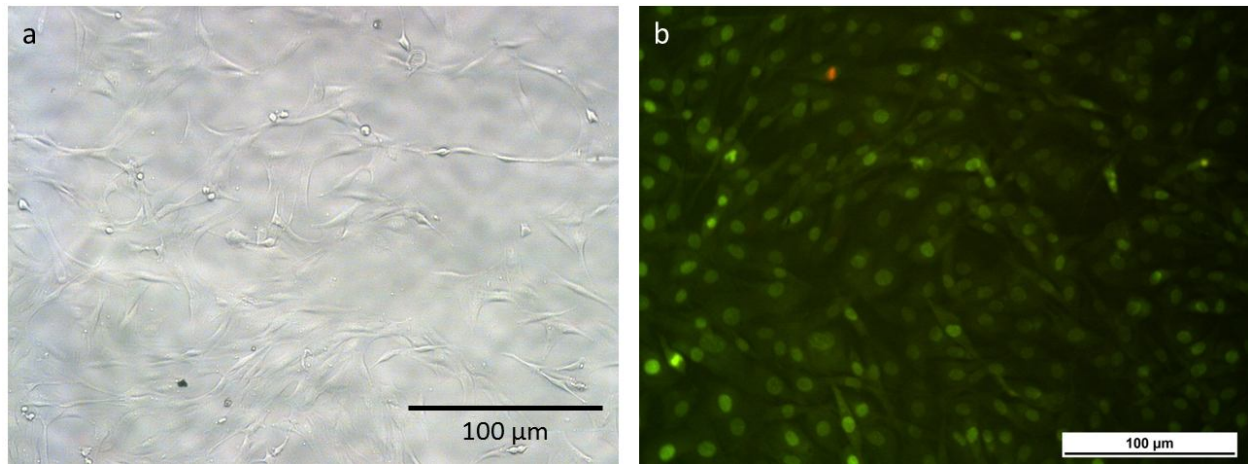SI 2: Water-uptake of 8PEG HAp hydrogel composites before UV curing.

SI 3: Water-uptake of 8PEG HAp hydrogel composites after UV curing.

Si 4: Scheme of ultraviolet radiation curing of 8PEG hydrogels

Chapter 4.4.3

SI 5: Adhesion experiments and cytotoxicity testing with osteoblasts (mouse osteoblast like MC3T3-E1) characterized with optical microscopy. (a) adhesion of osteoblasts on flat UV cured 8PEG 20HAp, (b) live-dead assay of osteoblasts on 8PEG 20HAp.